Towards Better Adaptation of Foundation Models

Zhuoyan Xu
University of Wisconsin - Madison
zhuoyan.xu@wisc.edu

ABSTRACT

Foundation models have revolutionized artificial intelligence, yet fundamental challenges remain in understanding and optimizing their capabilities in adaptation and inference. This document presents several interconnected contributions advancing the theoretical understanding and practical deployment of foundation models. First, we provide theoretical justification for multitask finetuning approaches in foundation models, demonstrating that diverse task selection leads to reduced error in target tasks with limited labeled data. We develop novel diversity and consistency metrics to quantify task relationships and propose an effective task selection algorithm. Second, we investigate the compositional abilities of large language models (LLMs) through in-context learning, revealing that while models excel at simpler composite tasks involving distinct input segments, they struggle with multi-step reasoning tasks. Our theoretical analysis explains this behavior, showing that compositional capability emerges when tasks process different input parts separately. Additionally, we contribute to collaborative work in understanding LLM behavior regarding the scale effects in in-context learning. Together, these contributions advance our understanding of capabilities and limitations in foundation models while providing practical insights for their effective utilization.

To further extend these advances, our ongoing work focuses on two areas: analyzing induction heads to understand out-of-distribution generalization mechanisms in LLM architectures, and developing adaptive inference frameworks for multimodal LLMs to improve deployment efficiency.

Our proposed future work will pursue two directions: First, we will develop token-level and model-level optimization techniques to improve inference efficiency while maintaining model performance, addressing the computational challenges in deploying large foundation models. Second, we will advance mechanistic interpretability by analyzing internal model representations and attention patterns during reasoning tasks, aiming to uncover how these models process and combine information to reach conclusions. These investigations will contribute fundamental insights into LLM capabilities while providing practical techniques for enhancing model performance and interpretability.

Contents

Chapter 1

Introduction

The emergence of foundation models [Bommasani et al., 2021] has fundamentally transformed the landscape of artificial intelligence (AI), enabling unprecedented capabilities across diverse domains. These models, exemplified by large language models (LLMs) (e.g., BERT [Devlin et al., 2019], Llama [Touvron et al., 2023a,b], GPT-3 [Brown et al., 2020], GPT-4 [OpenAI, 2023]), vision models (e.g., CLIP [Radford et al., 2021] and DINOv2 [Oquab et al., 2023]), and multimodal large language models (MLLMs) (e.g., GPT-4V(ision) [OpenAI, 2022b], Claude-3 [Anthropic, 2024], Llama-3 [Meta, 2024]) have demonstrated remarkable abilities across multiple modalities and tasks—from basic classification and recognition to complex understanding and reasoning, leading to some of the most exciting developments in AI to date.

Despite their remarkable capabilities, foundation models face a fundamental challenge as the "Specialization Gap"—the difficulty of transforming general-purpose models into efficient domain experts. This gap manifests through three interconnected barriers: (1) **Knowledge Barrier**: Models possess broad but shallow knowledge, struggling to develop the deep expertise required for specialized tasks without extensive labeled data. For instance, while a vision model may recognize general visual patterns from broad pretraining data, it struggles to adapt to specialized domains like identifying rare butterfly species or distinguishing subtle variations in cancer cell morphology; (2) **Reasoning Barrier**: Models lack the structured reasoning patterns needed for complex compositional tasks that require combining multiple concepts or executing multi-step logical processes, such as combining question-answering with translation, or text summarization with numerical extraction; and (3) **Efficiency Barrier**: Model's full capacity is unable to deployed under resource constraints, such as memory limitations on edge devices or latency requirements in real-time applications. Our research addresses the fundamental question: how can we bridge this specialization gap through adaptive transformation techniques that overcome these barriers simultaneously?"

My work addresses these by developing targeted adaptation techniques and analyzing the mechanisms behind compositional reasoning, and creating adaptive frameworks for resource-efficient deployment. We mainly address these challenges through theoretical analysis, empirical studies, and practical solutions.

Effective adaptation. First, we tackle the challenge of adapting foundation models to new tasks with limited labeled data. While these models excel at many tasks, their effective adaptation, especially in few-shot scenarios, remains both a practical challenge and a theoretical mystery. We present a theoretical framework for analyzing multitask finetuning, revealing that with a diverse set of relevant tasks, this approach can significantly reduce error in target tasks compared to direct adaptation. Our analysis quantifies the relationship between finetuning tasks and target tasks through novel diversity and consistency metrics, leading to practical algorithms for task selection that substantially improve adaptation performance.

Understanding compositional ability. Second, we delve into understanding the cognitive capabilities of large language models, specifically focusing on their ability to handle composite tasks. While these models demonstrate remarkable in-context learning capabilities, their approach to solving unseen complex tasks that combine multiple simple tasks remains poorly understood. Through systematic empirical studies, we uncover that models exhibit divergent behaviors: they show promising performance on simpler composite tasks that apply distinct operations to different input segments but struggle with multi-step reasoning tasks. Our theoretical analysis in a simplified setting provides insights into why models succeed in certain compositional scenarios while failing in others, contributing to our fundamental understanding of these systems.

Efficient Inference. Third, we have an ongoing work exploring adaptive inference techniques for foundation models under varying resource constraints. Our key insight is that an multimodal LLMs can be conceptualized as a collection of shallower models, which can be leveraged for dynamic reconfiguration during inference. We develop AdaLLaVA, a framework that dynamically adjusts model computation based on input content and latency constraints. Our initial results show promising directions for maintaining model performance while adapting to different computational budgets at inference time.

Beyond these primary contributions, we have also advanced the understanding of foundation models through several complementary investigations. Through collaborations, I contributed to understanding scale effects in in-context learning [Shi et al., 2024b] and investigating induction heads for out-of-distribution generalization [Song et al., 2024]. These investigations collectively enhance our understanding of model behavior and deployment considerations.

Building on our completed work in few-shot adaptation and compositional reasoning, and our ongoing work adaptive inference, my work investigates how to enhance foundation models' specialized capabilities. For the proposed work in my ongoing plan, we will focus on two aspect (details in Chapter 6). First, extending our work on adaptive inference, we aim to develop a comprehensive efficiency framework that dynamically optimizes model deployment through intelligent token selection and selective component activation. Second, we will conduct a systematic investigation of the relationship between model architecture and reasoning capabilities in LLMs. This work will analyze how architectural elements—particularly attention patterns and induction heads—influence in-context learning and compositional reasoning abilities. By identifying and strengthening key architectural components responsible for reasoning, we aim to develop more robust and efficient models that maintain strong performance on complex tasks while requiring fewer computational resources.

The remainder of this document is organized as follows: Chapter 2 provides necessary background and related work. Chapter 3 presents our theoretical analysis of multitask finetuning and its empirical validation. Chapter 4 explores the compositional abilities of large language models through both empirical studies and theoretical analysis. Chapters 5 and 6 discussed our ongoing and proposed works. Chapter 7 discussed my additional collaborative works and the connections between my research components and outlined the timeline for my proposed work and defense schedule.

Chapter 2

Background and Related Work

2.1 Adaptation of Foundation Models

Training Foundation Models. Foundation models [Bommasani et al., 2021] are typically trained using self-supervised learning over broad data. The most commonly used training approaches include *contrastive learning* in vision and *masked modeling* in NLP. Our theoretical analysis considers both approaches under a unified framework. Here we briefly review these approaches.

Contrastive learning, in a self-supervised setting, aims to group randomly augmented versions of the same data point while distinguishing samples from diverse groups. The success of this approach in vision and multi-modal training tasks [Oord et al., 2018; Chen et al., 2020; He et al., 2020; Tian et al., 2020a; Grill et al., 2020; Radford et al., 2021] has spurred considerable interest. Several recent studies [Arora et al., 2019; HaoChen et al., 2021; Tosh et al., 2021; Zimmermann et al., 2021; Wei et al., 2021; Wang and Isola, 2020; Wen and Li, 2021; Wang et al., 2022; Shi et al., 2023a; Huang et al., 2023; Sun et al., 2023b,a] seek to develop its theoretical understanding. Arora et al. [2019] established theoretical guarantees on downstream classification performance. HaoChen et al. [2021] provided analysis on spectral contrastive loss. Their analysis assumes the pretraining and target tasks share the same data distribution and focus on the effect of contrastive learning on direct adaptation. My prior work (details in Chapter 3) focuses on the novel class setting and investigates further finetuning the pretrained model with multitask to improve performance.

Masked modeling seeks to predict masked tokens in an input sequence. This self-supervised approach is the foundation of many large language models [Devlin et al., 2019; Liu et al., 2019; Chowdhery et al., 2022; Ni et al., 2022; Touvron et al., 2023a], and has been recently explored in vision [He et al., 2022]. In the theoretical frontier, Zhao et al. [2023] formulated masked language modeling as standard supervised learning with labels from the input text. They further investigated the relationship between pretrained data and testing data by diversity statement. My prior work (details in Chapter 3) subsumes their work as a special case, and can explain a broader family of pretraining methods.

Adapting Foundation Models. Adapting foundation models to downstream tasks has recently received significant attention. The conventional wisdom, mostly adopted in vision [Vinyals et al., 2016; Ge and Yu, 2017; Chen et al., 2020; He et al., 2020, 2022; Shi et al., 2023b], involves learning a simple function, such as linear probing, on the representation from a foundation model, while keeping the model frozen or minorly finetuning the whole model. In NLP, prompt-based finetuning [Gao et al., 2021a; Hu et al., 2022b; Chung et al., 2022; Song et al., 2022; Zhou et al., 2022b; Xie et al., 2023; Zhang et al., 2023a] was developed and widely used, in which a prediction task is transformed into a masked language modeling problem during finetuning. With the advances in large language models, parameter-efficient tuning has emerged as an attractive solution. Prompt tuning [Lester et al., 2021; Li and Liang, 2021; Roberts et al., 2023] learns an extra prompt token for a new task, while updating minimal or no parameters in the model backbone. Another promising approach is in-context learning [Min et al., 2022c; Wei et al., 2022a,b; Shi et al., 2023d; Xu et al., 2024b], where the model is tasked to make predictions based on contexts supplemented with a few examples, with no parameter updates. In this paper, we consider adapting foundation models to new tasks with limited labels. Parameter-efficient tuning, such as in-context learning, might face major challenges [Xie et al., 2022b] when the distribution of the new task deviates from those considered in pretraining. Instead, our approach finetunes the model using multiple relevant tasks. We empirically verify that doing so leads to better adaptation.

Multitask Learning. Multitask supervised learning has been considered for transfer learning to a target task [Zhong et al., 2021; Sanh et al., 2022; Chen et al., 2022b; Min et al., 2022b; Wang et al., 2023c]. Multitask has been shown to induce zero-shot generalization in large language models [Sanh et al., 2022], and also enable parameter efficient tuning by prompt tuning [Wang et al., 2023c]. My prior work (details in Chapter 3) leverages multitask learning to unlock better zero-shot and few-shot performance of pretrained models. Min et al. [2022b]; Chen et al. [2022b] primarily focus on in-context learning, Zhong et al. [2021] focuses on the idea of task conversion where transfer classification task as question-answer format, our approach is based on utilizing original examples, in alignment with our theoretical framework. A line of theoretical work provides the error bound of the target task in terms of sample complexity [Du et al., 2021; Tripuraneni et al., 2021; Shi et al., 2023a; Xu et al., 2023]. Tripuraneni et al. [2020] established a framework of multitask learning centered around the notion of task diversity for the training data. Their work mainly analyzed representations from supervised pretraining using multitasks. In contrast, my prior work (details in Chapter 3) considers representations from self-supervised pretraining, and focuses on multitask finetuning. Our approach and analysis guarantee that limited but diverse and consistent finetuning task can improve the prediction performance on a target task with novel classes.

Few-shot Learning and Meta Learning. Few-shot learning necessitates the generalization to new tasks with only a few labeled samples [Wang et al., 2020; Vu et al., 2021; Murty et al., 2021; Liu et al., 2021; Yang et al., 2022; Galanti et al., 2022]. Direct training with limited data is prone to overfitting. Meta learning offers a promising solution that allows the model to adapt to the few-shot setting [Finn et al., 2017; Raghu et al., 2020]. This solution has been previously developed for vision tasks [Vinyals et al., 2016; Snell et al., 2017; Chen et al., 2021b; Hu et al., 2022c]. Inspired by meta learning in the few-shot setting, our analysis extends the idea of multitask finetuning by providing sound theoretic justifications and demonstrating strong empirical results. We further introduce a task selection algorithm that bridges our theoretical findings with practical applications in multitask finetuning.

2.2 Compositional ability of LLMs

Large language model. LLMs are often Transformer-based [Vaswani et al., 2017] equipped with the enormous size of parameters and pretrained on vast training data. Typical LLMs includes BERT [Devlin et al., 2019], PaLM [Chowdhery et al., 2022], LLaMA[Touvron et al., 2023a], ChatGPT [OpenAI, 2022a], GPT4 [OpenAI, 2023]. Pretraining methods include masked language modeling [Devlin et al., 2019; Liu et al., 2019], contrastive learning [Gao et al., 2021b; Shi et al., 2023a; Sun et al., 2023c, 2024] and auto-regressive pretraining [Radford et al., 2018, 2019]. Several works [Madasu and Srivastava, 2022; Alajrami et al., 2023] investigate the effects of pretraining on language models. Adapting LLMs to various downstream tasks has received significant attention, e.g., adaptor [Hu et al., 2022a, 2023; Zhang et al., 2023a; Luo et al., 2024], prompt tuning [Lester et al., 2021; Li and Liang, 2021; Wei et al., 2023a; Gu et al., 2024c], multitask finetuning [Sanh et al., 2022; Wang et al., 2023c; Xu et al., 2023, 2024c], instruction tuning [Chung et al., 2022; Mishra et al., 2022], in-context learning [Min et al., 2022c; Dong et al., 2022; Yao et al., 2023], low-rank adaptation [Hu et al., 2022a; Zeng and Lee, 2024; Hu et al., 2024], reinforcement learning from human feedback (RLHF) [Ouyang et al., 2022] and inference acceleration [Gu et al., 2024b,d; Xu et al., 2024a].

In-context learning. LLM exhibits a remarkable ability for in-context learning (ICL) [Brown et al., 2020], particularly for generative models. Given a sequence of labeled examples and a testing example (combined as a prompt), the model can construct new predictors for testing examples without further parameter updates. Several empirical studies investigate the behavior of ICLs. Zhao et al. [2021]; Holtzman et al. [2021]; Lu et al. [2022] formulate the problems and report the sensitivity. Rubin et al. [2022]; Liu et al. [2022]; Hongjin et al. [2023]; Wang et al. [2023b] provide methods to better choose in-context learning examples. Chen et al. [2022a]; Min et al. [2022a] use meta training with an explicit in-context learning object to boost performance. Theoretically, Xie et al. [2022a]; Garg et al. [2022] provide a framework to explain the working mechanism of in-context learning. Von Oswald et al. [2023]; Akyürek et al. [2023]; Mahankali et al. [2023]; Zhang et al. [2023b], investigating with linear models, show how transformers can represent gradient descent and conduct linear regression. Based on these works, we provide an analysis showing how LLM can exhibit compositional ability in ICL.

Emergence of compositional ability. Scaling law was first proposed by Kaplan et al. [2020] and then followed up by Hoffmann et al. [2022], emphasizing both the scale of models and training data. Sometimes, increasing scale can lead to new behaviors of LLMs, termed *emergent abilities* [Wei et al., 2022a; Arora and Goyal, 2023], such as domain generalization [Shi et al., 2024a], math reasoning [Gu et al., 2024a], spatial reasoning [Wang et al., 2024] and so on. Recent works show LLMs with larger scales have distinct behavior compared to smaller language models [Wei et al., 2023b; Shi et al., 2023d, 2024b]. These behaviors can have positive or negative effects on performance. Solving complex tasks and reasoning is an active problem in the AI community [Huang and Chang, 2022]. There is a line of empirical works investigating the compositional ability in linguistic fashion [Kim and Linzen, 2020; Levy et al.,

2022; An et al., 2023a,b; Xu et al., 2024b]. LLMs are capable of learning abstract reasoning (e.g., grammar) to perform new tasks when finetuned or given suitable in-context examples. In our prior work (details in Chapter 4), we include linguistic experiments as part of our testing suite, illustrating LLMs' compositional ability. Ye et al. [2023]; Berglund et al. [2023]; Dziri et al. [2023] show LLMs will have difficulties solving tasks that require reasoning. Berglund et al. [2023] studies that LLMs trained on "A is B" fail to learn "B is A". In our work (details in Chapter 4), we conduct similar experiments showing LLMs will fail on composite if different steps of logical rules are mixed.

2.3 Efficient Inference of multimodal LLMs (MLLMs)

Multimodal Large Language Models. With the success of LLMs, increasing research focus on extends LLMs from pure text modality to other modalities such as image [Liu et al., 2023b], video [Li et al., 2024], and audio [Latif et al., 2023]. Such development leads to the emergence of MLLMs, often involving combine vision encoders with existing LLMs. Flamingo [Alayrac et al., 2022] inserts gated cross-attention dense blocks between vision encoder and LLMs, align vision and language modality. BLIP2 [Li et al., 2023] introduce Q-former with two-stage pretraining, bridge frozen image encoders and LLMs to enable visual instruction capability. LLaVA [Liu et al., 2023b,a] and MiniGPT-4 [Zhu et al., 2024a] use simple MLP to connect vision embedding space and text token space and show state-of-art performance on a variety of tasks. Our ongoing work (details in Chapter 5) builds on these developments and aims to enable adaptive inference of MLLMs.

Adaptive Inference. Adaptive inference refers to the capability in which the computational complexity of making predictions is dynamically adjusted based on the input data, latency budget, or desired accuracy levels [Han et al., 2021]. Early works focus on the selection of hand-crafted features in multi-stage prediction pipelines [Karayev et al., 2014; Xu et al., 2012; Grubb and Bagnell, 2012]. More recent works have extended these ideas to deep models. For convolutional networks, methods have been developed to downsample the input, skip layers or exist early during inference [Figurnov et al., 2017; Li et al., 2021; Wang et al., 2018b; Bengio et al., 2015; Wu et al., 2018; Hu et al., 2019; Jie et al., 2019; Meng et al., 2020]. For vision transformers, various approaches have been proposed to enhance efficiency, such as selecting different patches of images [Wang et al., 2021; Rao et al., 2021; Pan et al., 2021], and using different attention heads and blocks [Meng et al., 2022]. Similar ideas have also been explored for LLMs, where models selectively process tokens [Raposo et al., 2024] or execute a subset of the operations [Du et al., 2022; Rotem et al., 2023] during inference.

Our ongoing work (details in Chapter 5) builds upon these ideas by dynamically selecting a subset of model components during inference. Unlike existing methods, our approach specifically targets the inference of MLLMs under latency constraints, predicting feasible execution plans tailored for each input while adhering to varying budget budgets.

Efficient Inference for MLLMs. MLLMs face a major challenge in deployment, due to their high computational costs during inference. Several recent works design lightweight model architectures to reduce the costs. Examples include Phi-2 [Javaheripi et al., 2023], Tinygpt-v [Yuan et al., 2023] and LLaVA-ϕ [Zhu et al., 2024b].

Vary-toy [Wei et al., 2024] enhanced performance through specialized vision vocabulary in smaller models. TinyLLaVA [Zhou et al., 2024] and LLaVA-OneVision [Li et al., 2024] learn small-scale models with better training data and pipeline. MoE-LLaVA [Lin et al., 2024] and LLaVA-MoD [Shu et al., 2024] improve efficiency by incorporating mixture-of-experts architectures and parameter sparsity techniques. Another line of research investigates the selection of input tokens to improving efficiency. An input image or video can lead to a large number of vision tokens. To address this, MADTP [Cao et al., 2024] and LLaVA-PruMerge [Shang et al., 2024] introduce token pruning and merging technique to reduce the tokens counts. Pham et al. [Pham et al., 2024] propose to selectively disabling attention mechanisms for visual tokens in MLLMs.

While our ongoing work (details in Chapter 5) also aims to improve the efficiency of MLLMs, it focuses dynamically adjusting an MLLM to fit varying latency budget during inference. This makes our approach orthogonal to prior efforts centered on developing inherently efficient MLLMs. Through our experiments, we will demonstrate that our approach is compatible with smaller models and integrates seamlessly with existing token-pruning techniques *e.g.*, LLaVA-PruMerge [Shang et al., 2024].

Chapter 3

Few-Shot Adaptation via Multitask Finetuning

3.1 Introduction

In this work, we focus on the problem of adapting a pretrained foundation model to a new task with a few labeled samples, where the target task can differ significantly from pretraining and the limited labeled data are insufficient for finetuning. This few-shot learning problem has been a long-standing challenge in machine learning [Wang et al., 2020]. Prior approaches include learning from examples in the context prompt (in-context learning) [Brown et al., 2020], constructing simple classifiers based on the pretrained representation [Zhang et al., 2020], or finetuning the model using text prompts converted from labeled data [Gao et al., 2021a]. An emerging solution involves finetuning a pretrained model on multiple auxiliary tasks pertaining to the target task. This multitask finetuning approach, related to meta learning [Hospedales et al., 2021], has been recently explored in NLP and vision [Murty et al., 2021; Vu et al., 2021; Zhong et al., 2021; Hu et al., 2022c; Chen et al., 2022b; Min et al., 2022b]. For example, latest studies [Sanh et al., 2022; Muennighoff et al., 2023] show that finetuning language models on a large set of tasks enables strong zero-shot generalization on unseen tasks. Nonetheless, the lack of sound theoretical explanations behind these previous approaches raises doubts about their ability to generalize on real-world tasks [Perez et al., 2021].

To bridge the gap, we study the theoretical justification of multitask finetuning. We consider an intermediate step that finetunes a pretrained model with a set of relevant tasks before adapting to a target task. Each of these auxiliary tasks might have a small number of labeled samples, and categories of these samples might not overlap with those on the target task. Our key intuition is that a sufficiently diverse set of relevant tasks can capture similar latent characteristics as the target task, thereby producing meaningful representation and reducing errors in the target task. To this end, we present rigorous theoretical analyses, provide key insight into conditions necessary for successful multitask finetuning, and introduce a novel algorithm for selecting tasks suitable for finetuning.

Our key contributions are three folds. *Theoretically*, we present a framework for analyzing pretraining followed by multitask finetuning. Our analysis (Section 3.3) reveals that with limited labeled data from diverse tasks, finetuning can improve the prediction performance on a downstream task. *Empirically*, we perform extensive experiments on both vision and language tasks (Section 3.4) to verify our theorem. Our results suggest that our theorem successfully predicts the behavior of multitask finetuning across datasets and models. *Practically*, inspired by our theorem, we design *a task selection algorithm* for multitask finetuning. On the Meta-Dataset [Triantafillou et al., 2020], our algorithm shows significantly improved results in comparison to finetuning using all possible tasks.

3.2 Background: Multitask Finetuning for Few-Shot Learning

This section reviews the pretraining of foundation models and adaptation for few-shot learning, and then formalizes the multitask finetuning approach.

Pretraining Foundation Models. We consider three common pretraining methods: contrastive learning, masked language modeling, and supervised pretraining. *Contrastive learning* is widely considered in vision and multi-modal tasks. This approach pretrains a model ϕ from a hypothesis class Φ of foundation models via loss on contrastive pairs generated from data points x. First sample a point x and then apply some transformation to obtain x^+; independently

sample another point x^-. The population contrastive loss is then $\mathcal{L}_{con-pre}(\phi) := \mathbb{E}\left[\ell_u\left(\phi(x)^\top\left(\phi(x^+) - \phi(x^-)\right)\right)\right]$, where the loss function ℓ_u is a non-negative decreasing function. In particular, logistic loss $\ell_u(v) = \log\left(1 + \exp\left(-v\right)\right)$ recovers the typical contrastive loss in most empirical work [Logeswaran and Lee, 2018; Oord et al., 2018; Chen et al., 2020]. *Masked language modeling* is a popular self-supervised learning approach in NLP. It can be regarded as a kind of *supervised pretraining*: the masked word is viewed as the class (see Section 8.2 for more details). In what follows we provide a unified formulation. On top of the representation function ϕ, there is a linear function $f \in \mathcal{F} \subset \left\{\mathbb{R}^d \to \mathbb{R}^K\right\}$ predicting the labels where K is the number of classes. The supervised loss is: $\mathcal{L}_{sup-pre}(\phi) := \min_{f\in\mathcal{F}} \mathbb{E}\left[\ell\left(f \circ \phi(x), y\right)\right]$, where $\ell(\cdot, y)$ is the cross-entropy loss. To simplify the notation, we unify $\mathcal{L}_{pre}(\phi)$ as the pretraining loss.

Adapting Models for Few-shot Learning. A pretrained foundation model ϕ can be used for downstream target tasks $\mathcal{T}$ by learning linear classifiers on ϕ. We focus on binary classification (the general multiclass setting is in Section 8.3). A linear classifier on ϕ is given by $\boldsymbol{w}^\top\phi(x)$ where $\boldsymbol{w} \in \mathbb{R}^d$. The supervised loss of ϕ w.r.t the task $\mathcal{T}$ is then:

$$\mathcal{L}_{sup}(\mathcal{T}, \phi) := \min_{\boldsymbol{w}} \mathop{\mathbb{E}}_{(x,y)\sim\mathcal{D}_\mathcal{T}}\left[\ell\left(\boldsymbol{w}^\top\phi(x), y\right)\right], \tag{3.1}$$

where $\mathcal{D}_\mathcal{T}(x, y)$ is the distribution of data (x, y) in task $\mathcal{T}$. In few-shot learning with novel classes, there are *limited labeled data points* for learning the linear classifier. Further, the target task $\mathcal{T}_0$ may contain *classes different from those in pretraining*. We are interested in obtaining a model ϕ such that $\mathcal{L}_{sup}(\mathcal{T}_0, \phi)$ is small.

Multitask Finetuning. In the challenging setting of few-shot learning, the data in the target task is limited. On the other hand, we can have prior knowledge of the target task characteristics and its associated data patterns, and thus can collect additional data from relevant and accessible sources when available. Such data may cover the patterns in target task and thus can be used as auxiliary tasks to finetune the pretrained model before adaptation to the target task. Here we formalize this idea in a general form and provide analysis in later sections. Formally, suppose we have M auxiliary tasks $\{\mathcal{T}_1, \mathcal{T}_2, \ldots, \mathcal{T}_M\}$, each with m labeled samples $\mathcal{S}_i := \{(x_j^i, y_j^i) : j \in [m]\}$. The finetuning data are $\mathcal{S} := \cup_{i\in[M]}\mathcal{S}_i$. Given a pretrained model $\hat{\phi}$, we further finetune it using the objective:

$$\min_{\phi\in\Phi} \frac{1}{M}\sum_{i=1}^{M} \widehat{\mathcal{L}}_{sup}(\mathcal{T}_i, \phi), \quad \text{where } \widehat{\mathcal{L}}_{sup}(\mathcal{T}_i, \phi) := \min_{\boldsymbol{w}_i\in\mathbb{R}^d} \frac{1}{m}\sum_{j=1}^{m} \ell(\boldsymbol{w}_i^\top\phi(x_j^i), y_j^i). \tag{3.2}$$

This can be done via gradient descent from the initialization $\hat{\phi}$ (see Algorithm 2 in the Appendix). Multitask finetuning is conceptually simple, and broadly applicable to different models and datasets. While its effectiveness has been previously demonstrated [Murty et al., 2021; Vu et al., 2021; Zhong et al., 2021; Hu et al., 2022c; Chen et al., 2022b; Min et al., 2022b; Sanh et al., 2022; Muennighoff et al., 2023], the theoretical justification remains to be fully investigated and understood.

3.3 Theoretical Analysis: Benefit of Multitask Finetuning

To understand the potential benefit of multitask finetuning, we will compare the performance of $\hat{\phi}$ (from pretraining) and ϕ' (from pretraining and multitask finetuning) on a target task $\mathcal{T}_0$. That is, we will compare $\mathcal{L}_{sup}(\mathcal{T}_0, \hat{\phi})$ and $\mathcal{L}_{sup}(\mathcal{T}_0, \phi')$, where $\mathcal{L}_{sup}(\mathcal{T}, \phi)$ is the population supervised loss of ϕ on the task $\mathcal{T}$ defined in Eq. 3.1. For the analysis, we first formalize the data distributions and learning models, then introduce the key notions, and finally present the key theorems.

Data Distributions. Let $\mathcal{X}$ be the input space and $\overline{\mathcal{Z}} \subseteq \mathbb{R}^d$ be the output space of the foundation model. Following Arora et al. [2019], suppose there is a set of latent classes $\mathcal{C}$ with $|\mathcal{C}| = K$, and a distribution η over the classes; each class $y \in \mathcal{C}$ has a distribution $\mathcal{D}(y)$ over inputs x. In pretraining using contrastive learning, the distribution $\mathcal{D}_{\text{con}}(\eta)$ of the contrastive data (x, x^+, x^-) is given by: $(y, y^-) \sim \eta^2$ and $x, x^+ \sim \mathcal{D}(y),\ x^- \sim \mathcal{D}(y^-)$. In masked self-supervised or fully supervised pretraining, (x, y) is generated by $y \sim \eta, x \sim \mathcal{D}(y)$. In a task $\mathcal{T}$ with binary classes $\{y_1, y_2\}$, the data distribution $\mathcal{D}_\mathcal{T}(x, y)$ is by first uniformly drawing $y \in \{y_1, y_2\}$ and then drawing $x \sim \mathcal{D}(y)$. Finally, let ζ denote the conditional distribution of $(y_1, y_2) \sim \eta^2$ conditioned on $y_1 \neq y_2$, and suppose the tasks in finetuning are from ζ. Note that in few-shot learning with novel classes, the target task's classes may not be the same as those in the pretraining. Let $\mathcal{C}_0$ be the set of possible classes in the target task, which may or may not overlap with $\mathcal{C}$.

Learning Models. Recall that Φ is the hypothesis class of foundation models $\phi : \mathcal{X} \to \overline{\mathcal{Z}}$. To gauge the generalization performance, let $\phi^* \in \Phi$ denote the model with the lowest target task loss $\mathcal{L}_{sup}(\mathcal{T}_0, \phi^*)$ and $\phi_\zeta^* \in \Phi$ denote the model with the lowest average supervised loss over the set of auxiliary tasks $\mathcal{L}_{sup}(\phi_\zeta^*) := \mathbb{E}_{\mathcal{T}\sim\zeta}[\mathcal{L}_{sup}(\mathcal{T}, \phi_\zeta^*)]$. Note that if all $\phi \in \Phi$ have high supervised losses, we cannot expect the method to lead to a good generalization performance, and thus we need to calibrate w.r.t. ϕ^* and ϕ_ζ^*. We also need some typical regularity assumptions.

Assumption 3.3.1 (Regularity Assumptions). *$\|\phi\|_2 \le R$ and linear operator $\|\boldsymbol{w}\|_2 \le B$. The loss ℓ_u is bounded in $[0, C]$ and L-Lipschitz. The supervised loss $\mathcal{L}_{sup}(\mathcal{T}, \phi)$ is $\tilde{L}$-Lipschitz with respect to ϕ.*

Diversity and Consistency. Central to our theoretical analysis lies in the definitions of *diversity* in auxiliary tasks used for finetuning and their *consistency* with the target task.

Definition 3.3.2 (Diversity). *The averaged representation difference for two model $\phi, \tilde{\phi}$ on a distribution ζ over tasks is $\bar{d}_\zeta(\phi, \tilde{\phi}) := \mathop{\mathbb{E}}_{\mathcal{T}\sim\zeta}\left[\mathcal{L}_{sup}(\mathcal{T}, \phi) - \mathcal{L}_{sup}(\mathcal{T}, \tilde{\phi})\right] = \mathcal{L}_{sup}(\phi) - \mathcal{L}_{sup}(\tilde{\phi})$. The worst-case representation difference between representations $\phi, \tilde{\phi}$ on the family of classes $\mathcal{C}_0$ is $d_{\mathcal{C}_0}(\phi, \tilde{\phi}) := \sup_{\mathcal{T}_0\subseteq\mathcal{C}_0}\left|\mathcal{L}_{sup}(\mathcal{T}_0, \phi) - \mathcal{L}_{sup}(\mathcal{T}_0, \tilde{\phi})\right|$. We say the model class Φ has ν-diversity (for ζ and $\mathcal{C}_0$) with respect to ϕ^*_ζ, if for any $\phi \in \Phi$, $d_{\mathcal{C}_0}(\phi, \phi^*_\zeta) \le \bar{d}_\zeta(\phi, \phi^*_\zeta)/\nu$.*

Such diversity notion has been proposed and used to derive statistical guarantees (e.g., Tripuraneni et al. [2020]; Zhao et al. [2023]). Intuitively, diversity measures whether the data from ζ covers the characteristics of the target data in $\mathcal{C}_0$, e.g., whether the span of the linear mapping solutions $\boldsymbol{w}$'s for tasks from ζ can properly cover the solutions for tasks from $\mathcal{C}_0$ [Zhao et al., 2023]. Existing work showed that diverse pretraining data will lead to a large diversity parameter ν and can improve the generalization in the target task. Our analysis will show the diversity in finetuning tasks from ζ can benefit the performance of a target task from $\mathcal{C}_0$.

Definition 3.3.3 (Consistency). *We say the model class Φ has κ-consistency (for ζ and $\mathcal{C}_0$) with respect to ϕ^* and ϕ^*_ζ, where $\kappa := \sup_{\mathcal{T}_0\subseteq\mathcal{C}_0}\left[\mathcal{L}_{sup}(\mathcal{T}_0, \phi^*_\zeta) - \mathcal{L}_{sup}(\mathcal{T}_0, \phi^*)\right]$.*

This consistency notion measures the similarity between the data in tasks from ζ and the data in the target task from $\mathcal{C}_0$. Intuitively, when the tasks from ζ are similar to the target task $\mathcal{T}_0$, their solutions ϕ^*_ζ and ϕ^* will be similar to each other, resulting in a small κ. Below we will derive guarantees based on the diversity ν and consistency κ to explain the gain from multitask finetuning.

Key Results. We now present the results for a uniform distribution η, and include the full proof and results for general distributions in Section 8.2 and Section 8.3. Recall that we will compare the performance of $\hat{\phi}$ (the model from pretraining) and ϕ' (the model from pretraining followed by multitask finetuning) on a target task $\mathcal{T}_0$. For $\hat{\phi}$ without multitask finetuning, we have:

Theorem 3.3.4. (No Multitask Finetuning) *Assume Assumption 3.3.1 and that Φ has ν-diversity and κ-consistency with respect to ϕ^* and ϕ^*_ζ. Suppose $\hat{\phi}$ satisfies $\hat{\mathcal{L}}_{pre}(\hat{\phi}) \le \epsilon_0$. Let $\tau := \Pr_{(y_1,y_2)\sim\eta^2}\{y_1 = y_2\}$. Then for any target task $\mathcal{T}_0 \subseteq \mathcal{C}_0$,*

$$\mathcal{L}_{sup}(\mathcal{T}_0, \hat{\phi}) - \mathcal{L}_{sup}(\mathcal{T}_0, \phi^*) \le \frac{1}{\nu}\left[\frac{2\epsilon_0}{1-\tau} - \mathcal{L}_{sup}(\phi^*_\zeta)\right] + \kappa. \tag{3.3}$$

In Theorem 3.3.4, $\widehat{\mathcal{L}}_{pre}(\phi)$ is the empirical loss of $\mathcal{L}_{pre}(\phi)$ with pretraining sample size N. We now consider ϕ' obtained by multitask finetuning. Define the subset of models with pretraining loss smaller than $\tilde{\epsilon}$ as $\Phi(\tilde{\epsilon}) := \left\{\phi \in \Phi : \widehat{\mathcal{L}}_{pre}(\phi) \le \tilde{\epsilon}\right\}$. Recall the Rademacher complexity of Φ on n points is $\mathcal{R}_n(\Phi) := \mathop{\mathbb{E}}_{\{\sigma_j\}_{j=1}^n, \{x_j\}_{j=1}^n}\left[\sup_{\phi\in\Phi}\sum_{j=1}^n \sigma_j\phi(x_j)\right]$.

Theorem 3.3.5 below showing that the target prediction performance of the model ϕ' from multitask finetuning can be significantly better than that of $\hat{\phi}$ without multitask finetuning. In particular, achieves an error reduction $\frac{1}{\nu}\left[(1-\alpha)\frac{2\epsilon_0}{1-\tau}\right]$. The reduction is achieved when multitask finetuning is solved to a small loss ϵ_1 for a small α on sufficiently many finetuning data.

Theorem 3.3.5. (With Multitask Finetuning) *Assume Assumption 3.3.1 and that Φ has ν-diversity and κ-consistency with respect to ϕ^* and ϕ^*_ζ. Suppose for some constant $\alpha \in (0,1)$, we solve Eq. 3.2 with empirical loss lower than $\epsilon_1 = \frac{\alpha}{3}\frac{2\epsilon_0}{1-\tau}$ and obtain ϕ'. For any $\delta > 0$, if for $\tilde{\epsilon} = \widehat{\mathcal{L}}_{pre}(\phi')$,*

$$M \geq \frac{1}{\epsilon_1}\left[4\sqrt{2}\tilde{L}\mathcal{R}_M(\Phi(\tilde{\epsilon})) + \frac{4C^2}{\epsilon_1}\log(\frac{2}{\delta})\right], Mm \geq \frac{1}{\epsilon_1}\left[16LB\mathcal{R}_{Mm}(\Phi(\tilde{\epsilon})) + \frac{4C^2}{\epsilon_1}\log(\frac{2}{\delta})\right],$$

then with probability $1-\delta$, for any target task $\mathcal{T}_0 \subseteq \mathcal{C}_0$,

$$\mathcal{L}_{sup}(\mathcal{T}_0, \phi') - \mathcal{L}_{sup}(\mathcal{T}_0, \phi^*) \leq \frac{1}{\nu}\left[\alpha\frac{2\epsilon_0}{1-\tau} - \mathcal{L}_{sup}(\phi^*_\zeta)\right] + \kappa. \tag{3.4}$$

The requirement is that the number of tasks M and the total number of labeled samples Mm across tasks are sufficiently large. This implies when M is above the threshold, the total size Mm determines the performance, and increasing either M or m while freezing the other can improve the performance. We shall verify these findings in our experiments (Section 3.4.1).

Theorem 3.3.5 also shows the conditions for successful multitask finetuning, in particular, the impact of the diversity and consistency of the finetuning tasks. Besides small finetuning loss on sufficiently many data, a large diversity parameter ν and a small consistency parameter κ will result in a small target error bound. Ideally, data from the finetuning tasks should be similar to those from the target task, but also sufficiently diverse to cover a wide range of patterns that may be encountered in the target task. This inspires us to perform finer-grained analysis of diversity and consistency using a simplified data model (Section 3.3.1), which sheds light on the design of an algorithm to select a subset of finetuning tasks with better performance (Section 3.3.2).

3.3.1 Case Study of Diversity and Consistency

Our main results, rooted in notions of diversity and consistency, state the general conclusion of multitask finetuning on downstream tasks. A key remaining question is how relevant tasks should be selected for multitask finetuning in practice. Our intuition is that this task selection should promote both diversity (encompassing the characteristics of the target task) and consistency (focusing on the relevant patterns in achieving the target task's objective). To illustrate such theoretical concepts and connect them to practical algorithms, we specialize the general conclusion to settings that allow easy interpretation of diversity and consistency. In this section, we provide a toy linear case study and we put the proof and also the analysis of a more general setting in Section 8.4, e.g., more general latent class $\mathcal{C}, \mathcal{C}_0$, more general distribution ζ, input data with noise.

In what follows, we specify the data distributions and function classes under consideration, and present an analysis for this case study. Our goal is to explain the intuition behind diversity and consistency notions: *diversity is about coverage, and consistency is about similarity in the latent feature space*. This can facilitate the design of task selection algorithms.

Linear Data and Tasks. Inspired by classic dictionary learning and recent analysis on representation learning [Wen and Li, 2021; Shi et al., 2023a], we consider the latent class/representation setting where each latent class $z \in \{0,-1,+1\}^d$ is represented as a feature vector. We focus on individual binary classification tasks, where $\mathcal{Y} = \{-1,+1\}$ is the label space. Thus, each task has two latent classes z, z' (denote the task as $\mathcal{T}_{z,z'}$) and we randomly assign -1 and $+1$ to each latent class. Namely, $\mathcal{T}_{z,z'}$ is defined as: $x = \begin{cases} z, & \text{if } y=-1 \\ z', & \text{if } y=+1 \end{cases}$. We show a diagram in Figure 3.1, we denote each task containing two latent classes, namely (z, z'). Each task in diagram can be represented as (T_1 to $T_{z_1,z_1'}$, T_2 to $T_{z_2,z_2'}$). We further assume a balanced class setting in all tasks, i.e., $p(y=-1) = p(y=+1) = \frac{1}{2}$. Now, we define the latent classes seen in multitask finetuning tasks: $\mathcal{C} = \left\{(\underbrace{1,1,\ldots,1,1,-1}_{k_\mathcal{C}},\underbrace{0,\ldots,0}_{d-k_\mathcal{C}})^\top, (\underbrace{1,1,\ldots,1,-1,1}_{k_\mathcal{C}},\underbrace{0,\ldots,0}_{d-k_\mathcal{C}})^\top, \ldots, (\underbrace{-1,1,\ldots,1,1,1}_{k_\mathcal{C}},\underbrace{0,\ldots,0}_{d-k_\mathcal{C}})^\top\right\}$. Note that their feature vectors only encode the first $k_\mathcal{C}$ features, and $|\mathcal{C}| = k_\mathcal{C}$. We let $\mathcal{C}_0 := \{z^{(1)}, z^{(2)}\} \subseteq \{0,-1,+1\}^d$ which is

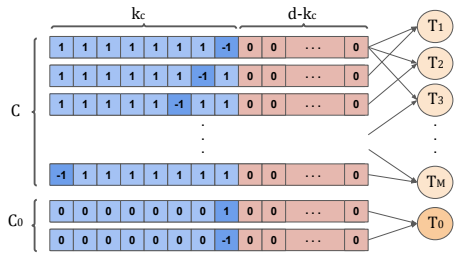

Figure 3.1: Illustration of features in linear data. Blue are the features encoded in $\mathcal{C}$ while red is not.

used for the target task, and assume that $z^{(1)}$ and $z^{(2)}$ only differ in 1 dimension, i.e., the target task can be done using this one particular dimension. Let ζ be a distribution uniformly sampling two different latent classes from $\mathcal{C}$. Then, our data generation pipeline for getting a multitask finetuning task is (1) sample two latent classes $(z, z') \sim \zeta$; (2) assign label $-1, +1$ to two latent classes.

Linear Model and Loss Function. We consider a linear model class with regularity Assumption 3.3.1, i.e., $\Phi = \{\phi \in \mathbb{R}^{d\times d} : \|\phi\|_F \leq 1\}$ and linear head $w \in \mathbb{R}^d$ where $\|w\|_2 \leq 1$. Thus, the final output of the model and linear head is $w^\top \phi x$. We use the loss in Shi et al. [2023a], i.e., $\ell\left(w^\top \phi x, y\right) = -yw^\top \phi x$.

Remark 3.3.1. *Although we have linear data, linear model, and linear loss, $\mathcal{L}_{sup}(\phi)$ is a non-linear function on ϕ as the linear heads are different across tasks, i.e., each task has its own linear head.*

Now we can link our diversity and consistency to features encoded by training or target tasks.

Theorem 3.3.6 (Diversity and Consistency)**.** *If $\mathcal{C}$ encodes the feature in $\mathcal{C}_0$, i.e., the different entry dimension of $z^{(1)}$ and $z^{(2)}$ in $\mathcal{C}_0$ is in the first $k_\mathcal{C}$ dimension, then we have ν is lower bounded by constant $\tilde{c} \geq \frac{2\sqrt{2}-2}{k_\mathcal{C}-1}$ and $\kappa \leq 1 - \sqrt{\frac{1}{k_\mathcal{C}}}$. Otherwise, we have $\nu \to 0$ and $\kappa \geq 1$.*

Theorem 3.3.6 establishes $\tilde{c}$-diversity and κ-consistency in Definition 3.3.2 and Definition 3.3.3. The analysis shows that diversity can be intuitively understood as the coverage of the finetuning tasks on the target task in the latent feature space: If the key feature dimension of the target task is covered by the features encoded by finetuning tasks, then we have lower-bounded diversity ν; if not covered, then the diversity ν tends to 0 (leading to vacuous error bound in Theorem 3.3.5). Also, consistency can be intuitively understood as similarity in the feature space: when $k_\mathcal{C}$ is small, a large fraction of the finetuning tasks are related to the target task, leading to a good consistency (small κ); when $k_\mathcal{C}$ is large, we have less relevant tasks, leading to a worse consistency. Such an intuitive understanding of diversity and consistency will be useful for designing practical task selection algorithms.

3.3.2 Task Selection

Our analysis suggests that out of a pool of candidate tasks, a subset S with good consistency (i.e., small κ) and large diversity (i.e., large ν) will yield better generalization to a target task. To realize this insight, we present a greedy selection approach, which sequentially adds tasks with the best consistency, and stops when there is no significant increase in the diversity of the selected subset. In doing so, our approach avoids enumerating all possible subsets and thus is highly practical.

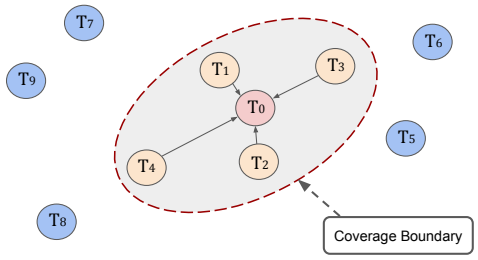

Figure 3.2: Illustration of the similarity and coverage. Target tasks ($\mathcal{T}_0$) with the most similar tasks in yellow and the rest in blue. The ellipsoid spanned by yellow tasks is the coverage for the target task. Adding more tasks in blue to the ellipsoid does not increase the coverage boundary.

A key challenge is to compute the consistency and diversity of the data. While the exact computation deems infeasible, we turn to approximations that capture the key notions of consistency and diversity. We show a simplified diagram for task selection in Figure 3.2. Specifically, given a foundation model ϕ, we assume any task data $\mathcal{T} = \{x_j\}$ follows a Gaussian distribution in the representation space: let $\phi(\mathcal{T}) = \{\phi(x_j)\}$ denote the representation vectors obtained by applying ϕ on the data points in $\mathcal{T}$; compute the sample mean $\mu_\mathcal{T}$ and covariance $C_\mathcal{T}$ for $\phi(\mathcal{T})$, and view it as the Gaussian $\mathcal{N}(\mu_\mathcal{T}, C_\mathcal{T})$. Further, following the intuition shown in the case study, we simplify consistency to similarity: for the target task $\mathcal{T}_0$ and a candidate task $\mathcal{T}_i$, if the cosine similarity

$\text{CosSim}(\mathcal{T}_0, \mathcal{T}_i) := \mu_{\mathcal{T}_0}^\top \mu_{\mathcal{T}_i} / (\|\mu_{\mathcal{T}_0}\|_2 \|\mu_{\mathcal{T}_i}\|_2)$ is large, we view $\mathcal{T}_i$ as consistent with $\mathcal{T}_0$. Next, we simplify diversity to coverage: if a dataset D (as a collection of finetuning tasks) largely "covers" the target data $\mathcal{T}_0$, we view D as diverse for $\mathcal{T}_0$. Regarding the task data as Gaussians, we note that the covariance ellipsoid of D covers the target data $\mu_{\mathcal{T}_0}$ iff $(\mu_D - \mu_{\mathcal{T}_0})^T C_D^{-1} (\mu_D - \mu_{\mathcal{T}_0}) \leq 1$. This inspires us to define the following coverage score as a heuristic for diversity: $\text{coverage}(D; \mathcal{T}_0) := 1/(\mu_D - \mu_{\mathcal{T}_0})^\top C_D^{-1} (\mu_D - \mu_{\mathcal{T}_0})$.

Using these heuristics, we arrive at the following selection algorithm: sort the candidate task in descending order of their cosine similarities to the target data; sequentially add tasks in the sorted order to L until $\text{coverage}(L; \mathcal{T}_0)$ has no significant increase. Algorithm 1 illustrates this key idea.

Algorithm 1 Consistency-Diversity Task Selection

Require: Target task $\mathcal{T}_0$, candidate finetuning tasks: $\{\mathcal{T}_1, \mathcal{T}_2, \ldots, \mathcal{T}_M\}$, model ϕ, threshold p.
1: Compute $\phi(\mathcal{T}_i)$ and $\mu_{\mathcal{T}_i}$ for $i = 0, 1, \ldots, M$.
2: Sort $\mathcal{T}_i$'s in descending order of similarity $(\mathcal{T}_0, \mathcal{T}_i)$. Denote the sorted list as $\{\mathcal{T}_1', \mathcal{T}_2', \ldots, \mathcal{T}_M'\}$.
3: $L \leftarrow \{\mathcal{T}_1'\}$
4: **for** $i = 2, \ldots, M$ **do**
5: If coverage$(L \cup \mathcal{T}_i'; \mathcal{T}_0) \geq (1 + p) \cdot$ coverage$(L; \mathcal{T}_0)$, then $L \leftarrow L \cup \mathcal{T}_i'$; otherwise, break.
6: **end for**
Ensure: selected data L for multitask finetuning.

3.4 Experiments

We now present our main results, organized in three parts. Section 3.4.1 explores how different numbers of finetuning tasks and samples influence the model's performance, offering empirical backing to our theoretical claims. Section 3.4.2 investigates whether our task selection algorithm can select suitable tasks for multitask finetuning. Section 3.4.3 provides a more extensive exploration of the effectiveness of multitask finetuning on various datasets and pretrained models. We defer other results to the appendix. Specifically, Section 8.5.4 shows that better diversity and consistency of finetuning tasks yield improved performance on target tasks under same sample complexity. Section 8.5.4 shows that finetuning tasks satisfying diversity yet without consistency lead to no performance gain even with increased sample complexity. Further, Section 8.6 and Section 8.7 present additional experiments using NLP and vision-language models, respectively.

Experimental Setup. We use four few-shot learning benchmarks: miniImageNet [Vinyals et al., 2016], tieredImageNet [Ren et al., 2018], DomainNet [Peng et al., 2019] and Meta-dataset [Triantafillou et al., 2020]. We use foundation models with different pretraining schemes (MoCo-v3 [Chen et al., 2021a], DINO-v2 [Oquab et al., 2023], and supervised learning with ImageNet [Russakovsky et al., 2015]) and architectures (ResNet [He et al., 2016] and ViT [Dosovitskiy et al., 2021]). We consider few-shot tasks consisting of N classes with K support samples and Q query samples per class (known as N-way K-shot). The goal is to classify the query samples based on the support samples. Tasks used for finetuning are constructed by samples from the training split. Each task is formed by randomly sampling 15 classes, with every class drawing 1 or 5 support samples and 10 query samples. Target tasks are similarly constructed from the test set. We follow [Chen et al., 2021b] for multitask finetuning and target task adaptation. During multitask finetuning, we update all parameters in the model using a nearest centroid classifier, in which all samples are encoded, class centroids are computed, and cosine similarity between a query sample and those centroids are treated as the class logits For adaptation to a target task, we only retain the model encoder and consider a similar nearest centroid classifier. This multitask finetuning protocol applies to all experiments (Sections 3.4.1 to 3.4.3). We provide full experimental set up in Section 8.5.

3.4.1 Verification of Theoretical Analysis

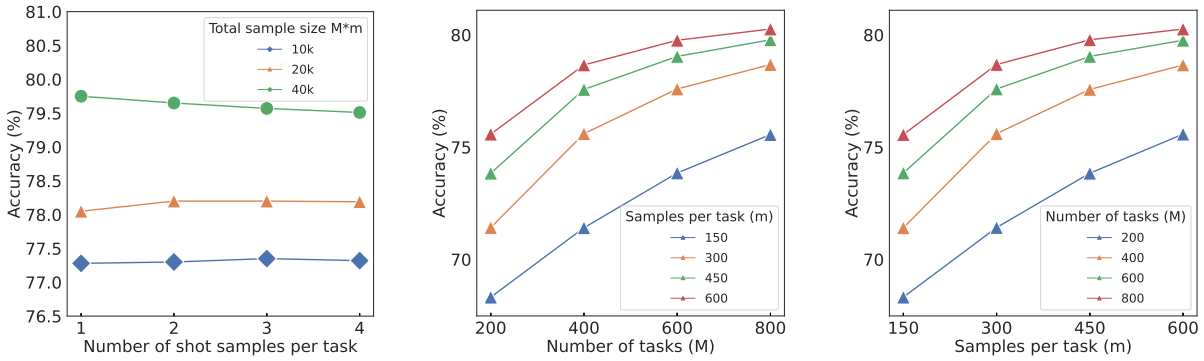

(a) # shots during finetuning. (b) # tasks during finetuning. (c) # samples during finetuning.

Figure 3.3: Results on ViT-B backbone pretrained by MoCo v3. (a) Accuracy v.s. number of shots per finetuning task. Different curves correspond to different total numbers of samples Mm. (b) Accuracy v.s. the number of tasks M. Different curves correspond to different numbers of samples per task m. (c) Accuracy v.s. number of samples per task m. Different curves correspond to different numbers of tasks M.

Pretrained	Selection	INet	Omglot	Acraft	CUB	QDraw	Fungi	Flower	Sign	COCO
CLIP	Random	56.29	65.45	31.31	59.22	36.74	31.03	75.17	33.21	30.16
	No Con.	60.89	72.18	31.50	66.73	40.68	35.17	81.03	37.67	34.28
	No Div.	56.85	73.02	32.53	65.33	40.99	33.10	80.54	34.76	31.24
	Selected	**60.89**	**74.33**	**33.12**	**69.07**	**41.44**	**36.71**	**80.28**	**38.08**	**34.52**
DINOv2	Random	83.05	62.05	36.75	93.75	39.40	52.68	98.57	31.54	47.35
	No Con.	83.21	76.05	36.32	93.96	50.76	53.01	98.58	34.22	47.11
	No Div.	82.82	79.23	36.33	93.96	55.18	52.98	98.59	35.67	44.89
	Selected	**83.21**	**81.74**	**37.01**	**94.10**	**55.39**	**53.37**	**98.65**	**36.46**	**48.08**
MoCo v3	Random	59.66	60.72	18.57	39.80	40.39	32.79	58.42	33.38	32.98
	No Con.	59.80	60.79	18.75	40.41	40.98	32.80	59.55	34.01	33.41
	No Div.	59.57	63.00	18.65	40.36	41.04	32.80	58.67	34.03	33.67
	Selected	**59.80**	**63.17**	**18.80**	**40.74**	**41.49**	**33.02**	**59.64**	**34.31**	**33.86**

Table 3.1: Results evaluating our task selection algorithm on Meta-dataset using ViT-B backbone. No Con.: Ignore consistency. No Div.: Ignore diversity. Random: Ignore both consistency and diversity.

We conduct experiments on the tieredImageNet dataset to confirm the key insight from our theorem — the impact of the number of finetuning tasks (M) and the number of samples per task (m).

Results. We first investigate the influence of the number of shots. We fix the target task as a 1-shot setting but vary the number of shots from 1 to 4 in finetuning, and vary the total sample size $Mm = [10k, 20k, 40k]$. The results in Figure 3.3a show no major change in accuracy with varying the number of shots in finetuning. It is against the common belief that meta-learning like Prototypical Networks [Snell et al., 2017] has to mimic the exact few-shot setting and that a mismatch will hurt the performance. The results also show that rather than the number of shots, the total sample size Mm determines the performance, which is consistent with our theorem. We next investigate the influence of M and m. We vary the number of tasks ($M = [200, 400, 600, 800]$) and samples per task ($m = [150, 300, 450, 600]$) while keeping all tasks have one shot sample. Figure 3.3b shows increasing M with fixed m improves accuracy, and Figure 3.3c shows increasing m with fixed M has similar behavior. Furthermore, different configurations of M and m for the same total sample size Mm have similar performance (e.g., $M = 400, m = 450$ compared to $M = 600, m = 300$ in Figure 3.3b). These again align with our theorem.

3.4.2 Task Selection

Setup. To evaluate our task selection Algorithm 1, we use the Meta-Dataset [Triantafillou et al., 2020]. It contains 10 extensive public image datasets from various domains, each partitioned into train/val/test splits. For each dataset except Describable Textures due to small size, we conduct an experiment, where the test-split of that dataset is used as the target task while the train-split from all the other datasets are used as candidate finetuning tasks. Each experiment follows the experiment protocol in Section 3.4. We performed ablation studies on the task selection algorithm, concentrating on either consistency or diversity, while violating the other. See details in Section 8.5.4.

Results. Table 3.1 compares the results from finetuning with tasks selected by our algorithm to those from finetuning with tasks selected by other methods. Our algorithm consistently attains performance gains. For instance, on Omniglot, our algorithm leads to significant accuracy gains over random selection of 8.9%, 19.7%, and 2.4% with CLIP, DINO v2, and MoCo v3, respectively. Violating consistency or diversity conditions generally result in a reduced performance compared to our approach. These results are well aligned with our expectations and affirm our diversity and consistency conclusions. We provide more ablatioin study on task selection in Table 8.7 in Section 8.5.4. We also apply task selection algorithm on DomainNet in Section 8.5.5. Furthermore, in Section 8.6, we employ our algorithm for NLP models on the GLUE dataset.

3.4.3 Effectiveness of Multitask Finetuning

Setup. We also conduct more extensive experiments on large-scale datasets across various settings to confirm the effectiveness of multitask finetuning. We compare to two baselines: *direct adaptation* where we directly adapt pretrained model encoder on target tasks without any finetuning, and *standard finetuning* where we append encoder with a linear head to map representations to class logits and finetune the whole model. During testing, we removed the linear layer and used the same few-shot testing process with the finetuned encoders. Please refer Table 8.12 in Section 8.5.8 for full results.

			miniImageNet		tieredImageNet		DomainNet	
pretrained	**backbone**	**method**	**1-shot**	**5-shot**	**1-shot**	**5-shot**	**1-shot**	**5-shot**
MoCo v3	ViT-B	Adaptation	75.33 (0.30)	92.78 (0.10)	62.17 (0.36)	83.42 (0.23)	24.84 (0.25)	44.32 (0.29)
		Standard FT	75.38 (0.30)	92.80 (0.10)	62.28 (0.36)	83.49 (0.23)	25.10 (0.25)	44.76 (0.27)
		Ours	**80.62** (0.26)	**93.89** (0.09)	**68.32** (0.35)	**85.49** (0.22)	**32.88** (0.29)	**54.17** (0.30)
	ResNet50	Adaptation	68.80 (0.30)	88.23 (0.13)	55.15 (0.34)	76.00 (0.26)	27.34 (0.27)	47.50 (0.28)
		Standard FT	68.85 (0.30)	88.23 (0.13)	55.23 (0.34)	76.07 (0.26)	27.43 (0.27)	47.65 (0.28)
		Ours	**71.16** (0.29)	**89.31** (0.12)	**58.51** (0.35)	**78.41** (0.25)	**33.53** (0.30)	**55.82** (0.29)
DINO v2	ViT-S	Adaptation	85.90 (0.22)	95.58 (0.08)	74.54 (0.32)	89.20 (0.19)	52.28 (0.39)	72.98 (0.28)
		Standard FT	86.75 (0.22)	95.76 (0.08)	74.84 (0.32)	89.30 (0.19)	54.48 (0.39)	74.50 (0.28)
		Ours	**88.70** (0.22)	**96.08** (0.08)	**77.78** (0.32)	**90.23** (0.18)	**61.57** (0.40)	**77.97** (0.27)
	ViT-B	Adaptation	90.61 (0.19)	97.20 (0.06)	82.33 (0.30)	92.90 (0.16)	61.65 (0.41)	79.34 (0.25)
		Standard FT	91.07 (0.19)	97.32 (0.06)	82.40 (0.30)	93.07 (0.16)	61.84 (0.39)	79.63 (0.25)
		Ours	**92.77** (0.18)	**97.68** (0.06)	**84.74** (0.30)	**93.65** (0.16)	**68.22** (0.40)	**82.62** (0.24)
Supervised pretraining on ImageNet	ViT-B	Adaptation	94.06 (0.15)	97.88 (0.05)	83.82 (0.29)	93.65 (0.13)	28.70 (0.29)	49.70 (0.28)
		Standard FT	95.28 (0.13)	98.33 (0.04)	86.44 (0.27)	94.91 (0.12)	30.93 (0.31)	52.14 (0.29)
		Ours	**96.91** (0.11)	**98.76** (0.04)	**89.97** (0.25)	**95.84** (0.11)	**48.02** (0.38)	**67.25** (0.29)
	ResNet50	Adaptation	81.74 (0.24)	94.08 (0.09)	65.98 (0.34)	84.14 (0.21)	27.32 (0.27)	46.67 (0.28)
		Standard FT	84.10 (0.22)	94.81 (0.09)	74.48 (0.33)	88.35 (0.19)	34.10 (0.31)	55.08 (0.29)
		Ours	**87.61** (0.20)	**95.92** (0.07)	**77.74** (0.32)	**89.77** (0.17)	**39.09** (0.34)	**60.60** (0.29)

Table 3.2: **Results of few-shot image classification.** We report average classification accuracy (%) with 95% confidence intervals on test splits. Adaptation: Direction adaptation without finetuning; Standard FT: Standard finetuning; Ours: Our multitask finetuning; 1-/5-shot: number of labeled images per class in the target task.

Results. Table 3.2 presents the results for various pretraining and finetuning methods, backbones, datasets, and few-shot learning settings. Multitask finetuning consistently outperforms the baselines in different settings. For example, in the most challenging setting of 1-shot on DomainNet, it attains a major gain of 7.1% and 9.3% in accuracy over standard finetuning and direct adaptation, respectively, when considering self-supervised pretraining with DINO v2 and using a Transformer model (ViT-S).

Interestingly, multitask finetuning achieves more significant gains for models pretrained with supervised learning than those pretrained with contrastive learning. For example, on DomainNet, multitask finetuning on supervised pretrained ViT-B achieves a relative gain of 67% and 35% for 1- and 5-shot, respectively. In contrast, multitask finetuning on DINO v2 pretrained ViT-B only shows a relative gain of 10% and 4%. This suggests that models from supervised pretraining might face a larger domain gap than models from DINO v2, and multitask finetuning helps to bridge this gap.

3.5 Conclusions

In this work, we studied the theoretical justification of multitask finetuning for adapting pretrained foundation models to downstream tasks with limited labels. Our analysis shows that, given sufficient sample complexity, finetuning using a diverse set of pertinent tasks can improve the performance on the target task. This claim was examined in our theoretical framework and substantiated by the empirical evidence accumulated throughout our study. Built on this theoretical insight, we further proposed a practical algorithm for selecting tasks for multitask finetuning, leading to significantly improved results when compared to using all possible tasks.

This work directly addresses the first challenge outlined in our thesis: efficiently adapting foundation models with limited labeled data. By providing theoretical foundations and practical algorithms for multitask finetuning, we contribute to transforming generalist models into task-specific experts more efficiently. These insights lay the groundwork for our ongoing investigations into model adaptation mechanisms, particularly in understanding how knowledge transfer occurs across tasks and how we can leverage this understanding to develop more effective adaptation techniques.

Chapter 4

Understanding Compositional Abilities

4.1 Introduction

While our theoretical analysis of multitask finetuning provides insights into how foundation models adapt to new tasks, it raises important questions about these models' fundamental reasoning capabilities. Particularly, understanding how these models combine knowledge from different tasks leads us to examine their compositional abilities.

LLMs have revolutionized the natural language processing (NLP) and general AI community. Recent advances have shown success in various fields. As model scale increases, larger models exhibit new behavior known as emergence ability. One remarkable emergence is the in-context learning ability (ICL) [Brown et al., 2020], where a model can solve new tasks given only a few examples as input, without any parameter updates. However, despite recent success, how LLMs solve complex reasoning tasks, particularly not seen in pre-training, remains an open question and largely lacks understanding.

In this paper, we focus on the problem of how LLMs tackle composite tasks that incorporate multiple simple tasks. Specifically, we investigate whether a model trained and in-context learned on individual tasks can effectively integrate these skills to tackle combined challenges, which are intuitive and simple for humans. For instance, in Figure 4.1, if a human is given examples where words following an asterisk (*) will be capitalized and words surrounded by parenthesis will be permuted, one can also understand words following an asterisk (*) surrounded by parenthesis will be capitalized and permuted simultaneously. This basic generalization seems trivial, yet we observe that LLMs fail to generalize in this way.

Compositional ability is an active problem in the AI community and is crucial for advancing Artificial General Intelligence (AGI). Recent studies have made significant contributions to the understanding of this area. Dziri et al. [2023] formulate compositional tasks as computation graphs to quantify each task's complexity level. Power et al. [2022]

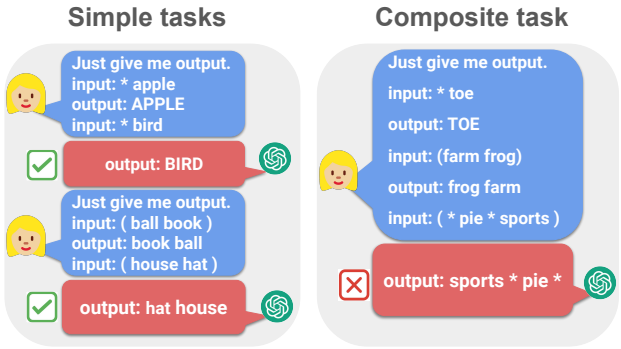

Figure 4.1: Inconsistent performance in GPT-4. Consider two simple tasks: If a word is followed by an asterisk (*), capitalize the letter. If two words are surrounded by parentheses, swap the positions. GPT-4 correctly solves two simple tasks based on demonstrations (left). The composite tasks have test inputs with both asterisk (*) and parenthesis. The correct answer should be *output: SPORTS PIE*. However, GPT-4 fails to solve the composite tasks (right). The same failure was observed in Claude 3.

show that models may develop generalization capabilities when trained extensively, beyond the point of overfitting, highlighting a phenomenon known as "grokking". An et al. [2023b] examines how LLMs acquire abstract reasoning and achieve compositional generalization in a linguistic context through ICL by testing LLMs on tasks that involve translating a formal language with a custom grammar. Although these studies offer insight, how LLMs compose tasks together is still not fully understood, especially in the ICL setting. Moreover, the absence of a solid theoretical framework in these discussions needs to be investigated concerning the underlying mechanisms of such behaviors.

Inspired by these seminal works, we further evaluate LLMs on a series of compositional tasks through ICL. The models were presented with examples of simple tasks and then asked to tackle composite tasks that they had not encountered during pretraining or in-context learning. We observe various behaviors: (1) for some composite tasks, the models showed a reasonable level of compositional skill, a capability that improved with larger model sizes; (2) for more complex composite tasks requiring sequential reasoning, the model struggle, and increasing the model size typically did not lead to better performance.

Our key intuition is that if the simple tasks that form a composite task can be easily separated into subtasks based on the inputs (e.g., performed separately on different parts of the input sentence), the model is more likely to complete such a composite task successfully (we call it "a separable composite task"). The performance of the model depends on how it connects and uses the information given for each part of the task. To clarify this insight, we present theoretical analyses in a simplified setting and provide key insights into conditions needed for success in such separable composite tasks.

Our contributions are twofold. *Empirically*, we introduce a variety of composite tasks from both the linguistic and logical domains to explore how the nature of these tasks influences the compositional performance of LLMs through ICL. *Theoretically*, we provide analysis on a simple yet insightful model: a one-layer single-head linear self-attention network [Von Oswald et al., 2023; Akyürek et al., 2023; Mahankali et al., 2023; Zhang et al., 2023b]. This framework allows us to demonstrate a clear separation in input embedding, effectively breaking down composite tasks into simpler components. We delve into the scaling of language models by examining the structure of the key and query matrices in the attention mechanism, arguing that larger models with a more complex internal structure exhibit enhanced performance on individual tasks, thereby improving their overall compositional capabilities on such separable tasks.

4.2 Warm-up: A Failure Case for Composition

Our goal is to understand the behavior of LLMs on compositional reasoning tasks. As a warm-up, we evaluate the **Capitalization & Swap** tasks (Figure 4.1) on different models. Recall the tasks: given words of common objects, ***** represents the operation of capitalizing the letters, **()** represents swapping the positions of the two words. We consider the standard in-context learning setting, which concatenates input-output examples $K = 10$ and one test input as the prompt for LLM. We perform experiments across various LLM families, e.g., Llama families [Touvron et al., 2023a] and GPTs [Radford et al., 2019; Black et al., 2021], see model details in Section 9.1.

Evaluation settings. To make thorough evaluations, we consider four settings: (1) capital: only on the capitalization task; (2) swap: only on swap; (3) composite: in-context examples are from simple tasks while the test input is about the composite task; (4) composite in-context: in-context examples and the test input are all drawn from the composite task. The composite in-context setting reduces the evaluation to another simple task, not requiring the model to composite the simple task ability but directly learning from the in-context examples. It serves as the gold standard performance for the composite task. See Table 4.1 for illustration.

	Composite	**Composite in-context**
Prompt	*input: * apple* *output: APPLE* *input: (farm frog)* *output: frog farm* *input: (* bell * ford)*	*input: (* good * zebra)* *output: ZEBRA GOOD* *input: (* bicycle * add)*
Truth	*output: FORD BELL*	*output: ADD BICYCLE*

Table 4.1: Examples of two settings on composite tasks. Composite: in-context examples are about simple tasks, while the test input is about the composite task. Composite in-context: both in-context examples and the test input are about the composite task.

Results. In Figure 4.2, somewhat surprisingly, we observe that LLMs cannot solve the composite task, although they perform well on simple tasks. There is a significant gap between the performance in these settings. Models in Llama families can solve capital and swap with nearly $\sim$90% accuracy but only achieve around 20% or below on the composite task. We also observe that composite in-context examples will significantly improve the performance: The accuracy of Llama families can go up to match the simple task accuracy. These observations show that *the models fail to compose the knowledge from the simple tasks, although they do have the representation*

power to solve the composite task (which can only be exploited when provided composite in-context examples) and *scaling up may not help*.

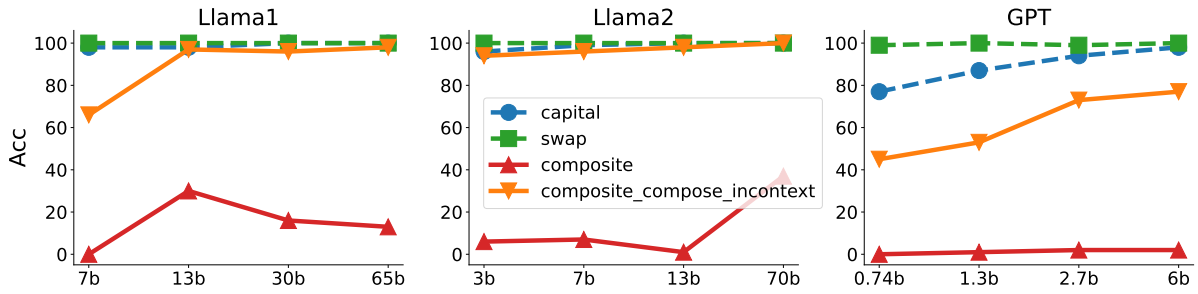

Figure 4.2: The exact match accuracy (y-axis) vs the model scale (x-axis, "b" stands for billion) for **Capitalization & Swap** tasks (example in Figure 4.1). Line *capital*: performance on the simple task of capitalization; *swap*: on the simple task of swap; *composite*: in-context examples are from simple tasks while test input from the composite task. *composite incontext*: in-context examples and test input are all from the composite task (example in Table 4.1).

4.3 Variability of Compositional Performance

The experiment on Capitalization & Swap shows failure cases while existing studies reported some successful composite abilities [Levy et al., 2022; An et al., 2023b]. This observation suggests a more refined perspective: LLMs exhibit variable compositional abilities, excelling in certain composite tasks while struggling in others. This section expands our exploration to additional composite tasks to further examine and understand this variability.

We introduce more composite tasks, including linguistic and logical challenges, wrapped as a testing suite. Similar to the Capitalization & Swap experiment, we design composite tasks that compose two simple tasks and evaluate the model in four settings: the two simple tasks, the composite setting, and the composite in-context setting (Table 4.1 show examples for the latter two). We consider two kinds of task: logical rules and linguistic translation. We first choose two simple tasks and compose them to construct a composite task.

To address concerns about data leakage and the possibility that models encounter similar tasks during pretraining, we opt for synthetic data in this work. While it is challenging to guarantee that test data has never been seen during pretraining, we take significant steps to mitigate this risk. Specifically, we construct our compositional test data using a unique syntax and mapping mechanism. This approach substantially shifts the data distribution away from existing web-scale data, making it highly improbable that our test data has been encountered during pretraining. By doing so, we aim to create novel composite tasks that comprehensively evaluate the models' compositional abilities.

Section 4.3.1 investigates logical tasks and Section 4.3.2 investigates translation tasks.

We perform experiments to answer the following questions: (**Q1**) How do LLMs perform in various tasks, where models might perform well in some scenarios while failing in others? (**Q2**) Does scaling up the model help in general? (**Q3**) Is the variability in performance relevant to the nature of tasks? Our experiments provide the following answers: (**A1**) A pattern of variable performance is observable across a range of composite tasks. (**A2**) Scaling-up helps when the model exhibits compositional ability for certain tasks but may not help when the model initially struggles. (**A3**) In tasks that involve processing inputs from varied segments or perspectives, especially simpler ones, the model tends to demonstrate compositional capabilities.

4.3.1 Composite Logical Rules

We enhance our suite of logical tasks by introducing a series of straightforward tasks that process either simple words or numerical values, with the output being a specific functional transformation of the input. These tasks are detailed in Table 4.2.

Composite tasks are created by merging two simple tasks. We conceptualize simple tasks as functions, $f(\cdot)$ and $g(\cdot)$ that map inputs to their respective outputs. We identify two distinct approaches to creating composite tasks: **(1) Compose by parts**: For inputs x, y, the result is $f(x), g(y)$. One example is **(A) + (F)** in Table 4.3. If a numerical number is given, it will increment by one; if the word is given, the letters will be capitalized; if both are given, perform both operations. **(2) Compose by steps**: Given input x, the result is $f(g(x))$. One example is **(A) + (B)** in Table 4.3. We use

Tasks	Task	Input	Output
Words	(A) Capitalization	apple	APPLE
	(B) Swap	bell ford	ford bell
	(C) Two Sum	twenty @ eleven	thirty-one
	(D) Past Tense	pay	paid
	(E) Opposite	Above	Below
Numerical	(F) Plus One	435	436
	(G) Modular	15 @ 6	3
	(H) Two Sum Plus One	12 # 5	18

Table 4.2: This table contains a collection of simple logical tasks. The *Words* category encompasses tasks that modify words at the character or structural level. The *Numerical* category is devoted to tasks that involve arithmetic computations performed on numbers.

Tasks	Simple Task	Simple Task	Composite
(A) + (B)	input: * apple output: APPLE	input: (farm frog) output: frog farm	input: (* bell * ford) output: FORD BELL
(A) + (F)	input: 435 output: 436	input: cow output: COW	input: 684 cat output: 685 CAT

Table 4.3: Examples of the two logical composite tasks. Full examples can be found in Section 9.1.

customized symbols as function mapping for composing two simple tasks. Examples are in Figure 4.1 and Table 4.3. Following existing work, we use exact match accuracy to evaluate the performance since the output for these tasks is usually simple and short.

Results. We provide our main results on composite tasks in Table 4.4. For the composed by parts tasks **(A) + (F)** and **(D) + (F)**, the models show strong compositional ability: the composite accuracy is high, improves with increasing scale, and eventually reaches similar performance as the "gold standard" composite in-context setting, as highlighted in red numbers. We refer to these tasks as "separable composite tasks", which are relatively easy for the model to solve. On the compose-by-step tasks, we observe the models have various performances. For composite tasks with sequential reasoning steps, the models exhibit various performances. For tasks involving capitalization **(A)** or swap **(B)**, the model has poor performance on a small scale (7b or lower) but has increased performance in increased model scale, such as 44% accuracy in **(A) + (C)** and 66% accuracy in **(B) + (D)**. One exception is Llama1-65b, which has lower accuracy than a smaller-scale model. We conjecture it is due to some unknown inductive bias during the pretraining. On composite steps tasks involving the arithmetic calculation of numerical numbers **(G) + (H)**, the model has the worst performance, and increasing the model scale does not provide benefits. A key observation is that compose-by-part tasks are separable compositions where the input can be broken down into two distinct segments. Such tasks are typically straightforward for a model to address. In all experiments, providing composed examples as in-context demonstrations will help the model understand and solve the composite tasks well, such as **Com. in-context** rows in all task combinations. We conclude that models fail to compose mechanisms of two simple tasks together; however, given composite examples, models can learn the composed mechanism efficiently. We also experimented with prompt demonstrations and found instructions provide no direct results; see more experimental details in Section 9.1.2. See more experimental results (including Llama3 [Meta, 2024]) and visualizations in Section 9.1.3.

4.3.2 Composite Linguistic Translation

Inspired by previous work in compositional generalization [An et al., 2023b; Levy et al., 2022; An et al., 2023a; Kim and Linzen, 2020], here we design our composite tasks by formal language translation tasks.

Our translation tasks are mainly derived from semantic parsing task COGS [Kim and Linzen, 2020] and compositional generalization task COFE An et al. [2023b]. These two datasets contain input as natural English sentences and output as a chain-ruled sentence following a customized grammar (see details in Section 9.2). We construct two composite

	Tasks	Mistral 7B	Mistral 8x7B	Llama2 7B	Llama2 13B	Llama2 70B	Llama1 7B	Llama1 13B	Llama1 30B	Llama1 65B
(A) + (B)	Capitalization	99	98	99	100	100	98	98	100	100
	swap	100	100	100	100	100	100	100	100	100
	Compose	16	42	7	1	37	0	30	16	13
	Com. in-context	95	96	96	98	100	66	97	96	98
(A) + (C)	twoSum	71	100	72	93	99	62	56	98	99
	Capitalization	98	99	100	95	99	97	98	99	99
	Compose	8	19	3	23	44	3	3	31	2
	Com. in-context	31	65	52	77	100	9	22	93	69
(A) + (F)	Capitalization	97	99	98	77	99	84	96	99	98
	PlusOne	100	99	100	100	100	100	100	100	100
	Compose	92	96	74	69	97	57	60	69	99
	Com. in-context	99	98	99	100	100	99	99	100	100
(B) + (D)	Swap	100	100	100	100	100	100	100	100	100
	Past Tense	97	99	97	100	99	97	98	100	100
	Compose	6	12	0	1	62	57	34	46	5
	Com. in-context	92	98	86	95	98	86	95	89	94
(B) + (E)	Swap	100	100	100	100	100	100	100	100	100
	Opposite	61	62	58	68	65	51	58	64	63
	Compose	0	0	0	0	0	0	0	0	0
	Com. in-context	35	32	12	37	37	0	9	7	9
(D) + (F)	Past Tense	100	100	98	100	100	100	100	100	100
	Plus One	100	100	100	100	100	99	100	100	100
	Compose	71	46	32	80	80	40	44	14	74
	Com. in-context	98	100	98	99	100	95	96	98	100
(G) + (H)	Modular	25	22	5	23	43	9	16	29	29
	twoSumPlus	38	42	3	77	90	14	10	40	87
	Compose	4	5	0	1	1	0	0	0	5
	Com. in-context	4	8	13	13	12	11	13	7	12

Table 4.4: Results are evaluated composite tasks on various models. The accuracy is in %.

tasks centered on compositional generalization utilizing the training datasets to create in-context examples. See details in Section 9.2.

We use the word error rate (WER) as the metric. It measures the minimum number of editing operations (deletion, insertion, and substitution) required to transform one sentence into another and is common for speech recognition or machine translation evaluations.

(T1) Phrase Recombination with Longer Chain. COFE proposed two compositional generalization tasks (Figure 2 in An et al. [2023b]). *Phrase Recombination*: integrate a prepositional phrase (e.g., "A in B") into a specific grammatical role (e.g., "subject", "object"); *Longer Chain*: Extend the tail of the logical form in sentences. We see them as simple tasks, and merge them to form a composite task: substitute the sentence subject in the Longer Chain task with a prepositional phrase from the Phrase Recombination task. Details and examples are in Table 9.5 of Section 9.2.

(T2) Passive to Active and Object to Subject Transformation. We consider two tasks from Kim and Linzen [2020]. *Passive to Active*: Transitioning sentences from passive to active voice. *Object to Subject*: Changing the same object (a common noun) from objective to subjective. They are merged to form our composite task, where both transformations are applied simultaneously to the input sentence. Details and examples are in Table 9.4 of Section 9.2.

Results. Figure 4.3 shows that LLMs can handle these composite tasks. The WER on the composite task is decent and improves with increasing model scale, particularly in Llamma2 models. These confirm the composite abilities of the models in these tasks.

Here, we notice that both composite tasks are separable composite tasks. If we break down these sentences into sub-sentences and phrases, the simple task operations occur in different parts or perspectives of the input sentences. So, the results here provide further support for composite abilities on separable composite tasks, where simple tasks that form the composite task are related to inputs from different parts or perspectives.

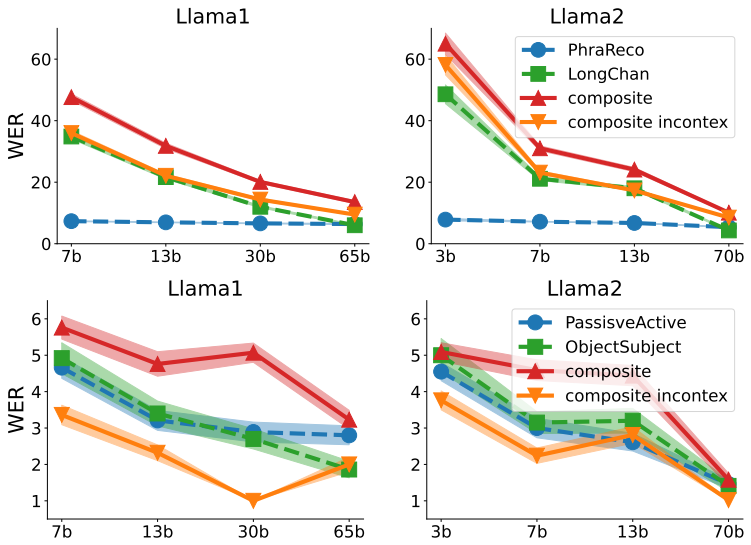

Figure 4.3: The word error rate (WER) vs the model scale on composite linguistic translation tasks. Dashed lines: simple tasks. Solid lines: composite tasks. Rows: **(T1)** Phrase Recombination with Longer Chain; **(T2)** Passive to Active and Object to Subject Transformation. Columns: different models. Lines: performance in different evaluation settings, e.g., the two simple tasks, the composite setting, and the composite in-context setting (examples are shown in Section 9.2).

We also observed the LLM exhibits better compositional ability on linguistic tasks than on logical tasks. We conclude natural language inputs can indeed help language models understand concepts better than special symbols or code. Natural language provides a richer context, which aligns better with how these models are trained on large text corpora. In contrast, logical and numerical tasks often rely on more rigid structures, which makes it harder for models to generalize without explicit training on such patterns.

Discussion. We observe the capability of models to handle composite tasks is significantly influenced by the task characteristics. If composite tasks contain simple tasks related to different parts or perspectives of the input, the model will tackle the composite tasks well.

One natural explanation is that the model processes the input in some hidden embedding space and decomposes the embedding of the input into different "regions". Here, each region is dedicated to specific types of information and thus related to different tasks, such as word-level modifications, arithmetic calculations, mapping mechanisms, semantic categorization, linguistic acceptability, or sentiment analysis. Then, suppose the two simple tasks correspond to two different task types that relate to separate regions of the embedding. In that case, the model can effectively manage the composite task by addressing each simple task operation within its corresponding region. As the model scales, its ability to handle individual tasks improves, leading to enhanced performance on composite tasks in such scenarios. For separable composite tasks, the inputs are divided into distinct regions and also reflected in embeddings, resulting in the model's high performance. However, when the simple tasks are not separable (e.g., requiring sequential steps in reasoning), their information mixes together, complicating the model's ability to discern and process them distinctly. Such overlap often leads to the model's inability to solve the composite task. This intuition is formalized in the following sections in a stylized theoretical setting.

4.4 Theoretical Analysis

4.4.1 Problem Setup

Despite the complex nature of non-linearity in transformers in LLMs, we note it is useful to appeal to the simple case of linear models to see if there are parallel insights that can help us better understand the phenomenon. In this section, we analyze a linear attention module and aim to provide rigorous proof about why LLMs can achieve compositional ability in some simple cases that could shed light on the more intricate behaviors observed in LLMs.

In-context learning. We follow existing work [Akyürek et al., 2023; Garg et al., 2022; Mahankali et al., 2023] with slight generalization to K simple tasks. A labeled example is denoted as (x, y) where $x \in \mathbb{R}^d, y \in \mathbb{R}^K$. In a simple task $k \in [K]$, y has only one non-zero entry $y^{(k)}$. In a composite task, y can have non-zero entries in dimensions corresponding to the combined simple tasks. The model takes a prompt $(x_1, y_1, \ldots, x_N, y_N, x_q)$ as input, which contains N in-context examples (x_i, y_i)'s and a query x_q, and aims to predict $\hat{y}_q$ close to the true label y_q for x_q. The prompt is usually stacked into an embedding matrix: $E := \begin{pmatrix} x_1 & x_2 & \ldots & x_N & x_q \\ y_1 & y_2 & \ldots & y_N & 0 \end{pmatrix} \in \mathbb{R}^{d_e \times (N+1)}$ where $d_e = d + K$. In in-context learning, we first pretrain the model using training prompts and then evaluate the model with evaluation prompts; see details below.

Pretraining procedure. We have B training data indexed by τ, each containing an input prompt $(x_{\tau,1}, y_{\tau,1}, \ldots, x_{\tau,N}, y_{\tau,N}, x_{\tau,q})$ and a corresponding true label $y_{\tau,q}$. Consider the following empirical loss: $\widehat{L}(\theta) = \sum_{k=1}^K \widehat{L}_k(\theta) = \frac{1}{2B} \sum_{\tau=1}^B \|\widehat{y}_{\tau,q} - y_{\tau,q}\|^2$ and the population loss (i.e., $B \to \infty$): $L(\theta) = \frac{1}{2}\mathbb{E}_{x_{\tau,1}, y_{\tau,1}, \cdots, x_{\tau,N}, y_{\tau,N}, x_{\tau,q}} \left[(\widehat{y}_{\tau,q} - y_{\tau,q})^2 \right]$.

Evaluation procedure. We now detail how to evaluate the model on downstream *composite* tasks. We consider the downstream classification task to be a multi-class classification problem, where the output label is a K-dimensional vector, and each entry corresponds to a simple binary classification task. For any given simple task k, the binary classification label is given by $\text{sgn}(y_q^{(k)})$, where sgn is the sign function. Similarly, our prediction is $\widetilde{y}_q^{(k)} = \text{sgn}\left(\widehat{y}_q^{(k)}\right)$. The accuracy of a composite task is defined as $\text{Acc}_\theta(x_1, \ldots, y_N, x_q) = \frac{1}{K} \sum_{k=1}^K \mathbb{1}\left(\text{sgn}\left(\widehat{y}_q^{(k)}\right) = \text{sgn}(y_q^{(k)})\right)$. We denote it as $\text{Acc}_\theta(\{x_i, y_i\}_{i=1}^N)$. Here we denote the model performance on each task as separate dimension, (e.g.letter capitalization, numbers increment), and the performance of composite tasks as the aggregation of multiple dimensions.

Data. Assume $x \overset{\text{i.i.d.}}{\sim} \mathcal{N}(0, \Lambda)$, where $\Lambda \in \mathbb{R}^{d \times d}$ is the covariance matrix. Assume $y = Wx$, where $W \in \mathbb{R}^{K \times d}$. For any simple task $k \in [K]$, its label is the k-th entry of y, which is $y^{(k)} = \langle w^{(k)}, x \rangle$, where $w^{(k)}$ is the k-th row of W. We assume each task weight $w^{(k)} \overset{\text{i.i.d.}}{\sim} \mathcal{N}(0, I_d)$.

Linear self-attention networks. These networks are widely studied [Von Oswald et al., 2023; Akyürek et al., 2023; Garg et al., 2022; Zhang et al., 2023b; Shi et al., 2023d]. Following them, we consider the following linear self-attention network with parameters $\theta = (W^{PV}, W^{KQ})$: $f_{\text{LSA},\theta}(E) = E + W^{PV} E \cdot \frac{E^\top W^{KQ} E}{N}$. The prediction of the model for x_q is $\hat{y}_q = [f_{\text{LSA},\theta}(E)]_{(d+1):(d+K),N+1}$, the bottom rightmost sub-vector of $f_{\text{LSA},\theta}(E)$ with length K.

Compositional ability. We now provide a formal definition about *compositional ability* of an LLM on composite tasks.

Definition 4.4.1 (Compositional Ability)**.** *Consider a composite task $\mathcal{T}$ that combines two simple tasks k and g. Let $\mathcal{S}_k$ denote N labeled examples from task k, and similarly for $\mathcal{S}_g$. Given an x_q from composite task $\mathcal{T}$, we say that the model has compositional ability on $\mathcal{T}$ if the model has higher accuracy using in-context examples from $\mathcal{S}_k \cup \mathcal{S}_g$ than from either single one, i.e.* $\max\{Acc_\theta(\mathcal{S}_k), Acc_\theta(\mathcal{S}_g)\} \leq Acc_\theta(\mathcal{S}_k \cup \mathcal{S}_g)$.

4.4.2 Theoretical Results

In this section, we present our theoretical results. We explain the observation in empirical results through the lens of confined supports in input embeddings corresponding to separate subspaces (modeling separable composition). We provide theoretical justification showing that separable composite task composite tasks whose inputs are composed by components adhere to certain conditions where models exhibit satisfactory performance. Models will fail when such conditions are violated. We first introduce the basic setup and definitions.

Disjoint subspaces of simple tasks. Recall that x lies in a d-dimensional space where each dimension represents a different characteristic. A simple task may depend only on a subset of these dimensions since its label only depends on a few features. Let $\mathbb{S} = [d]$ represent the dimensions of x. For a task k, the output $y^{(k)} = \langle w_k, x \rangle$ depends on a subset of dimensions in x. Denote this subset by $\mathbb{K} \subseteq \mathbb{S}$ and call it the active index set for task k.

In the following, we always assume that the K tasks have disjoint subspaces: for any two tasks $k \neq g$, their active index sets $\mathbb{K}$, and $\mathbb{G}$ are disjoint, i.e., $\mathbb{K} \cap \mathbb{G} = \varnothing$. In practice, the dimensions within $\mathbb{K}$ could be associated with numerical arithmetic operations, while those in $\mathbb{G}$ might pertain to semantic analysis. This illustrates the model's approach to address these tasks in their respective subspaces.

We now introduce a mild assumption regarding the distribution of input embeddings.

Assumption 4.4.2. *Given two disjoint subspaces $\mathbb{K}$ and $\mathbb{G}$, the covariance matrix Λ of the input distribution can be segmented into block matrices $\Lambda_{\mathbb{K}\mathbb{K}}, \Lambda_{\mathbb{K}\mathbb{G}}, \Lambda_{\mathbb{G}\mathbb{K}}$, and $\Lambda_{\mathbb{G}\mathbb{G}}$, then we assume $\sigma_{max}(\Lambda_{\mathbb{K}\mathbb{G}}) = \sigma_{max}(\Lambda_{\mathbb{G}\mathbb{K}}) \leq \epsilon$ for constant ϵ, where $\sigma(\cdot)$ denote the singular value of matrix.*

Assumption 4.4.2 implies that for two separate simple tasks, each associated with its respective feature subspace $\mathbb{K}$ and $\mathbb{G}$, the covariance between these two sets of features is bounded by a constant value. This is a natural assumption when inputs of composite tasks can be decomposed into parts. Suppose we have input embeddings from two tasks: arithmetic computations and semantic analysis. This assumption suggests that the feature subspaces of the input embeddings for two tasks are almost independent.

We now define confined support, which means that each task's input embedding only has support within its feature subspace.

Definition 4.4.3 (Confined Support)**.** *We say a task has confined support if the input x only has larger singular values within its active index set. The norm of entries outside the active index set is bounded by a small constant δ.*

This definition shows that each simple task only has large values within its corresponding subsets of dimensions of input embeddings. For example, let $\mathbb{K}$ represent the first d_1 dimensions of an input vector x, and $\mathbb{G}$ account for the remaining d_2 dimensions, with the total dimension being $d = d_1 + d_2$. The examples from task k will have input as $x = (x_1, x_{\delta_1})$ where $x_1 \in \mathbb{R}^{d_1}, x_{\delta_1} \in \mathbb{R}^{d_2}, \|x_{\delta_1}\| \leq \delta$. Similarly, the examples from task g will have inputs as $x = (x_{\delta_2}, x_2)$.

We now present our results of the compositional ability under a confined support of x.

Theorem 4.4.4. *Consider distinct tasks k and g with corresponding examples $\mathcal{S}_k, \mathcal{S}_g$. If two tasks have confined support, and Assumption 4.4.2 is true, then with high probability, the model has the compositional ability as defined in Definition 4.4.1. Moreover,*

$$Acc_\theta(\mathcal{S}_k) + Acc_\theta(\mathcal{S}_g) \leq Acc_\theta(\mathcal{S}_{k\cup g}).$$

Theorem 4.4.4 shows the compositional ability of LLMs to handle composite tasks that integrate two simple tasks, which have confined support in their own feature subspace.

An illustrative case involves the tasks of Capitalization **(A)** & Plus One **(F)** and Past Tense **(D)** & Plus One **(F)**, as depicted in Table 4.4. These two simple tasks involve word-level modification and arithmetic operation on separate parts of the input. Due to this separation, each task correlates with a specific segment of the input embedding. Therefore, it is observed that these tasks possess confined supports.

We further provide theory illustrating the **necessity of the confined supports**, we demonstrate that when the confined support is violated, simple tasks begin to show variations (indicated by large singular values) across the entire feature subspace of the input embedding. For instance, the composite task of Capitalization (A) & Swap (B), which involves mixed steps in reasoning as shown in Figure 4.2, shows poor performance of LLMs given both simple tasks' examples as in-context demonstrations. Another example is Modular (G) & Two Sum Plus (H) as shown in the last row of Table 4.4, where both simple tasks involve multisteps arithmetic operation. These two tasks share the same embedding space support, mixing their variations and causing the model to be unable to effectively address the composite tasks that integrate them. We further substantiate this observation with Section 4.4.2, which establishes that when two tasks share overlapping support in the embedding space, a scenario can arise where the model fails to demonstrate compositional ability.

If two tasks do not have confined support, there exists one setting in which we have

$$\text{Acc}_\theta(\mathcal{S}_k) = \text{Acc}_\theta(\mathcal{S}_g) = \text{Acc}_\theta(\mathcal{S}_{k\cup g}).$$

Section 4.4.2 demonstrates that a model's failure to solve tasks with mixed steps reasoning, which contains overlapping input embedding spaces, thereby diminishing the model's ability to solve them when presented together.

We also show the **scaling effect**: if simple tasks have confined support, the compositional ability of language models will increase as the model scale increases in Theorem 9.3.1 in Section 9.3.1. We demonstrate this by showing that the model's accuracy on each simple task improves with a larger model scale. We finally provide a **case study** on confined support for illustration in Section 9.3.2. We defer the full proof in Section 9.4.

4.5 Conclusion

In this work, we presented a distinct pattern in LLMs' behaviors when tackling composite tasks. We observed that if the composite task can be separated into two simple tasks whose inputs are from distinct perspectives, the models exhibit

decent compositional ability. Otherwise, LLMs will struggle, and scaling up the model size may not offer improvement. We illustrated this behavior across a variety of logical and linguistic challenges. We extended our discussion to the role of input embeddings in affecting model performance, providing a theoretical backup that connects the nature of tasks to how inputs are processed. We anticipate that our research will shed light on the compositional capabilities and reasoning of LLMs, and stimulate further exploration in this direction.

This work addresses the second core challenge we proposed in Chapter 1: understanding and enhancing complex compositional reasoning in foundation models. Our findings reveal fundamental patterns in how these models handle composite tasks, providing crucial insights into their cognitive limitations. These discoveries directly inform our ongoing collaborated work on analyzing induction heads and their role in out-of-distribution generalization, as understanding the mechanisms behind successful composition cases can help us develop more robust architectures for complex reasoning tasks. Furthermore, this improved understanding of compositional behavior helps bridge the gap between general-purpose models and specialized task performance, connecting back to our broader goal of efficient model adaptation.

Chapter 5

Adaptive Runtime Inference

Building on our completed work in few-shot adaptation and compositional reasoning, my work investigates how to enhance foundation models' specialized capabilities. With our ongoing work of adaptive inference, we aim to develop a framework that improve efficiency in adapting to downstream tasks.

5.1 Motivation

Foundation models have increasingly evolved toward multimodal capabilities, with multimodal LLMs emerging as key players in the field. While these models demonstrate remarkable visual reasoning abilities, they come with substantial computational costs. Several recent efforts seek to improve the efficiency of MLLMs by considering lightweight architectures, mixture of experts or token selection techniques [Lin et al., 2024; Shang et al., 2024]. A key characteristic of these prior approaches is that they produce models with static accuracy and latency footprint.

We argue that MLLMs with fixed computational footprint are insufficient for real-world deployment. Consider the example of deploying an MLLM on a server farm. Different requests may have distinct latency requirements, *e.g.*, requests from a mobile application, which requires instant feedback to an user vs. those from a recommendation system, which performs updates less frequently and thus can tolerate a higher latency. Further, the available computing resources may vary at any given point in time, as the overall loads of the system fluctuate. Similarly, when deployed on edges device, the latency budget often remains constant, yet the computing resources may vary due to contention produced by other on-device programs.

5.2 Proposed Work

In departure from prior approaches, we propose to address latency-aware adaptive inference for MLLMs, aiming to dynamically adjust a model's computational load based on input content and a specified latency budget. This problem

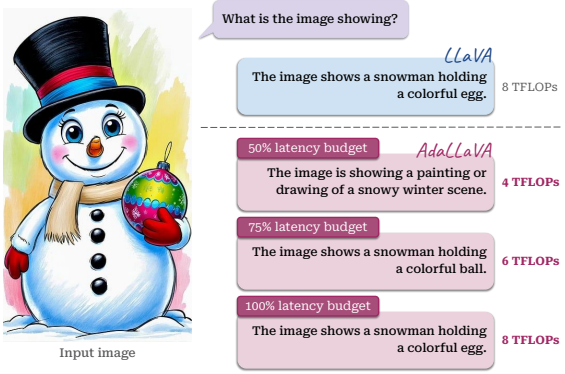

Figure 5.1: Given an image-query pair and latency constraints, AdaLLaVA learns to generate appropriate responses while adapting to varying computational budgets.

is of both conceptual interest and practical significance. Our key insight is that an MLLM can be conceptualized as a collection of shallower models, which can be leveraged for dynamic reconfiguration during inference. For example, previous works have shown that Transformer blocks in an LLM and some attention heads within these blocks can be bypassed with minor impact on accuracy [Wu et al., 2018; Meng et al., 2022]. Therefore, strategically selecting operations with varying accuracy impacts during inference leads to a set of models with shared parameters but distinct accuracy-latency tradeoffs, enabling the MLLM to flexibly respond to varying latency requirements.

To this end, we present **AdaLLaVA**, a learning-based framework for adaptive inference in MLLMs. As shown in Fig. 5.1, given query and the latency budget, the MLLM can answer the query without violation of the budget. Key to AdaLLaVA lies in a learned scheduler that dynamically generates an execution plan, selecting a subset of operations within an MLLM based on the input content and a specified latency budget. This execution plan ensures that inference is performed within the given latency constraint while maximizing expected accuracy. To enable effective learning of the scheduler, we introduce a probabilistic formulation in tandem with a dedicated sampling strategy to account for latency constraints at training time.

5.3 Contributions

We conduct extensive experiments and demonstrate that AdaLLaVA can achieve a range of accuracy-latency tradeoffs at runtime. AdaLLaVA maintains comparable performance to full models across several benchmarks while operating with higher efficiency. Further, AdaLLaVA exhibits strong adaptability to different latency budgets, effectively trading accuracy for speed during inference, particularly in extremely latency-constrained settings. In all cases, AdaLLaVA adheres to latency budgets. Additionally, AdaLLaVA can be further integrated with token selection techniques to further enhance efficiency, and demonstrates content-aware optimization by generating execution solutions tailored to specific input samples.

Our key **contributions** are three folds.

- We present AdaLLaVA, a novel adaptive inference framework for MLLM. Our method for the first time enables dynamic model execution based on a latency budget and input contents at inference time.
- Our key technical innovation lies in the design of a latency-aware scheduler, which reconfigures a base MLLM model at inference time, along with a probabilistic modeling approach that allows for the incorporation of hard latency constraints during MLLM training.
- Through extensive experiments, we show that AdaLLaVA can adapt to a range of latency requirements while preserving the performance of the base model, and that AdaLLaVA can be integrated with token selection techniques to further enhance efficiency.

5.4 Conclusion

This work advances my research goals by addressing the practical deployment challenges of foundation models, particularly in the emerging multimodal domain. While our earlier work focused on efficient adaptation and understanding compositional reasoning, this research complements those efforts by developing adaptive inference techniques that make these models more practically viable. Our framework for dynamic operation reconfiguration represents a crucial step toward our broader goal of transforming foundation models into practical, task-specific experts. Furthermore, this work opens new directions for our ongoing research in developing adaptive inference frameworks for multimodal LLMs, particularly in understanding how model behavior changes under different computational constraints and how we can maintain reasoning capabilities while optimizing for efficiency.

Chapter 6

Proposed Work

6.1 Broader Efficient Inference

Our previous work on adaptive inference demonstrated the potential of dynamic component selection in multimodal LLMs. However, achieving truly efficient and adaptable foundation models requires a more comprehensive approach that optimizes both at the token level and architectural level while maintaining reasoning capabilities.

6.1.1 Motivation

While foundation models have shown remarkable capabilities, their deployment remains constrained by computational costs and efficiency challenges. Our completed work on adaptive inference revealed that dynamic model reconfiguration can significantly improve efficiency, but also highlighted the need for more sophisticated optimization strategies. Current approaches primarily focus on model component selection, overlooking the potential of integrated token selection and computation routing strategies that have shown promise in recent work [Shang et al., 2024; Chen et al., 2025; Zhang et al., 2024]. Furthermore, recent advances in mechanistic interpretability have identified key components within LLMs that significantly impact model performance on comprehension benchmarks [Song et al., 2024; Reddy, 2024; Wang et al., 2023a]. These insights open new possibilities for developing training-free algorithms for component selection, offering a principled approach to efficiency optimization that maintains model capabilities.

6.1.2 Proposed Work

We propose to develop a comprehensive efficiency framework that operates at multiple perspectives:

- Token-Level Optimization: Develop content-aware token selection strategies that dynamically identify and retain crucial tokens for different tasks. Design predictive mechanisms to anticipate token importance based on task requirements and computational constraints.
- Architecture-Guided Component Selection: Leverage mechanistic interpretability insights to identify key induction heads and attention patterns crucial for specific tasks.

6.1.3 Contributions

This research will advance the field through novel algorithms for joint token and component optimization, and practical techniques for deploying foundation models under varying computational constraints.

6.1.4 Conclusion

This work will deepen our understanding of how model architecture influences reasoning capabilities in foundation models. By systematically analyzing and enhancing architectural components, we aim to develop more capable models for complex reasoning tasks. This research directly addresses our thesis goals of understanding and improving foundation models' specialized capabilities while maintaining efficiency.

6.2 Complex Reasoning

Building on our previous findings about compositional abilities in LLMs, we now aim to systematically investigate how architectural elements influence complex reasoning capabilities, particularly focusing on the interaction between model architecture and in-context learning performance.

6.2.1 Motivation

While our earlier work revealed patterns in how LLMs handle composite tasks, fundamental questions remain about the architectural mechanisms enabling complex reasoning. Recent work has shown that specific architectural components, particularly induction heads and attention patterns, play crucial roles in model behavior. However, we lack a systematic understanding of how these components contribute to reasoning capabilities and how they can be enhanced. Additionally, while techniques like Chain-of-Thought prompting have shown promise, their interaction with model architecture in solving compositional tasks remains poorly understood.

6.2.2 Proposed Work

We propose a comprehensive investigation of architectural influences on reasoning capabilities:

- Systematically analyze how different architectural components contribute to basic logical operations (negation, conjunction, disjunction).
- Map the relationship between attention patterns and specific reasoning steps.
- Develop methods to identify and strengthen key components responsible for compositional understanding.
- Analyze embedding similarities and prediction probabilities across model layers during reasoning.
- Create a comprehensive benchmark for evaluating compositional reasoning capabilities.

6.2.3 Contributions

This research will make several key contributions to the field of foundation models. First, it will provide a systematic understanding of how architectural elements enable logical reasoning, revealing the mechanisms behind basic and complex reasoning operations. Through novel architectural modifications, we will enhance models' compositional capabilities, particularly in handling multi-step reasoning tasks. Our development of a comprehensive benchmark for evaluating compositional reasoning will establish new standards for assessing model performance across different types of logical tasks. Furthermore, by investigating the interplay between prompting techniques and model architecture, we will uncover new insights into how different architectural components respond to and process various prompting strategies. Finally, these findings will translate into practical guidelines for designing more capable models, helping bridge the gap between theoretical understanding and practical implementation of stronger reasoning capabilities in foundation models.

6.2.4 Conclusion

This work will deepen our understanding of how model architecture influences reasoning capabilities in foundation models. By systematically analyzing and enhancing architectural components, we aim to develop more capable models for complex reasoning tasks. This research directly addresses our thesis goals of understanding and improving foundation models' specialized capabilities while maintaining efficiency.

Chapter 7

Conclusion

Our research addresses fundamental challenges in making foundation models more practical and capable through two complementary threads. In our completed work, we first tackled the challenge of efficient adaptation through theoretical analysis of multitask finetuning, revealing how diverse task sets can significantly improve adaptation performance with limited labeled data (Chapter 3). We then investigated compositional abilities in LLMs, uncovering distinct patterns in how these models handle different types of composite tasks and providing theoretical insights into their success and failure modes (Chapter 4). Our work on adaptive inference for multimodal LLMs demonstrated how dynamic model reconfiguration can improve deployment efficiency while maintaining performance (Chapter 5).

Building on these foundations, our proposed work extends in two crucial directions. First, we aim to develop a comprehensive efficiency framework that combines token-level optimization with mechanistic interpretability-guided component selection, advancing beyond our initial adaptive inference work to create more sophisticated optimization strategies (Chapter 6, Sec. 6.1). Second, we will deepen our investigation of compositional reasoning by analyzing how architectural elements influence reasoning capabilities, extending our earlier findings about compositional patterns to understand and enhance the mechanisms behind complex reasoning (Chapter 6, Sec. 6.2). Together, these research directions form a coherent approach to our central goal: transforming general-purpose foundation models into more efficient and capable task-specific experts. Our completed work established fundamental understanding and initial solutions, while our proposed work aims to develop more comprehensive frameworks for both efficient deployment and enhanced reasoning capabilities. This progression from theoretical foundations to practical solutions addresses the critical challenges of adaptation, efficiency, and reasoning that currently limit the practical impact of foundation models.

7.1 Additional collaborative work

While my research primarily focuses customize+ foundation models, I have also contributed to several related research directions that further our understanding of LLMs. Below, I briefly summarize these works and discuss their connections to the main themes of this document.

Understanding Scale Effects in In-Context Learning. In collaborative work [Shi et al., 2024b] investigating why larger language models perform in-context learning differently, we investigated how model scale affects in-context learning behavior in LLMs. Through theoretical analysis and empirical studies, we found that larger and smaller models process in-context examples differently: larger models tend to be more sensitive to noise in test contexts, while smaller models show increased robustness. Our theoretical framework explains this behavior by showing that smaller models focus on key features while larger models distribute attention across a broader range of features, providing new insights into how model scale influences learning dynamics. Our experiments demonstrate how LLMs of varying sizes perform differently in in-context learning tasks. This work provides additional theoretical insights into how model scale affects learning behaviors, complementing our analysis of compositional abilities.

Investigating OOD Generalization Through Induction Heads. We also contributed to research examining out-of-distribution generalization in transformers through the lens of induction heads [Song et al., 2024]. This work investigated the role of induction heads in transformer models through systematic ablation experiments. Using synthetic in-context learning tasks designed to test compositional reasoning, we examined how models perform when induction heads are removed or shuffled between layers. These experiments provided empirical evidence that induction heads are critical for compositional learning and out-of-distribution generalization. The experimental results showed clear

performance degradation on compositional tasks when induction head functionality was disrupted, supporting the theoretical framework about how transformers compose information across attention layers to achieve generalization.

7.2 Timeline

Our ongoing adaptive inference project (Chapter 5) will be completed by January 2025. The efficiency inference work (Chapter 6, Sec. 6.1) is scheduled for completion by summer 2025, with a submission-ready manuscript. Our research on reasoning capabilities (Chapter 6, Sec. 6.2) will start in spring 2025 and possibly extend through fall 2025. With these milestones in place, I am targeting a thesis defense in fall 2025, approximately one year from now.

7.3 Broader impact

In general, my future proposed thesis will advance the field of foundation models through contributions that address critical challenges in their practical deployment and theoretical understanding. Our work establishes new frameworks for efficient model adaptation, enhances our understanding of how these models approach complex reasoning tasks, and develops novel methods for efficient deployment. These contributions not only advance the theoretical foundations of machine learning but also provide practical solutions for making foundation models more accessible and effective in real-world applications. By bridging the gap between theoretical capabilities and practical deployment, this work helps pave the way for more efficient, capable, and practically viable AI systems.

Bibliography

Ekin Akyürek, Dale Schuurmans, Jacob Andreas, Tengyu Ma, and Denny Zhou. What learning algorithm is in-context learning? investigations with linear models. In *The Eleventh International Conference on Learning Representations*, 2023.

Ahmed Alajrami, Katerina Margatina, and Nikolaos Aletras. Understanding the role of input token characters in language models: How does information loss affect performance? In *The 2023 Conference on Empirical Methods in Natural Language Processing*, 2023. URL https://openreview.net/forum?id=Ra6gfR3XuI.

Jean-Baptiste Alayrac, Jeff Donahue, Pauline Luc, Antoine Miech, Iain Barr, Yana Hasson, Karel Lenc, Arthur Mensch, Katherine Millican, Malcolm Reynolds, et al. Flamingo: a visual language model for few-shot learning. *Advances in neural information processing systems*, 35:23716–23736, 2022.

Shengnan An, Zeqi Lin, Bei Chen, Qiang Fu, Nanning Zheng, and Jian-Guang Lou. Does deep learning learn to abstract? a systematic probing framework. In *The Eleventh International Conference on Learning Representations*, 2023a.

Shengnan An, Zeqi Lin, Qiang Fu, Bei Chen, Nanning Zheng, Jian-Guang Lou, and Dongmei Zhang. How do in-context examples affect compositional generalization? *arXiv preprint arXiv:2305.04835*, 2023b.

Anthropic. The claude 3 model family: Opus, sonnet, haiku. https://www-cdn.anthropic.com/de8ba9b01c9ab7cbabf5c33b80b7bbc618857627/Model_Card_Claude_3.pdf, 2024.

Sanjeev Arora and Anirudh Goyal. A theory for emergence of complex skills in language models. *arXiv preprint arXiv:2307.15936*, 2023.

Sanjeev Arora, Hrishikesh Khandeparkar, Mikhail Khodak, Orestis Plevrakis, and Nikunj Saunshi. A theoretical analysis of contrastive unsupervised representation learning. In *36th International Conference on Machine Learning, ICML 2019*. International Machine Learning Society (IMLS), 2019.

Emmanuel Bengio, Pierre-Luc Bacon, Joelle Pineau, and Doina Precup. Conditional computation in neural networks for faster models. *arXiv preprint arXiv:1511.06297*, 2015.

Lukas Berglund, Meg Tong, Max Kaufmann, Mikita Balesni, Asa Cooper Stickland, Tomasz Korbak, and Owain Evans. The reversal curse: Llms trained on" a is b" fail to learn" b is a". *arXiv preprint arXiv:2309.12288*, 2023.

Sid Black, Leo Gao, Phil Wang, Connor Leahy, and Stella Biderman. GPT-Neo: Large Scale Autoregressive Language Modeling with Mesh-Tensorflow. Technical report, Zenodo, March 2021. If you use this software, please cite it using these metadata.

David M Blei, Andrew Y Ng, and Michael I Jordan. Latent dirichlet allocation. *Journal of Machine Learning research*, 2003.

Rishi Bommasani, Drew A Hudson, Ehsan Adeli, Russ Altman, Simran Arora, Sydney von Arx, Michael S Bernstein, Jeannette Bohg, Antoine Bosselut, Emma Brunskill, et al. On the opportunities and risks of foundation models. *arXiv preprint arXiv:2108.07258*, 2021.

Samuel R. Bowman, Gabor Angeli, Christopher Potts, and Christopher D. Manning. A large annotated corpus for learning natural language inference. In *Proceedings of the 2015 Conference on Empirical Methods in Natural Language Processing*. Association for Computational Linguistics, 2015.

Tom Brown, Benjamin Mann, Nick Ryder, Melanie Subbiah, Jared D Kaplan, Prafulla Dhariwal, Arvind Neelakantan, Pranav Shyam, Girish Sastry, Amanda Askell, et al. Language models are few-shot learners. *Advances in neural information processing systems*, 2020.

Jianjian Cao, Peng Ye, Shengze Li, Chong Yu, Yansong Tang, Jiwen Lu, and Tao Chen. Madtp: Multimodal alignment-guided dynamic token pruning for accelerating vision-language transformer. In *Proceedings of the IEEE/CVF Conference on Computer Vision and Pattern Recognition*, pages 15710–15719, 2024.

Liang Chen, Haozhe Zhao, Tianyu Liu, Shuai Bai, Junyang Lin, Chang Zhou, and Baobao Chang. An image is worth 1/2 tokens after layer 2: Plug-and-play inference acceleration for large vision-language models. In *European Conference on Computer Vision*, pages 19–35. Springer, 2025.

Ting Chen, Simon Kornblith, Mohammad Norouzi, and Geoffrey Hinton. A simple framework for contrastive learning of visual representations. In *International conference on machine learning*. PMLR, 2020.

Xinlei Chen, Saining Xie, and Kaiming He. An empirical study of training self-supervised vision transformers. In *Proceedings of the IEEE/CVF International Conference on Computer Vision*, 2021a.

Yanda Chen, Ruiqi Zhong, Sheng Zha, George Karypis, and He He. Meta-learning via language model in-context tuning. In Smaranda Muresan, Preslav Nakov, and Aline Villavicencio, editors, *Proceedings of the 60th Annual Meeting of the Association for Computational Linguistics (Volume 1: Long Papers)*, pages 719–730, Dublin, Ireland, May 2022a. Association for Computational Linguistics. doi: 10.18653/v1/2022.acl-long.53.

Yanda Chen, Ruiqi Zhong, Sheng Zha, George Karypis, and He He. Meta-learning via language model in-context tuning. In *Proceedings of the 60th Annual Meeting of the Association for Computational Linguistics*, 2022b.

Yinbo Chen, Zhuang Liu, Huijuan Xu, Trevor Darrell, and Xiaolong Wang. Meta-baseline: Exploring simple meta-learning for few-shot learning. In *Proceedings of the IEEE/CVF International Conference on Computer Vision*, 2021b.

Aakanksha Chowdhery, Sharan Narang, Jacob Devlin, Maarten Bosma, Gaurav Mishra, Adam Roberts, Paul Barham, Hyung Won Chung, Charles Sutton, Sebastian Gehrmann, et al. Palm: Scaling language modeling with pathways. *arXiv preprint arXiv:2204.02311*, 2022.

Hyung Won Chung, Le Hou, Shayne Longpre, Barret Zoph, Yi Tay, William Fedus, Eric Li, Xuezhi Wang, Mostafa Dehghani, Siddhartha Brahma, et al. Scaling instruction-finetuned language models. *arXiv preprint arXiv:2210.11416*, 2022.

Jacob Devlin, Ming-Wei Chang, Kenton Lee, and Kristina Toutanova. BERT: Pre-training of deep bidirectional transformers for language understanding. In *Proceedings of the 2019 Conference of the North American Chapter of the Association for Computational Linguistics: Human Language Technologies*. Association for Computational Linguistics, 2019.

Qingxiu Dong, Lei Li, Damai Dai, Ce Zheng, Zhiyong Wu, Baobao Chang, Xu Sun, Jingjing Xu, and Zhifang Sui. A survey for in-context learning. *arXiv preprint arXiv:2301.00234*, 2022.

Alexey Dosovitskiy, Lucas Beyer, Alexander Kolesnikov, Dirk Weissenborn, Xiaohua Zhai, Thomas Unterthiner, Mostafa Dehghani, Matthias Minderer, Georg Heigold, Sylvain Gelly, Jakob Uszkoreit, and Neil Houlsby. An image is worth 16x16 words: Transformers for image recognition at scale. In *International Conference on Learning Representations*, 2021.

Nan Du, Yanping Huang, Andrew M Dai, Simon Tong, Dmitry Lepikhin, Yuanzhong Xu, Maxim Krikun, Yanqi Zhou, Adams Wei Yu, Orhan Firat, et al. Glam: Efficient scaling of language models with mixture-of-experts. In *International Conference on Machine Learning*, pages 5547–5569. PMLR, 2022.

Simon Shaolei Du, Wei Hu, Sham M. Kakade, Jason D. Lee, and Qi Lei. Few-shot learning via learning the representation, provably. In *9th International Conference on Learning Representations, ICLR 2021, Virtual Event, Austria, May 3-7, 2021*. OpenReview.net, 2021.

Nouha Dziri, Ximing Lu, Melanie Sclar, Xiang Lorraine Li, Liwei Jiang, Bill Yuchen Lin, Sean Welleck, Peter West, Chandra Bhagavatula, Ronan Le Bras, Jena D. Hwang, Soumya Sanyal, Xiang Ren, Allyson Ettinger, Zaid Harchaoui, and Yejin Choi. Faith and fate: Limits of transformers on compositionality. In *Thirty-seventh Conference on Neural Information Processing Systems*, 2023.

Michael Figurnov, Maxwell D Collins, Yukun Zhu, Li Zhang, Jonathan Huang, Dmitry Vetrov, and Ruslan Salakhutdinov. Spatially adaptive computation time for residual networks. In *Proceedings of the IEEE conference on computer vision and pattern recognition*, pages 1039–1048, 2017.

Chelsea Finn, Pieter Abbeel, and Sergey Levine. Model-agnostic meta-learning for fast adaptation of deep networks. In *International conference on machine learning*. PMLR, 2017.

Tomer Galanti, András György, and Marcus Hutter. Generalization bounds for transfer learning with pretrained classifiers. *arXiv preprint arXiv:2212.12532*, 2022.

Tianyu Gao, Adam Fisch, and Danqi Chen. Making pre-trained language models better few-shot learners. In *Proceedings of the 59th Annual Meeting of the Association for Computational Linguistics and the 11th International Joint Conference on Natural Language Processing*, 2021a.

Tianyu Gao, Xingcheng Yao, and Danqi Chen. SimCSE: Simple contrastive learning of sentence embeddings. In Marie-Francine Moens, Xuanjing Huang, Lucia Specia, and Scott Wen-tau Yih, editors, *Proceedings of the 2021 Conference on Empirical Methods in Natural Language Processing*, pages 6894–6910, Online and Punta Cana, Dominican Republic, November 2021b. Association for Computational Linguistics. doi: 10.18653/v1/2021.emnlp-main.552.

Tianyu Gao, Xingcheng Yao, and Danqi Chen. SimCSE: Simple contrastive learning of sentence embeddings. In *Empirical Methods in Natural Language Processing (EMNLP)*, 2021c.

Shivam Garg, Dimitris Tsipras, Percy S Liang, and Gregory Valiant. What can transformers learn in-context? a case study of simple function classes. *Advances in Neural Information Processing Systems*, 35:30583–30598, 2022.

Siddhant Garg and Yingyu Liang. Functional regularization for representation learning: A unified theoretical perspective. *Advances in Neural Information Processing Systems*, 2020.

Weifeng Ge and Yizhou Yu. Borrowing treasures from the wealthy: Deep transfer learning through selective joint fine-tuning. In *Proceedings of the IEEE conference on computer vision and pattern recognition*, 2017.

Xinyang Geng and Hao Liu. Openllama: An open reproduction of llama, May 2023. URL https://github.com/openlm-research/open_llama.

Sachin Goyal, Ananya Kumar, Sankalp Garg, Zico Kolter, and Aditi Raghunathan. Finetune like you pretrain: Improved finetuning of zero-shot vision models. In *Proceedings of the IEEE/CVF Conference on Computer Vision and Pattern Recognition*, 2023.

Jean-Bastien Grill, Florian Strub, Florent Altché, Corentin Tallec, Pierre Richemond, Elena Buchatskaya, Carl Doersch, Bernardo Avila Pires, Zhaohan Guo, Mohammad Gheshlaghi Azar, et al. Bootstrap your own latent-a new approach to self-supervised learning. *Advances in neural information processing systems*, 2020.

Alex Grubb and Drew Bagnell. Speedboost: Anytime prediction with uniform near-optimality. In *Artificial Intelligence and Statistics*, pages 458–466. PMLR, 2012.

Jiuxiang Gu, Chenyang Li, Yingyu Liang, Zhenmei Shi, Zhao Song, and Tianyi Zhou. Fourier circuits in neural networks: Unlocking the potential of large language models in mathematical reasoning and modular arithmetic. *arXiv preprint arXiv:2402.09469*, 2024a.

Jiuxiang Gu, Yingyu Liang, Heshan Liu, Zhenmei Shi, Zhao Song, and Junze Yin. Conv-basis: A new paradigm for efficient attention inference and gradient computation in transformers. *arXiv preprint arXiv:2405.05219*, 2024b.

Jiuxiang Gu, Yingyu Liang, Zhenmei Shi, Zhao Song, and Chiwun Yang. Toward infinite-long prefix in transformer. *arXiv preprint arXiv:2406.14036*, 2024c.

Jiuxiang Gu, Yingyu Liang, Zhenmei Shi, Zhao Song, and Yufa Zhou. Tensor attention training: Provably efficient learning of higher-order transformers. *arXiv preprint arXiv:2405.16411*, 2024d.

Yizeng Han, Gao Huang, Shiji Song, Le Yang, Honghui Wang, and Yulin Wang. Dynamic neural networks: A survey. *IEEE Transactions on Pattern Analysis and Machine Intelligence*, 44(11):7436–7456, 2021.

Jeff Z HaoChen, Colin Wei, Adrien Gaidon, and Tengyu Ma. Provable guarantees for self-supervised deep learning with spectral contrastive loss. *Advances in Neural Information Processing Systems*, 2021.

Kaiming He, Xiangyu Zhang, Shaoqing Ren, and Jian Sun. Deep residual learning for image recognition. In *Proceedings of the IEEE Conference on Computer Vision and Pattern Recognition*, 2016.

Kaiming He, Haoqi Fan, Yuxin Wu, Saining Xie, and Ross Girshick. Momentum contrast for unsupervised visual representation learning. In *Proceedings of the IEEE/CVF conference on computer vision and pattern recognition*, 2020.

Kaiming He, Xinlei Chen, Saining Xie, Yanghao Li, Piotr Dollár, and Ross Girshick. Masked autoencoders are scalable vision learners. In *Proceedings of the IEEE/CVF Conference on Computer Vision and Pattern Recognition*, 2022.

Jordan Hoffmann, Sebastian Borgeaud, Arthur Mensch, Elena Buchatskaya, Trevor Cai, Eliza Rutherford, Diego de Las Casas, Lisa Anne Hendricks, Johannes Welbl, Aidan Clark, et al. Training compute-optimal large language models. *arXiv preprint arXiv:2203.15556*, 2022.

Ari Holtzman, Peter West, Vered Shwartz, Yejin Choi, and Luke Zettlemoyer. Surface form competition: Why the highest probability answer isn't always right. In *Proceedings of the 2021 Conference on Empirical Methods in Natural Language Processing*, pages 7038–7051, 2021.

SU Hongjin, Jungo Kasai, Chen Henry Wu, Weijia Shi, Tianlu Wang, Jiayi Xin, Rui Zhang, Mari Ostendorf, Luke Zettlemoyer, Noah A Smith, et al. Selective annotation makes language models better few-shot learners. In *The Eleventh International Conference on Learning Representations*, 2023.

Timothy Hospedales, Antreas Antoniou, Paul Micaelli, and Amos Storkey. Meta-learning in neural networks: A survey. *IEEE Transactions on Pattern Analysis and Machine Intelligence*, 2021.

Edward J Hu, yelong shen, Phillip Wallis, Zeyuan Allen-Zhu, Yuanzhi Li, Shean Wang, Lu Wang, and Weizhu Chen. LoRA: Low-rank adaptation of large language models. In *International Conference on Learning Representations*, 2022a.

Edward J Hu, yelong shen, Phillip Wallis, Zeyuan Allen-Zhu, Yuanzhi Li, Shean Wang, Lu Wang, and Weizhu Chen. LoRA: Low-rank adaptation of large language models. In *International Conference on Learning Representations*, 2022b.

Hanzhang Hu, Debadeepta Dey, Martial Hebert, and J Andrew Bagnell. Learning anytime predictions in neural networks via adaptive loss balancing. In *Proceedings of the AAAI Conference on Artificial Intelligence*, volume 33, pages 3812–3821, 2019.

Jerry Yao-Chieh Hu, Maojiang Su, En-Jui Kuo, Zhao Song, and Han Liu. Computational limits of low-rank adaptation (lora) for transformer-based models. *arXiv preprint arXiv:2406.03136*, 2024.

Minqing Hu and Bing Liu. Mining and summarizing customer reviews. In *Proceedings of the tenth ACM SIGKDD international conference on Knowledge discovery and data mining*, 2004.

Shell Xu Hu, Da Li, Jan Stühmer, Minyoung Kim, and Timothy M Hospedales. Pushing the limits of simple pipelines for few-shot learning: External data and fine-tuning make a difference. In *Proceedings of the IEEE/CVF Conference on Computer Vision and Pattern Recognition*, 2022c.

Zhiqiang Hu, Lei Wang, Yihuai Lan, Wanyu Xu, Ee-Peng Lim, Lidong Bing, Xing Xu, Soujanya Poria, and Roy Lee. LLM-adapters: An adapter family for parameter-efficient fine-tuning of large language models. In Houda Bouamor, Juan Pino, and Kalika Bali, editors, *Proceedings of the 2023 Conference on Empirical Methods in Natural Language Processing*, pages 5254–5276, Singapore, December 2023. Association for Computational Linguistics. doi: 10.18653/v1/2023.emnlp-main.319.

Jie Huang and Kevin Chen-Chuan Chang. Towards reasoning in large language models: A survey. *arXiv preprint arXiv:2212.10403*, 2022.

Weiran Huang, Mingyang Yi, Xuyang Zhao, and Zihao Jiang. Towards the generalization of contrastive self-supervised learning. In *The Eleventh International Conference on Learning Representations*, 2023.

Mojan Javaheripi, Sébastien Bubeck, Marah Abdin, Jyoti Aneja, Sebastien Bubeck, Caio César Teodoro Mendes, Weizhu Chen, Allie Del Giorno, Ronen Eldan, Sivakanth Gopi, et al. Phi-2: The surprising power of small language models. *Microsoft Research Blog*, 2023.

Chao Jia, Yinfei Yang, Ye Xia, Yi-Ting Chen, Zarana Parekh, Hieu Pham, Quoc Le, Yun-Hsuan Sung, Zhen Li, and Tom Duerig. Scaling up visual and vision-language representation learning with noisy text supervision. In *International Conference on Machine Learning*. PMLR, 2021.

Zequn Jie, Peng Sun, Xin Li, Jiashi Feng, and Wei Liu. Anytime recognition with routing convolutional networks. *IEEE transactions on pattern analysis and machine intelligence*, 43(6):1875–1886, 2019.

Jared Kaplan, Sam McCandlish, Tom Henighan, Tom B Brown, Benjamin Chess, Rewon Child, Scott Gray, Alec Radford, Jeffrey Wu, and Dario Amodei. Scaling laws for neural language models. *arXiv preprint arXiv:2001.08361*, 2020.

Sergey Karayev, Mario Fritz, and Trevor Darrell. Anytime recognition of objects and scenes. In *Proceedings of the IEEE Conference on Computer Vision and Pattern Recognition*, pages 572–579, 2014.

Najoung Kim and Tal Linzen. COGS: A compositional generalization challenge based on semantic interpretation. In Bonnie Webber, Trevor Cohn, Yulan He, and Yang Liu, editors, *Proceedings of the 2020 Conference on Empirical Methods in Natural Language Processing (EMNLP)*, pages 9087–9105, Online, November 2020. Association for Computational Linguistics. doi: 10.18653/v1/2020.emnlp-main.731.

Ananya Kumar, Aditi Raghunathan, Robbie Matthew Jones, Tengyu Ma, and Percy Liang. Fine-tuning can distort pretrained features and underperform out-of-distribution. In *The Tenth International Conference on Learning Representations, ICLR 2022, Virtual Event, April 25-29, 2022*. OpenReview.net, 2022.

Brenden M Lake, Ruslan Salakhutdinov, and Joshua B Tenenbaum. Human-level concept learning through probabilistic program induction. *Science*, 2015.

Siddique Latif, Moazzam Shoukat, Fahad Shamshad, Muhammad Usama, Yi Ren, Heriberto Cuayáhuitl, Wenwu Wang, Xulong Zhang, Roberto Togneri, Erik Cambria, et al. Sparks of large audio models: A survey and outlook. *arXiv preprint arXiv:2308.12792*, 2023.

Brian Lester, Rami Al-Rfou, and Noah Constant. The power of scale for parameter-efficient prompt tuning. In *Proceedings of the 2021 Conference on Empirical Methods in Natural Language Processing*. Association for Computational Linguistics, 2021.

Itay Levy, Ben Bogin, and Jonathan Berant. Diverse demonstrations improve in-context compositional generalization. *arXiv preprint arXiv:2212.06800*, 2022.

Bo Li, Yuanhan Zhang, Dong Guo, Renrui Zhang, Feng Li, Hao Zhang, Kaichen Zhang, Yanwei Li, Ziwei Liu, and Chunyuan Li. Llava-onevision: Easy visual task transfer. *arXiv preprint arXiv:2408.03326*, 2024.

Hengduo Li, Zuxuan Wu, Abhinav Shrivastava, and Larry S Davis. 2d or not 2d? adaptive 3d convolution selection for efficient video recognition. In *Proceedings of the IEEE/CVF conference on computer vision and pattern recognition*, pages 6155–6164, 2021.

Junnan Li, Dongxu Li, Silvio Savarese, and Steven Hoi. Blip-2: Bootstrapping language-image pre-training with frozen image encoders and large language models. In *International conference on machine learning*, pages 19730–19742. PMLR, 2023.

Xiang Lisa Li and Percy Liang. Prefix-tuning: Optimizing continuous prompts for generation. In *Proceedings of the 59th Annual Meeting of the Association for Computational Linguistics and the 11th International Joint Conference on Natural Language Processing*. Association for Computational Linguistics, 2021.

Bin Lin, Zhenyu Tang, Yang Ye, Jiaxi Cui, Bin Zhu, Peng Jin, Jinfa Huang, Junwu Zhang, Yatian Pang, Munan Ning, et al. Moe-llava: Mixture of experts for large vision-language models. *arXiv preprint arXiv:2401.15947*, 2024.

Chen Liu, Yanwei Fu, Chengming Xu, Siqian Yang, Jilin Li, Chengjie Wang, and Li Zhang. Learning a few-shot embedding model with contrastive learning. In *Proceedings of the AAAI conference on artificial intelligence*, 2021.

Haotian Liu, Chunyuan Li, Yuheng Li, and Yong Jae Lee. Improved baselines with visual instruction tuning, 2023a.

Haotian Liu, Chunyuan Li, Qingyang Wu, and Yong Jae Lee. Visual instruction tuning. In *NeurIPS*, 2023b.

Jiachang Liu, Dinghan Shen, Yizhe Zhang, Bill Dolan, Lawrence Carin, and Weizhu Chen. What makes good in-context examples for GPT-3? In Eneko Agirre, Marianna Apidianaki, and Ivan Vulić, editors, *Proceedings of Deep Learning Inside Out (DeeLIO 2022): The 3rd Workshop on Knowledge Extraction and Integration for Deep Learning Architectures*, pages 100–114, Dublin, Ireland and Online, May 2022. Association for Computational Linguistics. doi: 10.18653/v1/2022.deelio-1.10.

Yinhan Liu, Myle Ott, Naman Goyal, Jingfei Du, Mandar Joshi, Danqi Chen, Omer Levy, Mike Lewis, Luke Zettlemoyer, and Veselin Stoyanov. RoBERTa: A robustly optimized BERT pretraining approach. *arXiv preprint arXiv:1907.11692*, 2019.

Lajanugen Logeswaran and Honglak Lee. An efficient framework for learning sentence representations. In *6th International Conference on Learning Representations, ICLR 2018, Vancouver, BC, Canada, April 30 - May 3, 2018, Conference Track Proceedings*. OpenReview.net, 2018.

Yao Lu, Max Bartolo, Alastair Moore, Sebastian Riedel, and Pontus Stenetorp. Fantastically ordered prompts and where to find them: Overcoming few-shot prompt order sensitivity. In Smaranda Muresan, Preslav Nakov, and Aline Villavicencio, editors, *Proceedings of the 60th Annual Meeting of the Association for Computational Linguistics (Volume 1: Long Papers)*, pages 8086–8098, Dublin, Ireland, May 2022. Association for Computational Linguistics. doi: 10.18653/v1/2022.acl-long.556.

Haozheng Luo, Jiahao Yu, Wenxin Zhang, Jialong Li, Jerry Yao-Chieh Hu, Xinyu Xing, and Han Liu. Decoupled alignment for robust plug-and-play adaptation. *arXiv preprint arXiv:2406.01514*, 2024.

Avinash Madasu and Shashank Srivastava. What do large language models learn beyond language? In Yoav Goldberg, Zornitsa Kozareva, and Yue Zhang, editors, *Findings of the Association for Computational Linguistics: EMNLP 2022*, pages 6940–6953, Abu Dhabi, United Arab Emirates, December 2022. Association for Computational Linguistics. doi: 10.18653/v1/2022.findings-emnlp.516. URL https://aclanthology.org/2022.findings-emnlp.516.

Arvind Mahankali, Tatsunori B Hashimoto, and Tengyu Ma. One step of gradient descent is provably the optimal in-context learner with one layer of linear self-attention. *arXiv preprint arXiv:2307.03576*, 2023.

Andreas Maurer. A vector-contraction inequality for rademacher complexities. In *International Conference on Algorithmic Learning Theory*. Springer, 2016.

Lingchen Meng, Hengduo Li, Bor-Chun Chen, Shiyi Lan, Zuxuan Wu, Yu-Gang Jiang, and Ser-Nam Lim. Adavit: Adaptive vision transformers for efficient image recognition. In *Proceedings of the IEEE/CVF Conference on Computer Vision and Pattern Recognition*, pages 12309–12318, 2022.

Yue Meng, Chung-Ching Lin, Rameswar Panda, Prasanna Sattigeri, Leonid Karlinsky, Aude Oliva, Kate Saenko, and Rogerio Feris. Ar-net: Adaptive frame resolution for efficient action recognition. In *Computer Vision–ECCV 2020: 16th European Conference, Glasgow, UK, August 23–28, 2020, Proceedings, Part VII 16*, pages 86–104. Springer, 2020.

Meta. Introducing meta llama 3: The most capable openly available llm to date. https://ai.meta.com/blog/meta-llama-3/, 2024.

Sewon Min, Mike Lewis, Luke Zettlemoyer, and Hannaneh Hajishirzi. MetaICL: Learning to learn in context. In Marine Carpuat, Marie-Catherine de Marneffe, and Ivan Vladimir Meza Ruiz, editors, *Proceedings of the 2022 Conference of the North American Chapter of the Association for Computational Linguistics: Human Language Technologies*, pages 2791–2809, Seattle, United States, July 2022a. Association for Computational Linguistics. doi: 10.18653/v1/2022.naacl-main.201.

Sewon Min, Mike Lewis, Luke Zettlemoyer, and Hannaneh Hajishirzi. MetaICL: Learning to learn in context. In *Proceedings of the 2022 Conference of the North American Chapter of the Association for Computational Linguistics: Human Language Technologies*, 2022b.

Sewon Min, Xinxi Lyu, Ari Holtzman, Mikel Artetxe, Mike Lewis, Hannaneh Hajishirzi, and Luke Zettlemoyer. Rethinking the role of demonstrations: What makes in-context learning work? In *Proceedings of the 2022 Conference on Empirical Methods in Natural Language Processing*. Association for Computational Linguistics, 2022c.

Swaroop Mishra, Daniel Khashabi, Chitta Baral, and Hannaneh Hajishirzi. Cross-task generalization via natural language crowdsourcing instructions. In *Proceedings of the 60th Annual Meeting of the Association for Computational Linguistics*, 2022.

Mehryar Mohri, Afshin Rostamizadeh, and Ameet Talwalkar. *Foundations of machine learning*. MIT press, 2018.

Niklas Muennighoff, Thomas Wang, Lintang Sutawika, Adam Roberts, Stella Biderman, Teven Le Scao, M. Saiful Bari, Sheng Shen, Zheng Xin Yong, Hailey Schoelkopf, Xiangru Tang, Dragomir Radev, Alham Fikri Aji, Khalid Almubarak, Samuel Albanie, Zaid Alyafeai, Albert Webson, Edward Raff, and Colin Raffel. Crosslingual generalization through multitask finetuning. In *Proceedings of the 61st Annual Meeting of the Association for Computational Linguistics (ACL)*, 2023.

Shikhar Murty, Tatsunori B Hashimoto, and Christopher D Manning. Dreca: A general task augmentation strategy for few-shot natural language inference. In *Proceedings of the 2021 Conference of the North American Chapter of the Association for Computational Linguistics: Human Language Technologies*, 2021.

Jianmo Ni, Gustavo Hernandez Abrego, Noah Constant, Ji Ma, Keith Hall, Daniel Cer, and Yinfei Yang. Sentence-t5: Scalable sentence encoders from pre-trained text-to-text models. In *Findings of the Association for Computational Linguistics: ACL 2022*, 2022.

B. Olshausen and D. Field. Sparse coding with an overcomplete basis set: A strategy employed by v1? *Vision Research*, 1997.

Aaron van den Oord, Yazhe Li, and Oriol Vinyals. Representation learning with contrastive predictive coding. *arXiv preprint arXiv:1807.03748*, 2018.

OpenAI. Introducing ChatGPT. https://openai.com/blog/chatgpt, 2022a. Accessed: 2022-11-30.

OpenAI. Gpt-4v(ision) system card. https://cdn.openai.com/papers/GPTV_System_Card.pdf, 2022b. Accessed: 2023-09-25.

OpenAI. GPT-4 technical report. *arXiv preprint arxiv:2303.08774*, 2023.

Maxime Oquab, Timothée Darcet, Theo Moutakanni, Huy V. Vo, Marc Szafraniec, Vasil Khalidov, Pierre Fernandez, Daniel Haziza, Francisco Massa, Alaaeldin El-Nouby, Russell Howes, Po-Yao Huang, Hu Xu, Vasu Sharma, Shang-Wen Li, Wojciech Galuba, Mike Rabbat, Mido Assran, Nicolas Ballas, Gabriel Synnaeve, Ishan Misra, Herve Jegou, Julien Mairal, Patrick Labatut, Armand Joulin, and Piotr Bojanowski. Dinov2: Learning robust visual features without supervision. *arXiv:2304.07193*, 2023.

Long Ouyang, Jeffrey Wu, Xu Jiang, Diogo Almeida, Carroll Wainwright, Pamela Mishkin, Chong Zhang, Sandhini Agarwal, Katarina Slama, Alex Ray, et al. Training language models to follow instructions with human feedback. *Advances in Neural Information Processing Systems*, 2022.

Bowen Pan, Rameswar Panda, Yifan Jiang, Zhangyang Wang, Rogerio Feris, and Aude Oliva. Ia-red2: Interpretability-aware redundancy reduction for vision transformers. *Advances in Neural Information Processing Systems*, 34: 24898–24911, 2021.

Bo Pang and Lillian Lee. A sentimental education: Sentiment analysis using subjectivity summarization based on minimum cuts. In *Proceedings of the 42nd Annual Meeting of the Association for Computational Linguistics*, 2004.

Bo Pang and Lillian Lee. Seeing stars: Exploiting class relationships for sentiment categorization with respect to rating scales. In *Proceedings of the 43rd Annual Meeting of the Association for Computational Linguistics (ACL'05)*, 2005.

Xingchao Peng, Qinxun Bai, Xide Xia, Zijun Huang, Kate Saenko, and Bo Wang. Moment matching for multi-source domain adaptation. In *Proceedings of the IEEE International Conference on Computer Vision*, 2019.

Ethan Perez, Douwe Kiela, and Kyunghyun Cho. True few-shot learning with language models. *Advances in neural information processing systems*, 2021.

Phu Pham, Wentian Zhao, Kun Wan, Yu-Jhe Li, Zeliang Zhang, Daniel Miranda, Ajinkya Kale, and Chenliang Xu. Quadratic is not what you need for multimodal large language models. *arXiv preprint arXiv:2410.06169*, 2024.

Alethea Power, Yuri Burda, Harri Edwards, Igor Babuschkin, and Vedant Misra. Grokking: Generalization beyond overfitting on small algorithmic datasets. *arXiv preprint arXiv:2201.02177*, 2022.

Alec Radford, Karthik Narasimhan, Tim Salimans, Ilya Sutskever, et al. Improving language understanding by generative pre-training. *OpenAI blog*, 2018.

Alec Radford, Jeffrey Wu, Rewon Child, David Luan, Dario Amodei, Ilya Sutskever, et al. Language models are unsupervised multitask learners. *OpenAI blog*, 1(8):9, 2019.

Alec Radford, Jong Wook Kim, Chris Hallacy, Aditya Ramesh, Gabriel Goh, Sandhini Agarwal, Girish Sastry, Amanda Askell, Pamela Mishkin, Jack Clark, et al. Learning transferable visual models from natural language supervision. In *International Conference on Machine Learning*. PMLR, 2021.

Aniruddh Raghu, Maithra Raghu, Samy Bengio, and Oriol Vinyals. Rapid learning or feature reuse? towards understanding the effectiveness of maml. In *International Conference on Learning Representations*, 2020.

Yongming Rao, Wenliang Zhao, Benlin Liu, Jiwen Lu, Jie Zhou, and Cho-Jui Hsieh. Dynamicvit: Efficient vision transformers with dynamic token sparsification. In A. Beygelzimer, Y. Dauphin, P. Liang, and J. Wortman Vaughan, editors, *Advances in Neural Information Processing Systems*, 2021. URL https://openreview.net/forum?id=jB0Nlbwlybm.

David Raposo, Sam Ritter, Blake Richards, Timothy Lillicrap, Peter Conway Humphreys, and Adam Santoro. Mixture-of-depths: Dynamically allocating compute in transformer-based language models. *arXiv preprint arXiv:2404.02258*, 2024.

Gautam Reddy. The mechanistic basis of data dependence and abrupt learning in an in-context classification task. In *The Twelfth International Conference on Learning Representations*, 2024. URL https://openreview.net/forum?id=aN4Jf6Cx69.

Mengye Ren, Sachin Ravi, Eleni Triantafillou, Jake Snell, Kevin Swersky, Josh B. Tenenbaum, Hugo Larochelle, and Richard S. Zemel. Meta-learning for semi-supervised few-shot classification. In *International Conference on Learning Representations*, 2018.

Nicholas Roberts, Xintong Li, Dyah Adila, Sonia Cromp, Tzu-Heng Huang, Jitian Zhao, and Frederic Sala. Geometry-aware adaptation for pretrained models. *arXiv preprint arXiv:2307.12226*, 2023.

Daniel Rotem, Michael Hassid, Jonathan Mamou, and Roy Schwartz. Finding the sweet spot: Analysis and improvement of adaptive inference in low resource settings. In *Proceedings of the 61st Annual Meeting of the Association for Computational Linguistics (Volume 1: Long Papers)*, pages 14836–14851, 2023.

Ohad Rubin, Jonathan Herzig, and Jonathan Berant. Learning to retrieve prompts for in-context learning. In *Proceedings of the 2022 Conference of the North American Chapter of the Association for Computational Linguistics: Human Language Technologies*, pages 2655–2671, 2022.

Olga Russakovsky, Jia Deng, Hao Su, Jonathan Krause, Sanjeev Satheesh, Sean Ma, Zhiheng Huang, Andrej Karpathy, Aditya Khosla, Michael Bernstein, et al. Imagenet large scale visual recognition challenge. *International journal of computer vision*, 2015.

Victor Sanh, Albert Webson, Colin Raffel, Stephen H Bach, Lintang Sutawika, Zaid Alyafeai, Antoine Chaffin, Arnaud Stiegler, Teven Le Scao, Arun Raja, et al. Multitask prompted training enables zero-shot task generalization. In *International Conference on Learning Representations*, 2022.

Yuzhang Shang, Mu Cai, Bingxin Xu, Yong Jae Lee, and Yan Yan. Llava-prumerge: Adaptive token reduction for efficient large multimodal models. *arXiv preprint arXiv:2403.15388*, 2024.

Zhenmei Shi, Junyi Wei, and Yingyu Liang. A theoretical analysis on feature learning in neural networks: Emergence from inputs and advantage over fixed features. In *International Conference on Learning Representations*, 2022.

Zhenmei Shi, Jiefeng Chen, Kunyang Li, Jayaram Raghuram, Xi Wu, Yingyu Liang, and Somesh Jha. The trade-off between universality and label efficiency of representations from contrastive learning. In *International Conference on Learning Representations*, 2023a.

Zhenmei Shi, Yifei Ming, Ying Fan, Frederic Sala, and Yingyu Liang. Domain generalization via nuclear norm regularization. In *Conference on Parsimony and Learning (Proceedings Track)*, 2023b.

Zhenmei Shi, Junyi Wei, and Yingyu Liang. Provable guarantees for neural networks via gradient feature learning. In *Thirty-seventh Conference on Neural Information Processing Systems*, 2023c.

Zhenmei Shi, Junyi Wei, Zhuoyan Xu, and Yingyu Liang. Why larger language models do in-context learning differently? In *R0-FoMo:Robustness of Few-shot and Zero-shot Learning in Large Foundation Models*, 2023d.

Zhenmei Shi, Yifei Ming, Ying Fan, Frederic Sala, and Yingyu Liang. Domain generalization via nuclear norm regularization. In *Conference on Parsimony and Learning*, pages 179–201. PMLR, 2024a.

Zhenmei Shi, Junyi Wei, Zhuoyan Xu, and Yingyu Liang. Why larger language models do in-context learning differently? In *Forty-first International Conference on Machine Learning*, 2024b. URL https://openreview.net/forum?id=W0a96EG26M.

Fangxun Shu, Yue Liao, Le Zhuo, Chenning Xu, Guanghao Zhang, Haonan Shi, Long Chen, Tao Zhong, Wanggui He, Siming Fu, et al. Llava-mod: Making llava tiny via moe knowledge distillation. *arXiv preprint arXiv:2408.15881*, 2024.

Jake Snell, Kevin Swersky, and Richard Zemel. Prototypical networks for few-shot learning. *Advances in neural information processing systems*, 2017.

Richard Socher, Alex Perelygin, Jean Wu, Jason Chuang, Christopher D Manning, Andrew Y Ng, and Christopher Potts. Recursive deep models for semantic compositionality over a sentiment treebank. In *Proceedings of the 2013 Conference on Empirical Methods in Natural Language Processing*, 2013.

Haoyu Song, Li Dong, Weinan Zhang, Ting Liu, and Furu Wei. Clip models are few-shot learners: Empirical studies on vqa and visual entailment. In *Proceedings of the 60th Annual Meeting of the Association for Computational Linguistics*, 2022.

Jiajun Song, Zhuoyan Xu, and Yiqiao Zhong. Out-of-distribution generalization via composition: a lens through induction heads in transformers. *arXiv preprint arXiv:2408.09503*, 2024.

Yiyou Sun, Zhenmei Shi, and Yixuan Li. A graph-theoretic framework for understanding open-world semi-supervised learning. In *Thirty-seventh Conference on Neural Information Processing Systems*, 2023a.

Yiyou Sun, Zhenmei Shi, Yingyu Liang, and Yixuan Li. When and how does known class help discover unknown ones? Provable understanding through spectral analysis. In *Proceedings of the 40th International Conference on Machine Learning*, Proceedings of Machine Learning Research. PMLR, 2023b.

Yiyou Sun, Zhenmei Shi, Yingyu Liang, and Yixuan Li. When and how does known class help discover unknown ones? provable understanding through spectral analysis. In *International Conference on Machine Learning*, pages 33014–33043. PMLR, 2023c.

Yiyou Sun, Zhenmei Shi, and Yixuan Li. A graph-theoretic framework for understanding open-world semi-supervised learning. *Advances in Neural Information Processing Systems*, 36, 2024.

Yonglong Tian, Dilip Krishnan, and Phillipf Isola. Contrastive multiview coding. In *European Conference on Computer Vision*. Springer, 2020a.

Yonglong Tian, Yue Wang, Dilip Krishnan, Joshua B Tenenbaum, and Phillip Isola. Rethinking few-shot image classification: a good embedding is all you need? In *European Conference on Computer Vision*. Springer, 2020b.

Christopher Tosh, Akshay Krishnamurthy, and Daniel Hsu. Contrastive learning, multi-view redundancy, and linear models. In *Algorithmic Learning Theory*. PMLR, 2021.

Hugo Touvron, Thibaut Lavril, Gautier Izacard, Xavier Martinet, Marie-Anne Lachaux, Timothée Lacroix, Baptiste Rozière, Naman Goyal, Eric Hambro, Faisal Azhar, et al. Llama: Open and efficient foundation language models. *arXiv preprint arXiv:2302.13971*, 2023a.

Hugo Touvron, Louis Martin, Kevin Stone, Peter Albert, Amjad Almahairi, Yasmine Babaei, Nikolay Bashlykov, Soumya Batra, Prajjwal Bhargava, Shruti Bhosale, et al. Llama 2: Open foundation and fine-tuned chat models. *arXiv preprint arXiv:2307.09288*, 2023b.

Eleni Triantafillou, Tyler Zhu, Vincent Dumoulin, Pascal Lamblin, Utku Evci, Kelvin Xu, Ross Goroshin, Carles Gelada, Kevin Swersky, Pierre-Antoine Manzagol, and Hugo Larochelle. Meta-dataset: A dataset of datasets for learning to learn from few examples. In *International Conference on Learning Representations*, 2020.

Nilesh Tripuraneni, Michael Jordan, and Chi Jin. On the theory of transfer learning: The importance of task diversity. *Advances in Neural Information Processing Systems*, 2020.

Nilesh Tripuraneni, Chi Jin, and Michael Jordan. Provable meta-learning of linear representations. In *International Conference on Machine Learning*. PMLR, 2021.

Ashish Vaswani, Noam Shazeer, Niki Parmar, Jakob Uszkoreit, Llion Jones, Aidan N Gomez, Łukasz Kaiser, and Illia Polosukhin. Attention is all you need. *Advances in neural information processing systems*, 30, 2017.

William E Vinje and Jack L Gallant. Sparse coding and decorrelation in primary visual cortex during natural vision. *Science*, 2000.

Oriol Vinyals, Charles Blundell, Timothy Lillicrap, Daan Wierstra, et al. Matching networks for one shot learning. *Advances in neural information processing systems*, 2016.

Johannes Von Oswald, Eyvind Niklasson, Ettore Randazzo, Joao Sacramento, Alexander Mordvintsev, Andrey Zhmoginov, and Max Vladymyrov. Transformers learn in-context by gradient descent. In Andreas Krause, Emma Brunskill, Kyunghyun Cho, Barbara Engelhardt, Sivan Sabato, and Jonathan Scarlett, editors, *Proceedings of the 40th International Conference on Machine Learning*, volume 202 of *Proceedings of Machine Learning Research*, pages 35151–35174. PMLR, 23–29 Jul 2023.

Ellen M Voorhees and Dawn M Tice. Building a question answering test collection. In *Proceedings of the 23rd annual international ACM SIGIR conference on Research and development in information retrieval*, 2000.

Tu Vu, Minh-Thang Luong, Quoc Le, Grady Simon, and Mohit Iyyer. Strata: Self-training with task augmentation for better few-shot learning. In *Proceedings of the 2021 Conference on Empirical Methods in Natural Language Processing*, 2021.

Alex Wang, Amanpreet Singh, Julian Michael, Felix Hill, Omer Levy, and Samuel Bowman. GLUE: A multi-task benchmark and analysis platform for natural language understanding. In *Proceedings of the 2018 EMNLP Workshop BlackboxNLP: Analyzing and Interpreting Neural Networks for NLP*. Association for Computational Linguistics, 2018a.

Jiayu Wang, Yifei Ming, Zhenmei Shi, Vibhav Vineet, Xin Wang, and Neel Joshi. Is a picture worth a thousand words? delving into spatial reasoning for vision language models. *arXiv preprint arXiv:2406.14852*, 2024.

Kevin Ro Wang, Alexandre Variengien, Arthur Conmy, Buck Shlegeris, and Jacob Steinhardt. Interpretability in the wild: a circuit for indirect object identification in GPT-2 small. In *The Eleventh International Conference on Learning Representations*, 2023a. URL https://openreview.net/forum?id=NpsVSN6o4ul.

Tongzhou Wang and Phillip Isola. Understanding contrastive representation learning through alignment and uniformity on the hypersphere. In *International Conference on Machine Learning*. PMLR, 2020.

Xin Wang, Fisher Yu, Zi-Yi Dou, Trevor Darrell, and Joseph E Gonzalez. Skipnet: Learning dynamic routing in convolutional networks. In *Proceedings of the European conference on computer vision (ECCV)*, pages 409–424, 2018b.

Xinyi Wang, Wanrong Zhu, Michael Saxon, Mark Steyvers, and William Yang Wang. Large language models are latent variable models: Explaining and finding good demonstrations for in-context learning. In *Thirty-seventh Conference on Neural Information Processing Systems*, 2023b.

Yaqing Wang, Quanming Yao, James T Kwok, and Lionel M Ni. Generalizing from a few examples: A survey on few-shot learning. *ACM computing surveys*, 2020.

Yifei Wang, Qi Zhang, Yisen Wang, Jiansheng Yang, and Zhouchen Lin. Chaos is a ladder: A new theoretical understanding of contrastive learning via augmentation overlap. In *International Conference on Learning Representations*, 2022.

Yulin Wang, Rui Huang, Shiji Song, Zeyi Huang, and Gao Huang. Not all images are worth 16x16 words: Dynamic transformers for efficient image recognition. In A. Beygelzimer, Y. Dauphin, P. Liang, and J. Wortman Vaughan, editors, *Advances in Neural Information Processing Systems*, 2021. URL https://openreview.net/forum?id=M0J1c3PqwKZ.

Zhen Wang, Rameswar Panda, Leonid Karlinsky, Rogerio Feris, Huan Sun, and Yoon Kim. Multitask prompt tuning enables parameter-efficient transfer learning. In *The Eleventh International Conference on Learning Representations*, 2023c.

Colin Wei, Kendrick Shen, Yining Chen, and Tengyu Ma. Theoretical analysis of self-training with deep networks on unlabeled data. In *International Conference on Learning Representations*, 2021.

Haoran Wei, Lingyu Kong, Jinyue Chen, Liang Zhao, Zheng Ge, En Yu, Jianjian Sun, Chunrui Han, and Xiangyu Zhang. Small language model meets with reinforced vision vocabulary. *arXiv preprint arXiv:2401.12503*, 2024.

Jason Wei, Yi Tay, Rishi Bommasani, Colin Raffel, Barret Zoph, Sebastian Borgeaud, Dani Yogatama, Maarten Bosma, Denny Zhou, Donald Metzler, Ed H. Chi, Tatsunori Hashimoto, Oriol Vinyals, Percy Liang, Jeff Dean, and William Fedus. Emergent abilities of large language models. *Transactions on Machine Learning Research*, 2022a.

Jason Wei, Xuezhi Wang, Dale Schuurmans, Maarten Bosma, Fei Xia, Ed Chi, Quoc V Le, Denny Zhou, et al. Chain-of-thought prompting elicits reasoning in large language models. *Advances in Neural Information Processing Systems*, 2022b.

Jerry Wei, Le Hou, Andrew Kyle Lampinen, Xiangning Chen, Da Huang, Yi Tay, Xinyun Chen, Yifeng Lu, Denny Zhou, Tengyu Ma, and Quoc V Le. Symbol tuning improves in-context learning in language models. In *The 2023 Conference on Empirical Methods in Natural Language Processing*, 2023a.

Jerry Wei, Jason Wei, Yi Tay, Dustin Tran, Albert Webson, Yifeng Lu, Xinyun Chen, Hanxiao Liu, Da Huang, Denny Zhou, et al. Larger language models do in-context learning differently. *arXiv preprint arXiv:2303.03846*, 2023b.

Zixin Wen and Yuanzhi Li. Toward understanding the feature learning process of self-supervised contrastive learning. In *International Conference on Machine Learning*. PMLR, 2021.

Janyce Wiebe, Theresa Wilson, and Claire Cardie. Annotating expressions of opinions and emotions in language. *Language resources and evaluation*, 2005.

Mitchell Wortsman, Gabriel Ilharco, Jong Wook Kim, Mike Li, Simon Kornblith, Rebecca Roelofs, Raphael Gontijo Lopes, Hannaneh Hajishirzi, Ali Farhadi, Hongseok Namkoong, et al. Robust fine-tuning of zero-shot models. In *Proceedings of the IEEE/CVF Conference on Computer Vision and Pattern Recognition*, 2022.

Zuxuan Wu, Tushar Nagarajan, Abhishek Kumar, Steven Rennie, Larry S Davis, Kristen Grauman, and Rogerio Feris. Blockdrop: Dynamic inference paths in residual networks. In *Proceedings of the IEEE conference on computer vision and pattern recognition*, pages 8817–8826, 2018.

Sang Michael Xie, Aditi Raghunathan, Percy Liang, and Tengyu Ma. An explanation of in-context learning as implicit bayesian inference. In *International Conference on Learning Representations*, 2022a.

Sang Michael Xie, Aditi Raghunathan, Percy Liang, and Tengyu Ma. An explanation of in-context learning as implicit bayesian inference. In *International Conference on Learning Representations*, 2022b.

Sang Michael Xie, Shibani Santurkar, Tengyu Ma, and Percy Liang. Data selection for language models via importance resampling. *arXiv preprint arXiv:2302.03169*, 2023.

Zhixiang Xu, Kilian Q Weinberger, and Olivier Chapelle. The greedy miser: learning under test-time budgets. In *Proceedings of the 29th International Coference on International Conference on Machine Learning*, pages 1299–1306, 2012.

Zhuoyan Xu, Zhenmei Shi, Junyi Wei, Yin Li, and Yingyu Liang. Improving foundation models for few-shot learning via multitask finetuning. In *ICLR 2023 Workshop on Mathematical and Empirical Understanding of Foundation Models*, 2023.

Zhuoyan Xu, Khoi Duc Nguyen, Preeti Mukherjee, Somali Chaterji, Yingyu Liang, and Yin Li. Adainf: Adaptive inference for resource-constrained foundation models. In *Workshop on Efficient Systems for Foundation Models II @ ICML2024*, 2024a. URL https://openreview.net/forum?id=A942VRmfhQ.

Zhuoyan Xu, Zhenmei Shi, and Yingyu Liang. Do large language models have compositional ability? an investigation into limitations and scalability. In *ICLR 2024 Workshop on Mathematical and Empirical Understanding of Foundation Models*, 2024b. URL https://openreview.net/forum?id=4XPeF0SbJs.

Zhuoyan Xu, Zhenmei Shi, Junyi Wei, Fangzhou Mu, Yin Li, and Yingyu Liang. Towards few-shot adaptation of foundation models via multitask finetuning. In *The Twelfth International Conference on Learning Representations*, 2024c.

Zhanyuan Yang, Jinghua Wang, and Yingying Zhu. Few-shot classification with contrastive learning. In *European Conference on Computer Vision*. Springer, 2022.

Shunyu Yao, Dian Yu, Jeffrey Zhao, Izhak Shafran, Thomas L. Griffiths, Yuan Cao, and Karthik R Narasimhan. Tree of thoughts: Deliberate problem solving with large language models. In *Thirty-seventh Conference on Neural Information Processing Systems*, 2023.

Jiacheng Ye, Zhiyong Wu, Jiangtao Feng, Tao Yu, and Lingpeng Kong. Compositional exemplars for in-context learning. In Andreas Krause, Emma Brunskill, Kyunghyun Cho, Barbara Engelhardt, Sivan Sabato, and Jonathan Scarlett, editors, *Proceedings of the 40th International Conference on Machine Learning*, volume 202 of *Proceedings of Machine Learning Research*, pages 39818–39833. PMLR, 23–29 Jul 2023.

Zhengqing Yuan, Zhaoxu Li, Weiran Huang, Yanfang Ye, and Lichao Sun. Tinygpt-v: Efficient multimodal large language model via small backbones. *arXiv preprint arXiv:2312.16862*, 2023.

Yuchen Zeng and Kangwook Lee. The expressive power of low-rank adaptation. In *The Twelfth International Conference on Learning Representations*, 2024.

Renrui Zhang, Jiaming Han, Aojun Zhou, Xiangfei Hu, Shilin Yan, Pan Lu, Hongsheng Li, Peng Gao, and Yu Qiao. Llama-adapter: Efficient fine-tuning of language models with zero-init attention. *arXiv preprint arXiv:2303.16199*, 2023a.

Ruiqi Zhang, Spencer Frei, and Peter L Bartlett. Trained transformers learn linear models in-context. *arXiv preprint arXiv:2306.09927*, 2023b.

Tianyi Zhang, Felix Wu, Arzoo Katiyar, Kilian Q Weinberger, and Yoav Artzi. Revisiting few-sample BERT fine-tuning. In *International Conference on Learning Representations*, 2020.

Zeliang Zhang, Phu Pham, Wentian Zhao, Kun Wan, Yu-Jhe Li, Jianing Zhou, Daniel Miranda, Ajinkya Kale, and Chenliang Xu. Treat visual tokens as text? but your mllm only needs fewer efforts to see. *arXiv preprint arXiv:2410.06169*, 2024.

Yulai Zhao, Jianshu Chen, and Simon Du. Blessing of class diversity in pre-training. In *International Conference on Artificial Intelligence and Statistics*. PMLR, 2023.

Zihao Zhao, Eric Wallace, Shi Feng, Dan Klein, and Sameer Singh. Calibrate before use: Improving few-shot performance of language models. In *International Conference on Machine Learning*, pages 12697–12706. PMLR, 2021.

Ruiqi Zhong, Kristy Lee, Zheng Zhang, and Dan Klein. Adapting language models for zero-shot learning by meta-tuning on dataset and prompt collections. In *Findings of the Association for Computational Linguistics: EMNLP 2021*. Association for Computational Linguistics, 2021.

Baichuan Zhou, Ying Hu, Xi Weng, Junlong Jia, Jie Luo, Xien Liu, Ji Wu, and Lei Huang. Tinyllava: A framework of small-scale large multimodal models. *arXiv preprint arXiv:2402.14289*, 2024.

Kaiyang Zhou, Jingkang Yang, Chen Change Loy, and Ziwei Liu. Conditional prompt learning for vision-language models. In *Proceedings of the IEEE/CVF Conference on Computer Vision and Pattern Recognition*, 2022a.

Kaiyang Zhou, Jingkang Yang, Chen Change Loy, and Ziwei Liu. Learning to prompt for vision-language models. *International Journal of Computer Vision*, 2022b.

Deyao Zhu, Jun Chen, Xiaoqian Shen, Xiang Li, and Mohamed Elhoseiny. MiniGPT-4: Enhancing vision-language understanding with advanced large language models. In *The Twelfth International Conference on Learning Representations*, 2024a. URL https://openreview.net/forum?id=1tZbq88f27.

Yichen Zhu, Minjie Zhu, Ning Liu, Zhicai Ou, Xiaofeng Mou, and Jian Tang. Llava-ϕ: Efficient multi-modal assistant with small language model. *arXiv preprint arXiv:2401.02330*, 2024b.

Roland S Zimmermann, Yash Sharma, Steffen Schneider, Matthias Bethge, and Wieland Brendel. Contrastive learning inverts the data generating process. In *International Conference on Machine Learning*. PMLR, 2021.

Chapter 8

Appendix of Chapter 3

In this appendix, we state our limitation in Section 8.1. The proof of our theoretical results for the binary case is presented in Section 8.2, where we formalize the theoretical settings and assumptions and elaborate on the results to contrastive pretraining in Section 8.2.1 and supervised pretraining in Section 8.2.2. We prove the main theory in Section 8.2.4, which is a direct derivative of 8.2.1 and 8.2.2. We generalize the setting to multiclass and provide proof in Section 8.3. We include the full proof of the general linear case study in Section 8.4. We provide additional experimental results of vision tasks in Section 8.5, language tasks in Section 8.6, and vision-language tasks in Sec. 8.7.

8.1 Limitation

We recognize an interesting phenomenon within multitask finetuning and dig into deeper exploration with theoretical analysis, while our experimental results may or may not beat state-of-the-art (SOTA) performance, as our focus is not on presenting multitask finetuning as a novel approach nor on achieving SOTA performance. On the other hand, the estimation of our diversity and consistency parameters accurately on real-world datasets is valuable but time-consuming. Whether there exists an efficient algorithm to estimate these parameters is unknown. We leave this challenging problem as our future work.

8.2 Deferred Proofs

In this section, we provide a formal setting and proof. We first formalize our setting in multiclass. Consider our task $\mathcal{T}$ contains r classes where $r \geq 2$.

Contrastive Learning. In contrastive learning, we sampled one example x from any latent class y, then apply the data augmentation module that randomly transforms such sample into another view of the original example denoted x^+. We also sample other $r-1$ examples $\{x_k^-\}_{k=1}^r$ from other latent classes $\{y_k^-\}_{k=1}^{r-1}$. We treat (x, x^+) as a positive pair and (x, x_k^-) as negative pairs. We define $\mathcal{D}_{\text{con}}(\eta)$ over sample $(x, x^+, x_1^-, \ldots, x_{r-1}^-)$ by following sampling procedure

$$(y, y_1^-, \ldots, y_{r-1}^-) \sim \eta^r \tag{8.1}$$

$$x \sim \mathcal{D}(y),\ x^+ \sim \mathcal{D}(y),\ x_k^- \sim \mathcal{D}(y_k^-), k = 1, \ldots, r-1. \tag{8.2}$$

We consider general contrastive loss $\ell_u\left(\left\{\phi(x)^\top\left(\phi(x^+) - \phi(x_k^-)\right)\right\}_{k=1}^{r-1}\right)$, where loss function ℓ_u is non-negative decreasing function. Minimizing the loss is equivalent to maximizing the similarity between positive pairs while minimizing it between negative pairs. In particular, logistic loss $\ell_u(\boldsymbol{v}) = \log\left(1 + \sum_i \exp\left(-\boldsymbol{v}_i\right)\right)$ for $\boldsymbol{v} \in \mathbb{R}^{r-1}$ recovers the one used in most empirical works: $-\log\left(\frac{\exp\left\{\phi(x)^\top\phi(x^+)\right\}}{\exp\{\phi(x)^\top\phi(x^+)\} + \sum_{i=1}^{r-1}\exp\left\{\phi(x)^\top\phi(x_i^-)\right\}}\right)$. The population contrastive loss is defined as $\mathcal{L}_{con-pre}(\phi) := \mathbb{E}\left[\ell_u\left(\left\{\phi(x)^\top\left(\phi(x^+) - \phi(x_k^-)\right)\right\}_{k=1}^{r-1}\right)\right]$. Let $\mathcal{S}_{con-pre} := \left\{x_j, x_j^+, x_{j1}^-, \ldots, x_{j(r-1)}^-\right\}_{j=1}^N$ denote our contrastive training set with N samples, sampled from $\mathcal{D}_{\text{con}}(\eta)$, we have empirical contrastive loss $\widehat{\mathcal{L}}_{con-pre}(\phi) := \frac{1}{N}\sum_{i=1}^N\left[\ell_u\left(\left\{\phi(x)^\top\left(\phi(x^+) - \phi(x_k^-)\right)\right\}_{k=1}^{r-1}\right)\right]$.

Supervised Learning. In supervised learning we have a labeled dataset denoted as $\mathcal{S}_{con-pre} := \{x_j, y_j\}_{j=1}^N$ with N samples, by following sampling procedure:

$$y \sim \eta \tag{8.3}$$
$$x \sim \mathcal{D}(y). \tag{8.4}$$

There are in total K classes, denote $\mathcal{C}$ as the set consists of all classes. On top of the representation function ϕ, there is a linear function $f \in \mathcal{F} \subset \left\{\mathbb{R}^d \to \mathbb{R}^K\right\}$ predicting the labels, denoted as $g(x) = f \circ \phi(x)$. We consider general supervised loss on data point (x, y) is

$$\ell(g(x), y) := \ell_u \left((g(x))_y - (g(x))_{y' \neq y, y' \in \mathcal{C}}\right). \tag{8.5}$$

where loss function ℓ_u is non-negative decreasing function. In particular, logistic loss $\ell_u(\boldsymbol{v}) = \log\left(1 + \sum_i \exp\left(-\boldsymbol{v}_i\right)\right)$ for $\boldsymbol{v} \in \mathbb{R}^{K-1}$ recovers the one used in most empirical works:

$$\ell(g(x), y) = \ell_u \left((g(x))_y - (g(x))_{y' \neq y, y' \in \mathcal{C}}\right) \tag{8.6}$$
$$= \log\left\{1 + \sum_{k \neq y}^{K} \exp\left(-\left[(g(x))_y - (g(x))_k\right]\right)\right\} \tag{8.7}$$
$$= -\log\left\{\frac{\exp(g(x))_y}{\sum_{k=1}^K \exp(g(x))_k}\right\}. \tag{8.8}$$

The population supervised loss is

$$\mathcal{L}_{sup-pre}(\phi) = \min_{f \in \mathcal{F}} \mathop{\mathbb{E}}_{x,y} \left[\ell\left(f \circ \phi(x), y\right)\right]. \tag{8.9}$$

For training set $\mathcal{S}_{sup-pre} := \{x_i, y_i\}_{i=1}^N$ with N samples, the empirical supervised pretraining loss is $\widehat{\mathcal{L}}_{sup-pre}(\phi) := \min_{f \in \mathcal{F}} \frac{1}{N} \sum_{i=1}^N \left[\ell\left(f \circ \phi(x_i), y_i\right)\right]$.

Masked Language Modeling. Masked language modeling is a self-supervised learning method. It can be viewed as a specific form of supervised pretraining above. The pretraining data is a substantial dataset of sentences, often sourced from Wikipedia. In the pretraining phase, a random selection of words is masked within each sentence, and the training objective is to predict these masked words using the context provided by the remaining words in the sentence. This particular pretraining task can be viewed as a multi-class classification problem, where the number of classes (denoted as K) corresponds to the size of the vocabulary. Considering BERT and its variations, we have function ϕ as a text encoder. This encoder outputs a learned representation, often known as `[CLS]` token. The size of such learned representation is d, which is 768 for $\text{BERT}_{\text{BASE}}$ or 1024 for $\text{BERT}_{\text{LARGE}}$.

Supervised Tasks. Given a representation function ϕ, we apply a task-specific linear transformation W to the representation to obtain the final prediction. Consider r-way supervised task $\mathcal{T}$ consist a set of distinct classes $(y_1, \ldots, y_r) \subseteq \mathcal{C}$. We define $\mathcal{D}_{\mathcal{T}}(y)$ as the distribution of randomly drawing $y \in (y_1, \ldots, y_r)$, we denote this process as $y \sim \mathcal{T}$. Let $\mathcal{S}_{\mathcal{T}} := \{x_j, y_j\}_{j=1}^m$ denote our labeled training set with m samples, sampled i.i.d. from $y_j \sim \mathcal{T}$ and $x_j \sim \mathcal{D}(y_j)$. Define $g(\phi(\mathbf{x})) := W\phi(x) \in \mathbb{R}^r$ as prediction logits, where $W \in \mathbb{R}^{r \times d}$. The typical supervised logistic loss is $\ell(g \circ \phi(x), y) := \ell_u\left(\left\{g(\phi(\mathbf{x}))_y - g(\phi(\mathbf{x}))_{y'}\right\}_{y' \neq y}\right)$. Similar to Arora et al. [2019], define supervised loss w.r.t the task $\mathcal{T}$

$$\mathcal{L}_{sup}(\mathcal{T}, \phi) := \min_{W \in \mathbb{R}^{r \times d}} \mathop{\mathbb{E}}_{y \sim \mathcal{T}} \mathop{\mathbb{E}}_{x \sim \mathcal{D}(y)} \left[\ell\left(W \cdot \phi(x), y\right)\right]. \tag{8.10}$$

Define supervised loss with mean classifier as $\mathcal{L}^{\mu}_{sup}(\mathcal{T}, \phi) := \mathop{\mathbb{E}}_{y \sim \mathcal{T}} \mathop{\mathbb{E}}_{x \sim \mathcal{D}(y)} \left[\ell\left(W^{\mu} \cdot \phi(x), y\right)\right]$ where each row of W^{μ} is the mean of each class in $\mathcal{T}$, $W^{\mu}_{y_k} := \mu_{y_k} = \mathop{\mathbb{E}}_{x \sim y_k}(\phi(x)), k = 1, \ldots, r$. In the target task, suppose we have r distinct classes from $\mathcal{C}$ with equal weights. Consider $\mathcal{T}$ follows a general distribution ζ. Define expected supervised loss as $\mathcal{L}_{sup}(\phi) := \mathop{\mathbb{E}}_{\mathcal{T} \sim \zeta}\left[\mathcal{L}_{sup}(\mathcal{T}, \phi)\right]$.

Mutlitask Finetuning. Suppose we have M auxiliary tasks $\{\mathcal{T}_1, \mathcal{T}_2, \ldots, \mathcal{T}_M\}$, each with m labeled samples $\mathcal{S}_i := \{(x^i_j, y^i_j) : j \in [m]\}$. The finetuning data are $\mathcal{S} := \cup_{i \in [M]} \mathcal{S}_i$. Given a pretrained model $\hat{\phi}$, we further finetune it using

Algorithm 2 Multitask Finetuning

Require: multitasks $\mathcal{T}_1, \ldots, \mathcal{T}_M$, pretrained model $\hat{\phi}$ with parameter θ, step size γ
1: Initialize ϕ with $\hat{\phi}$
2: **repeat**
3: **for all** $\mathcal{T}_i$ **do**
4: $\theta \leftarrow \theta - \gamma \nabla_\theta \widehat{\mathcal{L}}_{sup}(\mathcal{T}_i, \phi)$ { $\widehat{\mathcal{L}}_{sup}(\mathcal{T}_i, \phi)$ is defined in (3.2)}
5: **end for**
6: **until** converge
Ensure: The final model, denoted as ϕ'

the objective:

$$\min_{\phi \in \Phi} \frac{1}{M} \sum_{i=1}^{M} \widehat{\mathcal{L}}_{sup}(\mathcal{T}_i, \phi), \quad \text{where } \widehat{\mathcal{L}}_{sup}(\mathcal{T}_i, \phi) := \min_{\boldsymbol{w}_i \in \mathbb{R}^d} \frac{1}{m} \sum_{j=1}^{m} \ell(\boldsymbol{w}_i^\top \phi(x_j^i), y_j^i). \tag{8.11}$$

This can be done via gradient descent from the initialization $\hat{\phi}$ (see Algorithm 2).

Algorithm 2 has similar pipeline as Raghu et al. [2020] where in the inner loop only a linear layer on top of the embeddings is learned. However, our algorithm is centered on multitask finetuning, where no inner loop is executed.

Finally, we formalize our assumption Assumption 3.3.1 below.

Assumption 8.2.1 (Regularity Conditions)**.** *The following regularity conditions hold:*

- ***(A1)*** *Representation function ϕ satisfies $\|\phi\|_2 \leq R$.*
- ***(A2)*** *Linear operator W satisfies bounded spectral norm $\|W\|_2 \leq B$.*
- ***(A3)*** *The loss function ℓ_u are bounded by $[0, C]$ and $\ell(\cdot)$ is L-Lipschitz.*
- ***(A4)*** *The supervised loss $\mathcal{L}_{sup}(\mathcal{T}, \phi)$ is $\tilde{L}$-Lipschitz with respect to ϕ for $\forall \mathcal{T}$.*

8.2.1 Contrastive Pretraining

In this section, we will show how multitask finetuning improves the model from contrastive pretraining. We present pretraining error in binary classification and $\mathcal{D}_{\mathcal{T}}(y)$ as uniform. See the result for the general condition with multi-class in Section 8.3.

Contrastive Pretraining and Direct Adaptation

In this section, we show the error bound of a foundation model on a target task, where the model is pretrained by contrastive loss followed directly by adaptation.

We first show how pretraining guarantees the expected supervised loss:

$$\mathcal{L}_{sup}(\phi) = \mathop{\mathbb{E}}_{\mathcal{T} \sim \zeta} \left[\mathcal{L}_{sup}(\mathcal{T}, \phi) \right]. \tag{8.12}$$

The error on the target task can be bounded by $\mathcal{L}_{sup}(\phi)$. We use ϵ^* denote $\mathcal{L}_{sup}(\phi_\zeta^*)$.

Lemma 8.2.2 (Lemma 4.3 in Arora et al. [2019])**.** *For $\forall \phi \in \Phi$ pretrained in contrastive loss, we have $\mathcal{L}_{sup}(\phi) \leq \frac{1}{1-\tau}(\mathcal{L}_{con-pre}(\phi) - \tau)$.*

We state the theorem below.

Theorem 8.2.3. *Assume Assumption 3.3.1 and that Φ has ν-diversity and κ-consistency with respect to ϕ^*, ϕ_ζ^*. Suppose $\hat{\phi}$ satisfies $\hat{\mathcal{L}}_{con-pre}(\hat{\phi}) \leq \epsilon_0$. Let $\tau := \Pr_{(y_1, y_2) \sim \eta^2}\{y_1 = y_2\}$. Consider pretraining set $\mathcal{S}_{con-pre} = \left\{x_j, x_j^+, x_j^-\right\}_{j=1}^N$. For any $\delta \geq 0$, if*

$$N \geq \frac{1}{\epsilon_0} \left[8LR\mathcal{R}_N(\Phi) + \frac{8C^2}{\epsilon_0} \log(\frac{2}{\delta}) \right].$$

Then with probability $1-\delta$*, for any target task* $\mathcal{T}_0 \subset \mathcal{C}_0$*,*

$$\mathcal{L}_{sup}(\mathcal{T}_0, \hat{\phi}) - \mathcal{L}_{sup}(\mathcal{T}_0, \phi^*) \leq \frac{1}{\nu}\left[\frac{1}{1-\tau}(2\epsilon_0 - \tau) - \mathcal{L}_{sup}(\phi^*)\right] + \kappa. \tag{8.13}$$

The pretraining sample complexity is $O(\frac{\mathcal{R}_N(\Phi)}{\epsilon_0} + \frac{\log(1/\delta)}{\epsilon_0^2})$. The first term is the Rademacher complexity of the entire representation space Φ with sample size N. The second term relates to the generalization bound. Pretraining typically involves a vast and varied dataset, sample complexity is usually not a significant concern during this stage.

Proof of Theorem 8.2.3. Recall in binary classes, $\mathcal{S}_{con-pre} = \left\{x_j, x_j^+, x_j^-\right\}_{j=1}^N$ denote our contrastive training set, sampled from $\mathcal{D}_{\text{con}}(\eta)$. Then by Lemma A.2 in Arora et al. [2019], with **(A1)** and **(A3)**, we have for $\forall \phi \in \Phi$ with probability $1-\delta$,

$$\mathcal{L}_{con-pre}(\phi) - \widehat{\mathcal{L}}_{con-pre}(\phi) \leq \frac{4LR\mathcal{R}_N(\Phi)}{N} + C\sqrt{\frac{\log\frac{1}{\delta}}{N}}. \tag{8.14}$$

To have above $\leq \epsilon_0$, we have sample complexity

$$N \geq \frac{1}{\epsilon_0}\left[8LR\mathcal{R}_N(\Phi) + \frac{8C^2}{\epsilon_0}\log(\frac{2}{\delta})\right].$$

In pretraining, we have $\hat{\phi}$ such that

$$\hat{\mathcal{L}}_{con-pre}(\hat{\phi}) \leq \epsilon_0.$$

Then with the above sample complexity, we have pretraining $\hat{\phi}$

$$\mathcal{L}_{con-pre}(\hat{\phi}) \leq 2\epsilon_0.$$

Recall ν-diversity and κ-consistency, for target task $\mathcal{T}_0$, we have that for $\hat{\phi}$ and ϕ^*,

$$\begin{aligned}
\mathcal{L}_{sup}(\mathcal{T}_0, \hat{\phi}) - \mathcal{L}_{sup}(\mathcal{T}_0, \phi^*) &= \mathcal{L}_{sup}(\mathcal{T}_0, \hat{\phi}) - \mathcal{L}_{sup}(\mathcal{T}_0, \phi_\zeta^*) + \mathcal{L}_{sup}(\mathcal{T}_0, \phi_\zeta^*) - \mathcal{L}_{sup}(\mathcal{T}_0, \phi^*) && (8.15)\\
&\leq d_{\mathcal{C}_0}(\hat{\phi}, \phi_\zeta^*) + \mathcal{L}_{sup}(\mathcal{T}_0, \phi_\zeta^*) - \mathcal{L}_{sup}(\mathcal{T}_0, \phi^*) && (8.16)\\
&\leq \bar{d}_\zeta(\hat{\phi}, \phi_\zeta^*)/\nu + \kappa && (8.17)\\
&\leq \frac{1}{\nu}\left[\mathcal{L}_{sup}(\hat{\phi}) - \mathcal{L}_{sup}(\phi_\zeta^*)\right] + \kappa && (8.18)\\
&= \frac{1}{\nu}\left[\frac{1}{1-\tau}(\mathcal{L}_{con-pre}(\hat{\phi}) - \tau) - \epsilon^*\right] + \kappa && (8.19)\\
&\leq \frac{1}{\nu}\left[\frac{1}{1-\tau}(2\epsilon_0 - \tau) - \epsilon^*\right] + \kappa, && (8.20)
\end{aligned}$$

where the second to last inequality comes from Theorem 8.2.2. □

Contrastive Pretraining and Multitask Finetuning

In this section, we show the error bound of a foundation model on a target task can be further reduced by multitask finetuning. We achieve this by showing that expected supervised loss $\mathcal{L}_{sup}(\phi)$ can be further reduced after multitask finetuning. The error on the target task can be bounded by $\mathcal{L}_{sup}(\phi)$. We use ϵ^* denote $\mathcal{L}_{sup}(\phi_\zeta^*)$.

Following the intuition in Garg and Liang [2020], we first re-state the definition of representation space.

Definition 8.2.4. *The subset of representation space is*

$$\Phi(\tilde{\epsilon}) = \left\{\phi \in \Phi : \hat{\mathcal{L}}_{pre}(\phi) \leq \tilde{\epsilon}\right\}.$$

Recall $\mathcal{S} = \{(x_j^i, y_j^i) : i \in [M], j \in [m]\}$ as finetuning dataset.

We define two function classes and associated Rademacher complexity.

Definition 8.2.5. *Consider function class*

$$\mathcal{G}_\ell(\tilde{\epsilon}) = \left\{ g_{W,\phi}(x,y) : g_{W,\phi}(x,y) = \ell(W\phi(x_j^i), y_j^i), \phi \in \Phi(\tilde{\epsilon}), \|W\|_2 \le B \right\}.$$

We define Rademacher complexity as

$$\mathcal{R}_n(\mathcal{G}_\ell(\tilde{\epsilon})) = \mathop{\mathbb{E}}_{\{\sigma_i\}_{j=1}^n, \{x_j, y_j\}_{j=1}^n} \left[\sup_{\ell \in \mathcal{G}_\ell(\tilde{\epsilon})} \sum_{j=1}^n \sigma_j \ell(W \cdot \phi(x_j), y_j) \right].$$

Definition 8.2.6. *Consider function class*

$$\mathcal{G}(\tilde{\epsilon}) = \{ g_\phi : g_\phi(\mathcal{T}) = \mathcal{L}_{sup}(T, \phi), \phi \in \Phi(\tilde{\epsilon}) \}.$$

We define Rademacher complexity as

$$\mathcal{R}_M(\mathcal{G}(\tilde{\epsilon})) = \mathop{\mathbb{E}}_{\{\sigma_i\}_{i=1}^M, \{\mathcal{T}_i\}_{i=1}^M} \left[\sup_{\phi \in \Phi(\tilde{\epsilon})} \sum_{i=1}^M \sigma_i \mathcal{L}_{sup}(\mathcal{T}_i, \phi) \right].$$

The key idea is multitask finetuning further reduce the expected supervised loss of a pretrained foundation model ϕ:

$$\mathcal{L}_{sup}(\phi) = \mathop{\mathbb{E}}_{\mathcal{T} \sim \zeta} \left[\mathcal{L}_{sup}(\mathcal{T}, \phi) \right]. \tag{8.21}$$

We first introduce some key lemmas. These lemmas apply to general r classes in a task $\mathcal{T}$.

Lemma 8.2.7 (Bounded Rademacher complexity)**.** *By (A2) and (A3), we have for* $\forall n$

$$\mathcal{R}_n(\mathcal{G}_\ell(\tilde{\epsilon})) \le 4\sqrt{r-1} LB \mathcal{R}_n(\Phi(\tilde{\epsilon})).$$

Proof of Theorem 8.2.7. We first prove $\ell(g(\phi(x)), y)$ is $\sqrt{2(r-1)}LB$-Lipschitz with respect to ϕ for all $\forall y \in \mathcal{C}$. Consider

$$f_y(g(\phi(\mathbf{x}))) = \{ g(\phi(\mathbf{x}))_y - g(\phi(\mathbf{x}))_{y'} \}_{y' \neq y},$$

where $f_y : \mathbb{R}^r \to \mathbb{R}^{r-1}$. Note that

$$\begin{aligned} \ell(g \circ \phi(x), y) &= \ell\left(\{ g(\phi(\mathbf{x}))_y - g(\phi(\mathbf{x}))_{y'} \}_{y' \neq y} \right) \\ &= \ell(f_y(g(\phi(\mathbf{x})))). \end{aligned}$$

By **(A3)**, we have ℓ is L-Lipschitz. We then prove f_y is $\sqrt{2(r-1)}$-Lipschitz. Without loss generality, consider $y = r$. We have $f_y(y) = [y_r - y_i]_{i=1}^{r-1}$. We have $\frac{\partial f_j}{y_i} = -\mathbb{1}\{j = i\}, i = 1, \ldots, r-1$, $\frac{\partial f_j}{y_r} = 1$. The Jacobian J satisfies $\|J\|_2 \le \|J\|_F = \sqrt{2(r-1)}$.

Since g is B-Lipschitz by **(A2)**:$\|W\|_2 \le B$. Then $\ell(g(\phi(x)), y)$ is $\sqrt{2(r-1)}LB$-Lipschitz with respect to ϕ for all $\forall y \in \mathcal{C}$. The conclusion follows Corollary 4 in Maurer [2016]. □

Lemma 8.2.8 (Bounded $\tilde{\epsilon}$)**.** *After finite steps in Multitask finetuning in Algorithm 2, we solve Eq. 3.2 with empirical loss lower than* $\epsilon_1 = \frac{\alpha}{3}\frac{1}{1-\tau}(2\epsilon_0 - \tau)$ *and obtain* ϕ'*. Then there exists a bounded* $\tilde{\epsilon}$ *such that* $\phi' \in \Phi(\tilde{\epsilon})$*.*

Proof of Theorem 8.2.8. Given finite number of steps and finite step size γ in Algorithm 2, we have bounded $\|\phi' - \hat{\phi}\|$. Then with **(A2)** and **(A3)**, using Theorem 8.2.7 we have $\ell(g(\phi(x)), y)$ is $\sqrt{2(r-1)}LB$-Lipschitz with respect to ϕ for all $\forall y$, using theorem A.2 in Arora et al. [2019] we have l_u is LC-Lipschitz with respect to ϕ, we have $\widehat{\mathcal{L}}_{pre}(\phi)$ is M-Lipschitz with respect to ϕ with bounded M. We have $\exists\, \epsilon$ such that $\widehat{\mathcal{L}}_{pre}(\phi') - \widehat{\mathcal{L}}_{pre}(\hat{\phi}) \le \epsilon\|\phi' - \hat{\phi}\|$. We have $\widehat{\mathcal{L}}_{pre}(\phi') \le \epsilon_0 + \epsilon\|\phi' - \hat{\phi}\|$. Take $\tilde{\epsilon} = \epsilon_0 + \epsilon\|\phi' - \hat{\phi}\|$ yields the result. □

Lemma 8.2.9. *Assume Assumption 3.3.1 and that* Φ *has* ν*-diversity and* κ*-consistency with respect to* ϕ^*, ϕ_ζ^**. Suppose for some small constant* $\alpha \in (0,1)$ *and* $\tilde{\epsilon}$*, we solve Eq. 3.2 with empirical loss lower than* $\epsilon_1 = \frac{\alpha}{3}\frac{1}{1-\tau}(2\epsilon_0 - \tau)$ *and obtain* ϕ'*. For any* $\delta > 0$*, if*

$$M \ge \frac{1}{\epsilon_1}\left[4\sqrt{2}\tilde{L}\mathcal{R}_M(\Phi(\tilde{\epsilon})) + \frac{4C^2}{\epsilon_1}\log(\frac{2}{\delta}) \right], Mm \ge \frac{1}{\epsilon_1}\left[8\sqrt{r-1}LB\mathcal{R}_{Mm}(\Phi(\tilde{\epsilon})) + \frac{4C^2}{\epsilon_1}\log(\frac{2}{\delta}) \right],$$

then expected supervised loss $\mathcal{L}_{sup}(\phi') \le \alpha\frac{1}{1-\tau}(2\epsilon_0 - \tau)$*, with probability* $1 - \delta$*.*

Proof of Theorem 8.2.9. Recall $\mathcal{S} := \{(x_j^i, y_j^i) : i \in [M], j \in [m]\}$ as finetuning dataset. Consider in Eq. 3.2 we have $\widehat{\mathbf{W}} := (\widehat{W}_1, \ldots, \widehat{W}_M)$ and ϕ' such that $\frac{1}{M}\sum_{i=1}^M \frac{1}{m}\sum_{j=1}^m \ell(\widehat{W}_i \cdot \phi'(x_j^i), y_j^i) \le \epsilon_1 < \frac{\alpha}{3}\epsilon_0$.

We tried to bound

$$\mathcal{L}_{sup}(\phi') - \frac{1}{m}\sum_{j=1}^m \ell(\widehat{W}_i \cdot \phi'(x_j^i), y_j^i).$$

Recall that

$$\mathcal{L}_{sup}(\mathcal{T}_i, \phi) = \min_{W \in \mathbb{R}^{r\times d}} \mathop{\mathbb{E}}_{y\sim\mathcal{T}_i} \mathop{\mathbb{E}}_{x\sim\mathcal{D}(y)} \left[\ell\left(W \cdot \phi(x), y\right)\right].$$

For $\forall \phi \in \Phi(\tilde{\epsilon})$

$$\mathcal{L}_{sup}(\phi) = \mathbb{E}_{\mathcal{T}\sim\zeta}\left[\mathcal{L}_{sup}(\mathcal{T}, \phi)\right] = \mathbb{E}_{\mathcal{T}\sim\zeta}\left[\min_{W \in \mathbb{R}^{r\times d}} \mathop{\mathbb{E}}_{y\sim\mathcal{T}} \mathop{\mathbb{E}}_{x\sim\mathcal{D}(y)} \left[\ell\left(W \cdot \phi(\mathbf{x}), y\right)\right]\right].$$

We have for $\forall \phi \in \Phi(\tilde{\epsilon})$, by uniform convergence (see Mohri et al. [2018] Theorem 3.3), we have with probability $1 - \delta/2$

$$\mathbb{E}_{\mathcal{T}\sim\zeta}\left[\mathcal{L}_{sup}(\mathcal{T}, \phi)\right] - \frac{1}{M}\sum_{i=1}^M \mathcal{L}_{sup}(\mathcal{T}_i, \phi) \le \frac{2\mathcal{R}_M(\mathcal{G}(\tilde{\epsilon}))}{M} + \sqrt{\frac{\log(2/\delta)}{M}} \tag{8.22}$$

$$\le \frac{2\sqrt{2}\tilde{L}\mathcal{R}_M(\Phi(\tilde{\epsilon}))}{M} + \sqrt{\frac{\log(2/\delta)}{M}}, \tag{8.23}$$

where the last inequality comes from **(A4)** and Corollary 4 in Maurer [2016]. To have above $\le \epsilon_1/2$, we have sample complexity

$$M \ge \frac{1}{\epsilon_1}\left[4\sqrt{2}\tilde{L}\mathcal{R}_M(\Phi(\tilde{\epsilon})) + \frac{4C^2}{\epsilon_1}\log(\frac{2}{\delta})\right].$$

Then we consider generalization bound for $\forall \phi$ and $\mathbf{W} := (W_1, \ldots, W_M)$

$$\mathcal{L}_{sup}(\phi, \mathbf{W}) = \frac{1}{M}\sum_{i=1}^M \mathop{\mathbb{E}}_{y^i\sim\mathcal{T}_i} \mathop{\mathbb{E}}_{x^i\sim\mathcal{D}(y^i)} \ell\left(W_i \cdot \phi(x^i), y^i\right) \tag{8.24}$$

$$\hat{\mathcal{L}}_{sup}(\phi, \mathbf{W}) = \frac{1}{M}\sum_{i=1}^M \frac{1}{m}\sum_{j=1}^m \ell(W_i \cdot \phi(x_j^i), y_j^i), \tag{8.25}$$

where $\mathbf{W} = (W_1, \ldots, W_M)$.

By uniform convergence (see Mohri et al. [2018] Theorem 3.3), we have with probability $1 - \delta/2$,

$$\mathcal{L}_{sup}(\phi, \mathbf{W}) - \hat{\mathcal{L}}_{sup}(\phi, \mathbf{W}) \le \frac{2\mathcal{R}_{Mm}(\mathcal{G}_\ell)}{Mm} + \sqrt{\frac{\log(2/\delta)}{Mm}} \le \frac{8\sqrt{r-1}LB\mathcal{R}_{Mm}(\Phi(\tilde{\epsilon}))}{Mm} + C\sqrt{\frac{\log(2/\delta)}{Mm}},$$

where the last inequality comes from Theorem 8.2.7. To have above $\le \epsilon_1/2$, we have sample complexity

$$Mm \ge \frac{1}{\epsilon_1}\left[8\sqrt{r-1}LB\mathcal{R}_{Mm}(\Phi(\tilde{\epsilon})) + \frac{4C^2}{\epsilon_1}\log(\frac{2}{\delta})\right],$$

satisfying $\forall \phi \in \Phi(\tilde{\epsilon})$

$$\begin{aligned}
\frac{1}{M}\sum_{i=1}^M \mathcal{L}_{sup}(\mathcal{T}_i, \phi) &= \frac{1}{M}\sum_{i=1}^M \min_{W \in \mathbb{R}^{r\times d}} \mathop{\mathbb{E}}_{y\sim\mathcal{T}_i} \mathop{\mathbb{E}}_{x\sim\mathcal{D}(y)} \left[\ell\left(W \cdot \phi(x), y\right)\right] \\
&\le \frac{1}{M}\sum_{i=1}^M \mathop{\mathbb{E}}_{y\sim\mathcal{T}_i} \mathop{\mathbb{E}}_{x\sim\mathcal{D}(y)} \left[\ell\left(\widehat{W}_i \cdot \phi(x), y\right)\right] \\
&= \mathcal{L}_{sup}(\phi, \widehat{\mathbf{W}}) \\
&\le \hat{\mathcal{L}}_{sup}(\phi, \widehat{\mathbf{W}}) + \epsilon_1/2.
\end{aligned}$$

Then combine above with Eq. 8.22

$$\begin{aligned}\mathcal{L}_{sup}(\phi) &= \mathop{\mathbb{E}}_{\mathcal{T}\sim\zeta}\left[\mathcal{L}_{sup}(\mathcal{T},\phi)\right] \\ &\le \hat{\mathcal{L}}_{sup}(\phi,\widehat{\mathbf{W}}) + \epsilon_1.\end{aligned}$$

We have

$$\mathcal{L}_{sup}(\phi') - \frac{1}{m}\sum_{j=1}^{m}\ell(\widehat{W}_i\cdot\phi'(x_j^i), y_j^i) \le \epsilon_1$$

$$\mathcal{L}_{sup}(\phi') \le 2\epsilon_1 \le \alpha\frac{1}{1-\tau}(2\epsilon_0-\tau).$$

The boundedness of $\tilde{\epsilon}$ follows Theorem 8.2.8. □

We state the theorem below.

Theorem 8.2.10. *Assume Assumption 3.3.1 and that Φ has ν-diversity and κ-consistency with respect to ϕ^*, ϕ_ζ^*. Suppose for some small constant $\alpha\in(0,1)$, we solve Eq. 3.2 with empirical loss lower than $\epsilon_1 = \frac{\alpha}{3}\frac{1}{1-\tau}(2\epsilon_0-\tau)$ and obtain ϕ'. For any $\delta>0$, if*

$$M \ge \frac{1}{\epsilon_1}\left[4\sqrt{2}\tilde{L}\mathcal{R}_M(\Phi(\tilde{\epsilon})) + \frac{4C^2}{\epsilon_1}\log(\frac{2}{\delta})\right], Mm \ge \frac{1}{\epsilon_1}\left[8LB\mathcal{R}_{Mm}(\Phi(\tilde{\epsilon})) + \frac{4C^2}{\epsilon_1}\log(\frac{2}{\delta})\right],$$

then with probability $1-\delta$, for any target task $\mathcal{T}_0\subseteq\mathcal{C}_0$,

$$\mathcal{L}_{sup}(\mathcal{T}_0,\phi') - \mathcal{L}_{sup}(\mathcal{T}_0,\phi^*) \le \frac{1}{\nu}\left[\alpha\frac{1}{1-\tau}(2\epsilon_0-\tau) - \mathcal{L}_{sup}(\phi_\zeta^*)\right] + \kappa. \tag{8.26}$$

Proof of Theorem 8.2.10. Recall with ν-diversity and κ-consistency with respect to ϕ^*, ϕ_ζ^*, for target task $\mathcal{T}_0$, we have that for ϕ' and ϕ^*,

$$\begin{aligned}\mathcal{L}_{sup}(\mathcal{T}_0,\phi') - \mathcal{L}_{sup}(\mathcal{T}_0,\phi^*) &= \mathcal{L}_{sup}(\mathcal{T}_0,\phi') - \mathcal{L}_{sup}(\mathcal{T}_0,\phi_\zeta^*) + \mathcal{L}_{sup}(\mathcal{T}_0,\phi_\zeta^*) - \mathcal{L}_{sup}(\mathcal{T}_0,\phi^*) \\ &\le \frac{1}{\nu}\bar{d}_\zeta(\phi',\phi_\zeta^*) + \kappa \\ &\le \frac{1}{\nu}\left[\mathcal{L}_{sup}(\phi') - \mathcal{L}_{sup}(\phi_\zeta^*)\right] + \kappa \\ &\le \frac{1}{\nu}\left[\alpha\frac{1}{1-\tau}(2\epsilon_0-\tau) - \epsilon^*\right] + \kappa,\end{aligned}$$

where the last inequality comes from Theorem 8.2.9, where taking $r=2$. □

8.2.2 Supervised Pretraining

In this section, we will show how multitask finetuning improves the model from supervised pretraining. We present pretraining error in binary classification and $\mathcal{D}_\mathcal{T}(y)$ as uniform. See the result for the general condition with multi-class in Section 8.3.

Supervised Pretraining and Direct Adaptation

In this section, we show the error bound of a foundation model on a target task, where the model is pretrained by supervised loss followed directly by adaptation. For general $y\sim\eta$. Let $p_i := \Pr_{y\sim\eta}\{y=y_i\}$, where $\sum_{i=1}^K p_i = 1$.

Lemma 8.2.11. *Suppose $y\sim\eta$ and $l \le \Pr_{y\sim\eta}\{y=y_i\} \le u$. Consider a task $\mathcal{T}$ containing r classes, which is a subset of the total class set $\mathcal{C}$. We have $\forall\phi\in\Phi$,*

$$\mathcal{L}_{sup}(\phi) \le \left(\frac{u}{l}\right)^r \mathcal{L}_{sup-pre}(\phi),$$

where

$$\mathcal{L}_{sup-pre}(\phi) = \min_{f\in\mathcal{F}}\mathop{\mathbb{E}}_{x,y}\left[\ell\left(f\circ\phi(x),y\right)\right]. \tag{8.27}$$

Proof of Section 8.2.2. We first prove $r = 3$, where $\mathcal{T} = \{y_1, y_2, y_3\}$. Then in supervised pretraining, we have:

$$\mathcal{L}_{sup-pre}(\phi) = \min_{f \in \mathcal{F}} \mathop{\mathbb{E}}_{y \sim \mathcal{T}} \mathop{\mathbb{E}}_{x \sim y} \left[\ell\left(f \circ \phi(x), y\right)\right]. \tag{8.28}$$

Let $f = (f_1, f_2, f_3)^\top$ be the best linear classifier on top of ϕ, the prediction logits are $g(x) = f \circ \phi(x) = (g_1(x), g_2(x), g_3(x))^\top$. Then we have:

$$\mathop{\mathbb{E}}_{x \sim y_1} \left[\ell\left(g \circ \phi(x), y\right)\right] = -\log \frac{\exp(g_1(x))}{\sum_{k=1}^3 \exp(g_k(x))}.$$

We let $y_k(x) = \exp(g_k(x)), k = 1, 2, 3$. Then

$$\begin{aligned}
&\mathcal{L}_{sup-pre}(\phi) \\
=&-\left[p_1 \mathop{\mathbb{E}}_{x \sim y_1}\left(\log \frac{y_1(x)}{\sum_{k=1}^3 y_k(x)}\right) + p_2 \mathop{\mathbb{E}}_{x \sim y_2}\left(\log \frac{y_2(x)}{\sum_{k=1}^3 y_k(x)}\right) + p_3 \mathop{\mathbb{E}}_{x \sim y_3}\left(\log \frac{y_3(x)}{\sum_{k=1}^3 y_k(x)}\right)\right] \\
=&p_1 \mathop{\mathbb{E}}_{x \sim y_1}\left(\log \frac{\sum_{k=1}^3 y_k(x)}{y_1(x)}\right) + p_2 \mathop{\mathbb{E}}_{x \sim y_2}\left(\log \frac{\sum_{k=1}^3 y_k(x)}{y_2(x)}\right) + p_3 \mathop{\mathbb{E}}_{x \sim y_3}\left(\log \frac{\sum_{k=1}^3 y_k(x)}{y_3(x)}\right).
\end{aligned}$$

Recall

$$\mathcal{L}_{sup}(\mathcal{T}, \phi) := \min_{\boldsymbol{w}} \mathop{\mathbb{E}}_{y \sim \mathcal{T}} \mathop{\mathbb{E}}_{x \sim \mathcal{D}(y)} \left[\ell\left(\boldsymbol{w}^\top \phi(x), y\right)\right]. \tag{8.29}$$

Consider

$$\mathcal{L}^*_{sup}(\mathcal{T}, \phi) := \mathop{\mathbb{E}}_{y \sim \mathcal{T}} \mathop{\mathbb{E}}_{x \sim \mathcal{D}(y)} \left[\ell\left(\boldsymbol{w}^\top \phi(x), y\right)\right], \tag{8.30}$$

where $\boldsymbol{w}$ is the corresponding sub-vector of f according to task (for e.g., $\boldsymbol{w} = (f_1, f_2)^\top$ if $\mathcal{T} = \{y_1, y_2\}$). Then we have

$$\begin{aligned}
\mathcal{L}^*_{sup}(\mathcal{T}, \phi) =& -\frac{p_1 p_2}{p_1 p_2 + p_1 p_3 + p_2 p_3} \cdot \frac{1}{2}\left[\mathop{\mathbb{E}}_{x \sim y_1}\left(\log \frac{y_1(x)}{y_1(x) + y_2(x)}\right) + \mathop{\mathbb{E}}_{x \sim y_2}\left(\log \frac{y_2(x)}{y_1(x) + y_2(x)}\right)\right] \\
&-\frac{p_1 p_3}{p_1 p_2 + p_1 p_3 + p_2 p_3} \cdot \frac{1}{2}\left[\mathop{\mathbb{E}}_{x \sim y_1}\left(\log \frac{y_1(x)}{y_1(x) + y_3(x)}\right) + \mathop{\mathbb{E}}_{x \sim y_3}\left(\log \frac{y_3(x)}{y_1(x) + y_3(x)}\right)\right] \\
&-\frac{p_2 p_3}{p_1 p_2 + p_1 p_3 + p_2 p_3} \cdot \frac{1}{2}\left[\mathop{\mathbb{E}}_{x \sim y_2}\left(\log \frac{y_2(x)}{y_2(x) + y_3(x)}\right) + \mathop{\mathbb{E}}_{x \sim y_3}\left(\log \frac{y_3(x)}{y_2(x) + y_3(x)}\right)\right] \\
=&\frac{p_1 p_2}{p_1 p_2 + p_1 p_3 + p_2 p_3} \cdot \frac{1}{2}\left[\mathop{\mathbb{E}}_{x \sim y_1}\left(\log \frac{y_1(x) + y_2(x)}{y_1(x)}\right) + \mathop{\mathbb{E}}_{x \sim y_2}\left(\log \frac{y_1(x) + y_2(x)}{y_2(x)}\right)\right] \\
&\frac{p_1 p_3}{p_1 p_2 + p_1 p_3 + p_2 p_3} \cdot \frac{1}{2}\left[\mathop{\mathbb{E}}_{x \sim y_1}\left(\log \frac{y_1(x) + y_3(x)}{y_1(x)}\right) + \mathop{\mathbb{E}}_{x \sim y_3}\left(\log \frac{y_1(x) + y_3(x)}{y_3(x)}\right)\right] \\
&\frac{p_2 p_3}{p_1 p_2 + p_1 p_3 + p_2 p_3} \cdot \frac{1}{2}\left[\mathop{\mathbb{E}}_{x \sim y_2}\left(\log \frac{y_2(x) + y_3(x)}{y_2(x)}\right) + \mathop{\mathbb{E}}_{x \sim y_3}\left(\log \frac{y_2(x) + y_3(x)}{y_3(x)}\right)\right].
\end{aligned}$$

By observing the terms with $y_1(x)$ as denominator (similar as $y_2(x), y_3(x)$), we want to prove:

$$p_1 \left(\frac{u}{l}\right)^2 \geq \frac{1}{2}\left(\frac{p_1 p_2 + p_1 p_3}{p_1 p_2 + p_1 p_3 + p_2 p_3}\right).$$

This obtained by $\left(\frac{u}{l}\right)^2 \geq \frac{1}{3}\frac{u}{l^2}$.

We have

$$\mathcal{L}^*_{sup}(\mathcal{T}, \phi) \leq \left(\frac{u}{l}\right)^2 \mathcal{L}_{sup-pre}(\phi).$$

For the general K-class setting, we follow similar steps, we have

$$\mathcal{L}_{sup-pre}(\phi) = -\left[\sum_{i=1}^r p_i \mathop{\mathbb{E}}_{x \sim y_i}\left(\log \frac{y_i(x)}{\sum_{k=1}^K y_k(x)}\right)\right].$$

We denote J as all possible r product of $p_i \in \{p_1, \ldots, p_K\}$, $J = \{p_1 \cdots p_r, \ldots\}$. Similarly, we have

$$\mathcal{L}^*_{sup}(\mathcal{T}, \phi) = -\frac{1}{r}\left\{\sum_{\mathcal{T}\subsetneq\mathcal{C}}\left[\frac{\prod_{i\in\mathcal{T}} p_i}{J}\sum_{i\in\mathcal{T}}\mathop{\mathbb{E}}_{x\sim y_i}\left(\log\frac{y_i(x)}{\sum_{j\in\mathcal{T}} y_j(x)}\right)\right]\right\}$$

where $\mathcal{T}$ are all tasks with r classes. By observing, inside the summation there are in total $\binom{K-1}{r-1}$ terms with $y_1(x)$ as the numerator, where corresponding probability is

$$\frac{p_1\prod_{i\in\mathcal{T}, i\neq 1} p_i}{J},$$

where each term can be upper bounded by $-\left(\frac{u}{l}\right)^r p_1 \mathop{\mathbb{E}}_{x\sim y_i}\left(\log\frac{y_i(x)}{\sum_{k=1}^K y_k(x)}\right)$ (similar as $y_j(x), j \in \mathcal{T}$). □

We state the theorem below.

Theorem 8.2.12. *Assume Assumption 3.3.1 and that Φ has ν-diversity and κ-consistency with respect to ϕ^*, ϕ^*_ζ. Suppose $\hat{\phi}$ satisfies $\hat{\mathcal{L}}_{sup-pre}(\hat{\phi}) \le \epsilon_0$. Let $p_i := \Pr_{y\sim\eta}\{y = y_i\}$, where $\sum_{i=1}^K p_i = 1$. Let $\rho := \frac{\max_i p_i}{\min_j p_j}$. Consider pretraining set $\mathcal{S}_{sup-pre} := \{x_i, y_i\}_{i=1}^N$, for any $\delta \ge 0$, if*

$$N \ge \frac{1}{\epsilon_0}\left[8LR\sqrt{K}\mathcal{R}_N(\Phi) + \frac{8C^2}{\epsilon_0}\log(\frac{2}{\delta})\right].$$

Then with probability $1-\delta$, for any target task $\mathcal{T}_0 \subset \mathcal{C}_0$,

$$\mathcal{L}_{sup}(\mathcal{T}_0, \hat{\phi}) - \mathcal{L}_{sup}(\mathcal{T}_0, \phi^*) \le \frac{1}{\nu}\left[2\rho^2\epsilon_0 - \epsilon^*\right] + \kappa. \tag{8.31}$$

Proof of Theorem 8.2.12. The proof follows similar steps in Theorem 8.2.3. For supervised pretraining, the sample complexity is similar to Theorem 8.2.3, note that there is an extra $\sqrt{K}$ term. We show how we have this term below:

Consider function class

$$\mathcal{G}_\ell = \left\{g_{W,\phi}(x,y) : g_{W,\phi}(x,y) = \ell(W^\top\phi(x^i_j), y^i_j), \phi \in \Phi, \|W\|_2 \le B\right\}.$$

The Rademacher complexity is

$$\mathcal{R}_n(\mathcal{G}_\ell) = \mathop{\mathbb{E}}_{\{\sigma_i\}_{j=1}^n, \{x_j, y_j\}_{j=1}^n}\left[\sup_{\ell\in\mathcal{G}_\ell}\sum_{j=1}^n \sigma_j \ell(W\cdot\phi(x_j), y_j)\right].$$

Then from Theorem 8.2.7, the pretraining is a large task with classification among K classes.

$$\mathcal{R}_n(\mathcal{G}_\ell) \le 4\sqrt{K}LB\mathcal{R}_n(\Phi).$$

Then by Theorem 3.3 in Mohri et al. [2018], with **(A1)** and **(A3)**, we have for $\forall\phi \in \Phi$ with probability $1-\delta$,

$$\mathcal{L}_{sup-pre}(\phi) - \widehat{\mathcal{L}}_{sup-pre}(\phi) \le \frac{4LR\sqrt{K}\mathcal{R}_N(\Phi)}{N} + C\sqrt{\frac{\log\frac{1}{\delta}}{N}}. \tag{8.32}$$

To have above $\le \epsilon_0$, we have sample complexity

$$N \ge \frac{1}{\epsilon_0}\left[8LR\sqrt{K}\mathcal{R}_N(\Phi) + \frac{8C^2}{\epsilon_0}\log(\frac{2}{\delta})\right].$$

With the above sample complexity of $\mathcal{S}_{sup-pre} = \{x_i, y_i\}_{i=1}^N$, we have pretraining $\hat{\phi}$

$$\mathcal{L}_{sup-pre}(\hat{\phi}) \le 2\epsilon_0.$$

Recall ν-diversity and κ-consistency, with respect to ϕ^*, ϕ^*_ζ, for target task $\mathcal{T}_0$, we have that for $\hat{\phi}$ and ϕ^*,

$$\mathcal{L}_{sup}(\mathcal{T}_0, \hat{\phi}) - \mathcal{L}_{sup}(\mathcal{T}_0, \phi^*) \leq d_{\mathcal{C}_0}(\hat{\phi}, \phi_\zeta^*) + \mathcal{L}_{sup}(\mathcal{T}_0, \phi_\zeta^*) - \mathcal{L}_{sup}(\mathcal{T}_0, \phi^*) \tag{8.33}$$
$$\leq \bar{d}_\zeta(\hat{\phi}, \phi_\zeta^*)/\nu + \kappa \tag{8.34}$$
$$\leq \frac{1}{\nu}\left[\mathcal{L}_{sup}(\hat{\phi}) - \mathcal{L}_{sup}(\phi_\zeta^*)\right] + \kappa \tag{8.35}$$
$$\leq \frac{1}{\nu}\left[\rho^2 \mathcal{L}_{sup-pre}(\hat{\phi}) - \epsilon^*\right] + \kappa \tag{8.36}$$
$$\leq \frac{1}{\nu}\left[2\rho^2\epsilon_0 - \epsilon^*\right] + \kappa \tag{8.37}$$

where the second to last inequality comes from Theorem 8.2.11.

□

Supervised Pretraining and Multitask Finetuning

In this section, we show the error bound of a supervised pretrained foundation model on a target task can be further reduced by multitask finetuning. We follow similar steps in Section 8.2.1. Recall Definition 8.2.4, similar to Theorem 8.2.9, we introduce the following lemma under supervised pretraining loss.

Lemma 8.2.13. *Assume Assumption 3.3.1 and that Φ has (ν, ϵ)-diversity for ζ and $\mathcal{C}_0$. Suppose for some small constant $\alpha \in (0, 1)$, we solve Eq. 3.2 with empirical loss lower than $\epsilon_1 = \frac{\alpha}{3} 2\rho^2\epsilon_0$ and obtain ϕ'. For any $\delta > 0$, if*

$$M \geq \frac{1}{\epsilon_1}\left[4\sqrt{2}\tilde{L}\mathcal{R}_M(\Phi(\tilde{\epsilon})) + \frac{4C^2}{\epsilon_1}\log(\frac{2}{\delta})\right], Mm \geq \frac{1}{\epsilon_1}\left[16LB\mathcal{R}_{Mm}(\Phi(\tilde{\epsilon})) + \frac{4C^2}{\epsilon_1}\log(\frac{2}{\delta})\right],$$

then expected supervised loss $\mathcal{L}_{sup}(\phi') \leq 2\alpha\rho^2\epsilon_0$, with probability $1 - \delta$.

Proof of Theorem 8.2.13. The steps follow similar steps in Theorem 8.2.9. □

We state the main theorem below.

Theorem 8.2.14. *Assume Assumption 3.3.1 and that Φ has (ν, ϵ)-diversity for ζ and $\mathcal{C}_0$. Suppose for some small constant $\alpha \in (0, 1)$, we solve Eq. 3.2 with empirical loss lower than $\epsilon_1 = \frac{\alpha}{3} 2\rho^2\epsilon_0$ and obtain ϕ'. For any $\delta > 0$, if*

$$M \geq \frac{1}{\epsilon_1}\left[4\sqrt{2}\tilde{L}\mathcal{R}_M(\Phi(\tilde{\epsilon})) + \frac{4C^2}{\epsilon_1}\log(\frac{2}{\delta})\right], Mm \geq \frac{1}{\epsilon_1}\left[16LB\mathcal{R}_{Mm}(\Phi(\tilde{\epsilon})) + \frac{4C^2}{\epsilon_1}\log(\frac{2}{\delta})\right],$$

then with probability $1 - \delta$, for any target task $\mathcal{T}_0 \subseteq \mathcal{C}_0$,

$$\mathcal{L}_{sup}(\mathcal{T}_0, \phi') - \mathcal{L}_{sup}(\mathcal{T}_0, \phi^*) \leq \frac{1}{\nu}\left(2\alpha\rho^2\epsilon_0 - \mathcal{L}_{sup}(\phi^*)\right) + \epsilon. \tag{8.38}$$

Proof of Theorem 8.2.14. Recall ν-diversity and κ-consistency, with respect to ϕ^*, ϕ_ζ^*, for target task $\mathcal{T}_0$, we have that for $\hat{\phi}$ and ϕ^*,

$$\mathcal{L}_{sup}(\mathcal{T}_0, \phi') - \mathcal{L}_{sup}(\mathcal{T}_0, \phi^*) \leq d_{\mathcal{C}_0}(\phi', \phi_\zeta^*) + \mathcal{L}_{sup}(\mathcal{T}_0, \phi_\zeta^*) - \mathcal{L}_{sup}(\mathcal{T}_0, \phi^*) \tag{8.39}$$
$$\leq \bar{d}_\zeta(\phi', \phi_\zeta^*)/\nu + \kappa \tag{8.40}$$
$$\leq \frac{1}{\nu}\left[\mathcal{L}_{sup}(\phi') - \mathcal{L}_{sup}(\phi_\zeta^*)\right] + \kappa \tag{8.41}$$
$$\leq \frac{1}{\nu}\left(2\alpha\rho^2\epsilon_0 - \epsilon^*\right) + \kappa, \tag{8.42}$$

where the last inequality comes from Theorem 8.2.13.

□

8.2.3 Masked Language Pretraining

The theoretical guarantee in masked language pretraining follows the same error bound in supervised pretraining, with K representing the size of the vocabulary.

8.2.4 Unified Main Theory

We now prove the main theory below. We first re-state the theorem.

Theorem 3.3.4. (No Multitask Finetuning) *Assume Assumption 3.3.1 and that Φ has ν-diversity and κ-consistency with respect to ϕ^* and ϕ_ζ^*. Suppose $\hat{\phi}$ satisfies $\hat{\mathcal{L}}_{pre}(\hat{\phi}) \le \epsilon_0$. Let $\tau := \Pr_{(y_1,y_2)\sim\eta^2}\{y_1 = y_2\}$. Then for any target task $\mathcal{T}_0 \subseteq \mathcal{C}_0$,*

$$\mathcal{L}_{sup}(\mathcal{T}_0, \hat{\phi}) - \mathcal{L}_{sup}(\mathcal{T}_0, \phi^*) \le \frac{1}{\nu}\left[\frac{2\epsilon_0}{1-\tau} - \mathcal{L}_{sup}(\phi_\zeta^*)\right] + \kappa. \tag{3.3}$$

Proof of Theorem 3.3.4. The result is a direct combination of Theorem 8.2.3 and Theorem 8.2.12. □

Theorem 3.3.5. (With Multitask Finetuning) *Assume Assumption 3.3.1 and that Φ has ν-diversity and κ-consistency with respect to ϕ^* and ϕ_ζ^*. Suppose for some constant $\alpha \in (0,1)$, we solve Eq. 3.2 with empirical loss lower than $\epsilon_1 = \frac{\alpha}{3}\frac{2\epsilon_0}{1-\tau}$ and obtain ϕ'. For any $\delta > 0$, if for $\tilde{\epsilon} = \widehat{\mathcal{L}}_{pre}(\phi')$,*

$$M \ge \frac{1}{\epsilon_1}\left[4\sqrt{2}\tilde{L}\mathcal{R}_M(\Phi(\tilde{\epsilon})) + \frac{4C^2}{\epsilon_1}\log(\frac{2}{\delta})\right], Mm \ge \frac{1}{\epsilon_1}\left[16LB\mathcal{R}_{Mm}(\Phi(\tilde{\epsilon})) + \frac{4C^2}{\epsilon_1}\log(\frac{2}{\delta})\right],$$

then with probability $1-\delta$, for any target task $\mathcal{T}_0 \subseteq \mathcal{C}_0$,

$$\mathcal{L}_{sup}(\mathcal{T}_0, \phi') - \mathcal{L}_{sup}(\mathcal{T}_0, \phi^*) \le \frac{1}{\nu}\left[\alpha\frac{2\epsilon_0}{1-\tau} - \mathcal{L}_{sup}(\phi_\zeta^*)\right] + \kappa. \tag{3.4}$$

Proof of Theorem 3.3.5. Follow the similar steps in proof of Theorem 8.2.9, we have

$$\mathcal{L}_{sup}(\phi') \le 2\epsilon_1 \le \alpha\frac{2\rho^2}{1-\tau}\epsilon_0.$$

Recall ν-diversity and κ-consistency, with respect to ϕ^*, ϕ_ζ^*, for target task $\mathcal{T}_0$, we have that for ϕ' and ϕ^*,

$$\begin{aligned}
\mathcal{L}_{sup}(\mathcal{T}_0, \phi') - \mathcal{L}_{sup}(\mathcal{T}_0, \phi^*) &\le d_{\mathcal{C}_0}(\phi', \phi_\zeta^*) + \mathcal{L}_{sup}(\mathcal{T}_0, \phi_\zeta^*) - \mathcal{L}_{sup}(\mathcal{T}_0, \phi^*) && (8.43)\\
&\le \bar{d}_\zeta(\phi', \phi_\zeta^*)/\nu + \kappa && (8.44)\\
&\le \frac{1}{\nu}\left[\mathcal{L}_{sup}(\phi') - \mathcal{L}_{sup}(\phi_\zeta^*)\right] + \kappa && (8.45)\\
&\le \frac{1}{\nu}\left[\alpha\frac{2\rho^2}{1-\tau}\epsilon_0 - \epsilon^*\right] + \kappa. && (8.46)
\end{aligned}$$

□

The sample complexity of finetuning depends on $\tilde{\epsilon} = \widehat{\mathcal{L}}_{pre}(\phi')$. Below we show that $\tilde{\epsilon}$ can be upper bounded in finite step finetuning.

Lemma 8.2.15 (Bounded $\tilde{\epsilon}$)**.** *After finite steps in Multitask finetuning in Algorithm 2, we solve Eq. 3.2 with empirical loss lower than $\epsilon_1 = \frac{\alpha}{3}\frac{1}{1-\tau}(2\epsilon_0 - \tau)$ and obtain ϕ'. Then there exists a bounded $\tilde{\epsilon}$ such that $\phi' \in \Phi(\tilde{\epsilon})$.*

Proof of Theorem 8.2.15. Given finite number of steps and finite step size γ in Algorithm 2, we have bounded $\|\phi' - \hat{\phi}\|$. Then with **(A2)** and **(A3)**, using Theorem 8.2.7 and lemma A.3 in Arora et al. [2019], we have $\widehat{\mathcal{L}}_{pre}(\phi)$ is M-Lipschitz with respect to ϕ with bounded M. We have $\exists\ \epsilon$ such that $\widehat{\mathcal{L}}_{pre}(\phi') - \widehat{\mathcal{L}}_{pre}(\hat{\phi}) \le \epsilon\|\phi' - \hat{\phi}\|$. We have $\widehat{\mathcal{L}}_{pre}(\phi') \le \epsilon_0 + \epsilon\|\phi' - \hat{\phi}\|$. Take $\tilde{\epsilon} = \epsilon_0 + \epsilon\|\phi' - \hat{\phi}\|$ yields the result. □

8.2.5 Bounded Task Loss by Task Diversity

By the previous lemma and claim, we have the below corollary.

Corollary 8.2.16. *Suppose we have ϕ in pretraining: for $\forall \phi \in \Phi$, $\mathcal{L}_{sup}(\phi) \leq \frac{1}{1-\tau}\left(\frac{u}{l}\right)^r \mathcal{L}_{pre}(\phi)$, where $\mathcal{L}_{pre}(\phi)$ is $\mathcal{L}_{con-pre}(\phi)$ if contrastive learning and $\mathcal{L}_{sup-pre}(\phi)$ if supervised learning.*

Consider $\rho = \frac{u}{l}$ and Theorem 8.2.16,

Recall ν-diversity and κ-consistency, with respect to ϕ^*, ϕ_ζ^*, for target task $\mathcal{T}_0$, we have that for $\hat{\phi}$ and ϕ^*,

$$\begin{aligned}
\mathcal{L}_{sup}(\mathcal{T}_0, \hat{\phi}) - \mathcal{L}_{sup}(\mathcal{T}_0, \phi^*) &\leq d_{\mathcal{C}_0}(\hat{\phi}, \phi_\zeta^*) + \mathcal{L}_{sup}(\mathcal{T}_0, \phi_\zeta^*) - \mathcal{L}_{sup}(\mathcal{T}_0, \phi^*) && (8.47)\\
&\leq \bar{d}_\zeta(\hat{\phi}, \phi_\zeta^*)/\nu + \kappa && (8.48)\\
&\leq \frac{1}{\nu}\left[\mathcal{L}_{sup}(\hat{\phi}) - \mathcal{L}_{sup}(\phi_\zeta^*)\right] + \kappa && (8.49)\\
&\leq \frac{1}{\nu}\left[\frac{\rho^r}{1-\tau}\mathcal{L}_{pre}(\hat{\phi}) - \mathcal{L}_{sup}(\phi^*)\right] + \kappa. && (8.50)
\end{aligned}$$

8.3 Multi-class Classification

In this section, we provide a general result for multi-classes.

8.3.1 Contrastive Pretraining

Lemma 8.3.1 (Theorem 6.1 in Arora et al. [2019])**.** *For multi-classes, we have*

$$\mathcal{L}_{sup}(\phi) \leq \mathcal{L}_{sup}^{\mu}(\phi) \leq \frac{1}{1-\tau_r}\mathcal{L}_{con-pre}(\phi), \tag{8.51}$$

where $\tau_r = \mathop{\mathbb{E}}_{(y, y_1^-, \ldots, y_{r-1}^-) \sim \eta^r} \mathbb{1}\{y \text{ does not appear in } (y_1^-, \ldots, y_{r-1}^-)\}$.

Proof of Theorem 8.3.1. The proof of Theorem 8.3.1 follows the first two steps in the proof of Theorem B.1 of Arora et al. [2019]. we denote distribution of $y \sim \mathcal{T}$ as $\mathcal{D}_{\mathcal{T}}(y)$ and it's uniform distribution. □

We first provide contrastive pretraining error similar to Theorem 8.2.3 in a multiclass setting.

Theorem 8.3.2. *Assume Assumption 3.3.1 and that Φ has ν-diversity and κ-consistency with respect to ϕ^*, ϕ_ζ^*. Suppose $\hat{\phi}$ satisfies $\hat{\mathcal{L}}_{con-pre}(\hat{\phi}) \leq \epsilon_0$. Consider a pretraining set $\mathcal{S}_{un} = \left\{x_j, x_j^+, x_{j1}^-, \ldots, x_{j(r-1)}\right\}_{j=1}^N$. For target task $\mathcal{T}_0$, with sample complexity*

$$N \geq \frac{1}{\epsilon_0}\left[8LR\sqrt{r-1}\mathcal{R}_N(\Phi) + \frac{8C^2}{\epsilon_0}\log(\frac{2}{\delta})\right],$$

it's sufficient to learn an $\hat{\phi}$ with classification error $\mathcal{L}_{sup}(\mathcal{T}_0, \hat{\phi}) - \mathcal{L}_{sup}(\mathcal{T}_0, \phi^*) \leq \frac{1}{\nu}\left[\frac{2}{1-\tau_r}\epsilon_0 - \epsilon^*\right] + \epsilon$, with probability $1-\delta$.

Proof of Theorem 8.3.2. Following similar step of proof of Theorem 8.2.3, we have with

$$N \geq \frac{1}{\epsilon_0}\left[8LR\sqrt{r-1}\mathcal{R}_N(\Phi) + \frac{8C^2}{\epsilon_0}\log(\frac{2}{\delta})\right].$$

Then pretraining $\hat{\phi}$

$$\mathcal{L}_{con-pre}(\hat{\phi}) \leq 2\epsilon_0.$$

Recall ν-diversity and κ-consistency, for target task $\mathcal{T}_0$, we have that for $\hat{\phi}$ and ϕ^*,

$$\mathcal{L}_{sup}(\mathcal{T}_0, \hat{\phi}) - \mathcal{L}_{sup}(\mathcal{T}_0, \phi^*) \leq \bar{d}_\zeta(\hat{\phi}, \phi_\zeta^*)/\nu + \kappa \tag{8.52}$$

$$\leq \frac{1}{\nu}\left[\mathcal{L}_{sup}(\hat{\phi}) - \mathcal{L}_{sup}(\phi_\zeta^*)\right] + \kappa \tag{8.53}$$

$$\tag{8.54}$$

Consider Theorem 8.3.1, we have:

$$\mathcal{L}_{sup}(\mathcal{T}_0, \hat{\phi}) - \mathcal{L}_{sup}(\mathcal{T}_0, \phi^*) \leq \frac{1}{\nu}\left[\frac{1}{1-\tau_r}\mathcal{L}_{con-pre}(\hat{\phi}) - \epsilon^*\right] + \kappa \tag{8.55}$$

$$= \frac{1}{\nu}\left(\frac{2\epsilon_0}{1-\tau_r} - \epsilon^*\right) + \kappa. \tag{8.56}$$

□

Below, we provide our main result similar to Theorem 8.2.10 for multi-classes setting.

Theorem 8.3.3. *For target evaluation task $\mathcal{T}_0$, consider the error bound in pretraining is $\mathcal{L}_{sup}(\mathcal{T}_0, \hat{\phi}) - \mathcal{L}_{sup}(\mathcal{T}_0, \phi^*) \leq \frac{1}{\nu}\left[\frac{2\epsilon_0}{1-\tau_r} - \epsilon^*\right] + \kappa$. Consider α as any small constant, for any $\epsilon_1 < \frac{\alpha}{3}\frac{2\epsilon_0}{1-\tau_r}$, consider a multitask finetuning set $\mathcal{S} = \{(x_j^i, y_j^i) : i \in [M], j \in [m]\}$, with M number of tasks, and m number of samples in each task. Then, with sample complexity*

$$M \geq \frac{1}{\epsilon_1}\left[4\sqrt{2}\tilde{L}\mathcal{R}_M(\Phi(\tilde{\epsilon})) + \frac{4C^2}{\epsilon_1}\log(\frac{2}{\delta})\right]$$

$$Mm \geq \frac{1}{\epsilon_1}\left[8LB\sqrt{r-1}\mathcal{R}_{Mm}(\Phi(\tilde{\epsilon})) + \frac{4C^2}{\epsilon_1}\log(\frac{2}{\delta})\right].$$

Solving Eq. 3.2 with empirical risk lower than ϵ_1 is sufficient to learn an ϕ' with classification error $\mathcal{L}_{sup}(\mathcal{T}_0, \phi') - \mathcal{L}_{sup}(\mathcal{T}_0, \phi^*) \leq \frac{1}{\nu}(\alpha\frac{2\epsilon_0}{1-\tau_r} - \epsilon^*) + \kappa$, with probability $1-\delta$.

Proof of Theorem 8.3.3. Recalling Theorem 8.2.7 and Theorem 8.2.9, the proof follows the same steps in the proof of Theorem 8.2.10, with different r.

□

8.3.2 Supervised Pretraining

We first provide contrastive pretraining error similar to Theorem 8.2.12 in the multiclass setting.

Theorem 8.3.4. *Assume Assumption 3.3.1 and that Φ has ν-diversity and κ-consistency with respect to ϕ^*, ϕ_ζ^*. Suppose $\hat{\phi}$ satisfies $\hat{\mathcal{L}}_{sup-pre}(\hat{\phi}) \leq \epsilon_0$. Let $p_i := \Pr_{y\sim\eta}\{y = y_i\}$, where $\sum_{i=1}^K p_i = 1$. Let $\rho := \frac{\max_i p_i}{\min_j p_j}$. Consider pretraining set $\mathcal{S}_{sup-pre} := \{x_i, y_i\}_{i=1}^N$, for any $\delta \geq 0$, if*

$$N \geq \frac{1}{\epsilon_0}\left[8LR\sqrt{K}\mathcal{R}_N(\Phi) + \frac{8C^2}{\epsilon_0}\log(\frac{2}{\delta})\right].$$

Then with probability $1-\delta$, for any target task $\mathcal{T}_0 \subset \mathcal{C}_0$,

$$\mathcal{L}_{sup}(\mathcal{T}_0, \hat{\phi}) - \mathcal{L}_{sup}(\mathcal{T}_0, \phi^*) \leq \frac{1}{\nu}\left[2\rho^r\epsilon_0 - \mathcal{L}_{sup}(\phi_\zeta^*)\right] + \kappa. \tag{8.57}$$

Proof of Theorem 8.3.4. The proof follows similar steps of Theorem 8.2.12. □

Below, we provide our main result similar to Theorem 8.2.14 for multi-classes setting.

Theorem 8.3.5. *Assume Assumption 3.3.1 and that Φ has ν-diversity and κ-consistency with respect to ϕ^*, ϕ_ζ^*. Suppose for some small constant $\alpha \in (0,1)$, we solve Eq. 3.2 with empirical loss lower than $\epsilon_1 = \frac{\alpha}{3} 2\rho^r \epsilon_0$ and obtain ϕ'. For any $\delta > 0$, if*

$$M \geq \frac{1}{\epsilon_1}\left[4\sqrt{2}\tilde{L}\mathcal{R}_M(\Phi(\tilde{\epsilon})) + \frac{4C^2}{\epsilon_1}\log(\frac{2}{\delta})\right], Mm \geq \frac{1}{\epsilon_1}\left[8LB\sqrt{r-1}\mathcal{R}_{Mm}(\Phi(\tilde{\epsilon})) + \frac{4C^2}{\epsilon_1}\log(\frac{2}{\delta})\right],$$

then with probability $1-\delta$, for any target task $\mathcal{T}_0 \subseteq \mathcal{C}_0$,

$$\mathcal{L}_{sup}(\mathcal{T}_0, \phi') - \mathcal{L}_{sup}(\mathcal{T}_0, \phi^*) \leq \frac{1}{\nu}\left(2\alpha\rho^r\epsilon_0 - \mathcal{L}_{sup}(\phi_\zeta^*)\right) + \kappa. \tag{8.58}$$

Proof of Theorem 8.3.5. Recalling Theorem 8.2.7 and Theorem 8.2.9, the proof follows the same steps in the proof of Theorem 8.2.14, with different r. □

8.4 Linear Case Study

In this section, we provide a full analysis of the linear case study to provide intuition about our consistency, diversity, and task selection algorithm. Intuitively, we have multiple classes, each centered around its mean vector. Target data has a subset of classes, while training data has another subset of classes. Consistency and diversity are related to how these two subsets overlap, i.e., the number of shared features and the number of disjoint features. Then, we can link it to the task selection algorithm.

In this section, z_i means the i-th dimension of vector z rather than the sample index.

8.4.1 Problem Setup

Linear Data and Tasks. We consider dictionary learning or sparse coding settings, which is a classic data model (e.g., Olshausen and Field [1997]; Vinje and Gallant [2000]; Blei et al. [2003]; Shi et al. [2022, 2023c]). Let $\mathcal{X} \subseteq \mathbb{R}^d$ be the input space and we have input data $x \in \mathcal{X}$. Suppose $Q \in \mathbb{R}^{d \times D}$ is an unknown dictionary with D columns that can be regarded as patterns or features. For simplicity, assume $d = D$ and Q is orthonormal. We have $z \in \{0, -1, +1\}^d$ as a latent class, where z is a hidden vector that indicates the presence of each pattern. Each latent class z has a distribution $\mathcal{D}_z(x)$ over inputs x. We assume $\mathcal{D}_z(x)$ be a distribution with mean Qz, i.e., $x = Qz + \boldsymbol{e}_z$, where $\boldsymbol{e}_z \in \mathbb{R}^d$ is some noise vector drawing from a zero-mean distribution.

For simplicity, we consider each task to be a binary classification task, where $\mathcal{Y} = \{-1, +1\}$ is the label space. In each task (in multitask finetuning or target task), we have two latent classes z, z' (denote the task as $\mathcal{T}_{z,z'}$) and we randomly assign -1 and $+1$ to each latent class. W.l.o.g., we have in $\mathcal{T}_{z,z'}$:

$$x = \begin{cases} Qz + \boldsymbol{e}_z, & \text{if } y = -1 \\ Qz' + \boldsymbol{e}_{z'}, & \text{if } y = +1. \end{cases} \tag{8.59}$$

For simplicity, we consider a balanced class setting in all tasks, i.e., $p(y=-1) = p(y=+1) = \frac{1}{2}$.

Now, we define multitask finetuning tasks and target tasks. Suppose there is a set of latent classes $\mathcal{C} \subseteq \{0, -1, +1\}^d$ used for multitask finetuning tasks, which has an index set $J_\mathcal{C} \subseteq [d], k_\mathcal{C} := |J_\mathcal{C}|$ such that for any $z \in \mathcal{C}$, we have $z_{J_\mathcal{C}} \in \{-1, +1\}^{k_\mathcal{C}}$ and $z_{[d]\setminus J_\mathcal{C}} \in \{0\}^{d-k_\mathcal{C}}$. Similarly, suppose there is a set of latent classes $\mathcal{C}_0 \subseteq \{0, -1, +1\}^d$ used for target tasks whose index set is $J_0 \subseteq [d], k_0 := |J_0|$. Note that $J_\mathcal{C}$ may or may not overlap with J_0 and denote the set of features encoded both by $\mathcal{C}_0$ and $\mathcal{C}$ as $L_\mathcal{C} := J_0 \cap J_\mathcal{C}, l_\mathcal{C} := |L_\mathcal{C}|$. Intuitively, $L_\mathcal{C}$ represents the target features covered by training data. Let ζ over $\mathcal{C} \times \mathcal{C}$ be the distribution of multitask finetuning tasks. Then, in short, our data generation pipeline for multitask finetuning tasks is (1) sample two latent classes $(z, z') \sim \zeta$ as a task $\mathcal{T}_{z,z'}$; (2) assign label $-1, +1$ to two latent classes; (3) sample input data from $\mathcal{D}_z(x)$ and $\mathcal{D}_{z'}(x)$ with balanced probabilities.

For simplicity, we have a symmetric assumption and a non-degenerate assumption for ζ. Symmetric assumption means each dimension is equal important and non-degenerate assumption means any two dimensions are not determined by each other in all tasks.

Assumption 8.4.1 (Symmetric)**.** *We assume for any multitask finetuning tasks distribution ζ, for any $j, k \in J_\mathcal{C}$, switching two dimensions z_j and z_k does not change the distribution ζ.*

Assumption 8.4.2 (Non-degenerate)**.** *We assume for any multitask finetuning tasks distribution ζ, for any $j, k \in J_\mathcal{C}$, over ζ we have $p(z_j = z'_j, z_k \neq z'_k) > 0$.*

Remark 8.4.1. *There exists many ζ satisfying above assumptions, e.g., (1) $z_{J_\mathcal{C}}$ and $z'_{J_\mathcal{C}}$ uniformly sampling from $\{-1,+1\}^{k_\mathcal{C}}$; or (2) let $k_\mathcal{C}=2$, $z_{J_\mathcal{C}}$ and $z'_{J_\mathcal{C}}$ uniformly sampling from $\{(+1,+1),(-1,+1),(+1,-1)\}$ (note that uniformly sampling from $\{(+1,+1),(-1,-1)\}$ does not satisfy non-degenerate assumption). Also, we note that even when $\mathcal{C}=\mathcal{C}_0$, the target latent class may not exist in the multitask finetuning tasks.*

Linear Model and Loss Function. Let Φ be the hypothesis class of models $\phi:\mathcal{X}\to\overline{\mathcal{Z}}$, where $\overline{\mathcal{Z}}\subseteq\mathbb{R}^d$ is the output space of the model. We consider a linear model class with regularity Assumption 3.3.1, i.e., $\Phi=\{\phi\in\mathbb{R}^{d\times d}:\|\phi\|_F\le R\}$ and linear head $w\in\mathbb{R}^d$ where $\|w\|_2\le B$. Thus, the final output of the model and linear head is $w^\top\phi x$. We use linear loss in Shi et al. [2023a], i.e., $\ell\left(w^\top\phi x,y\right)=-yw^\top\phi x$ and we have

$$\mathcal{L}_{sup}(\mathcal{T},\phi):=\min_{w\in\mathbb{R}^d,\|w\|_2\le B}\mathop{\mathbb{E}}_{z,y\sim\mathcal{T}}\mathop{\mathbb{E}}_{x\sim\mathcal{D}_z(x)}\left[\ell\left(w^\top\phi x,y\right)\right] \tag{8.60}$$

$$\mathcal{L}_{sup}(\phi):=\mathop{\mathbb{E}}_{\mathcal{T}\sim\zeta}\left[\mathcal{L}_{sup}(\mathcal{T},\phi)\right] \tag{8.61}$$

$$\phi^*_\zeta:=\arg\min_{\phi\in\Phi}\mathcal{L}_{sup}(\phi), \tag{8.62}$$

where ϕ^*_ζ is the optimal representation for multitask finetuning.

8.4.2 Diversity and Consistency Analysis

Optimal Representation for Multitask Finetuning

Lemma 8.4.3. *Assume Assumption 8.4.1 and Assumption 8.4.2. We have $\phi^*_\zeta=U\Lambda^*Q^{-1}$, where U is any orthonormal matrix, $\Lambda^*=diag(\lambda^*)$. For any $i\in J_\mathcal{C}$, $\lambda^*_i=\frac{R}{\sqrt{k_\mathcal{C}}}$ and $\lambda^*_i=0$ otherwise.*

Proof of Theorem 8.4.3. We have the singular value decomposition $\phi=U\Lambda V^\top$, where $\Lambda=\mathrm{diag}(\lambda)$, where $\lambda\in\mathbb{R}^d$. Then, we have

$$\mathcal{L}_{sup}(\phi)=\mathop{\mathbb{E}}_{\mathcal{T}\sim\zeta}\left[\mathcal{L}_{sup}(\mathcal{T},\phi)\right] \tag{8.63}$$

$$=\mathop{\mathbb{E}}_{\mathcal{T}\sim\zeta}\left[\min_{w\in\mathbb{R}^d,\|w\|_2\le B}\mathop{\mathbb{E}}_{z,y\sim\mathcal{T}}\mathop{\mathbb{E}}_{x\sim\mathcal{D}_z(x)}\left[\ell\left(w^\top\phi x,y\right)\right]\right] \tag{8.64}$$

$$=\mathop{\mathbb{E}}_{\mathcal{T}_{z,z'}\sim\zeta}\left[\min_{w\in\mathbb{R}^d,\|w\|_2\le B}\frac{1}{2}\left(\mathop{\mathbb{E}}_{x\sim\mathcal{D}_z(x)}\left[\ell\left(w^\top\phi x,-1\right)\right]+\mathop{\mathbb{E}}_{x\sim\mathcal{D}_{z'}(x)}\left[\ell\left(w^\top\phi x,+1\right)\right]\right)\right] \tag{8.65}$$

$$=\frac{1}{2}\mathop{\mathbb{E}}_{\mathcal{T}_{z,z'}\sim\zeta}\left[\min_{w\in\mathbb{R}^d,\|w\|_2\le B}\mathop{\mathbb{E}}_{x\sim\mathcal{D}_z(x)}\left[w^\top\phi x\right]+\mathop{\mathbb{E}}_{x\sim\mathcal{D}_{z'}(x)}\left[-w^\top\phi x\right]\right] \tag{8.66}$$

$$=\frac{1}{2}\mathop{\mathbb{E}}_{\mathcal{T}_{z,z'}\sim\zeta}\left[\min_{w\in\mathbb{R}^d,\|w\|_2\le B}w^\top\phi Qz-w^\top\phi Qz'\right] \tag{8.67}$$

$$=-\frac{B}{2}\mathop{\mathbb{E}}_{\mathcal{T}_{z,z'}\sim\zeta}\left[\|\phi Q(z-z')\|_2\right] \tag{8.68}$$

$$=-\frac{B}{2}\mathop{\mathbb{E}}_{\mathcal{T}_{z,z'}\sim\zeta}\left[\|\Lambda V^\top Q(z-z')\|_2\right]. \tag{8.69}$$

W.l.o.g., we can assume $V^\top=Q^{-1}$. As $\|\phi\|_F=\|\Lambda\|_F=\|\lambda\|_2$ thus we have

$$\begin{aligned}
\min_{\phi\in\Phi}\mathcal{L}_{sup}(\phi) &= -\frac{B}{2}\max_{\|\Lambda\|_F\le R}\mathop{\mathbb{E}}_{\mathcal{T}_{z,z'}\sim\zeta}[\|\Lambda(z-z')\|_2] \\
&= -\frac{B}{2}\max_{\|\lambda\|_2\le R}\mathop{\mathbb{E}}_{\mathcal{T}_{z,z'}\sim\zeta}\left[\sqrt{\sum_{i=1}^{d}\lambda_i^2(z_i-z_i')^2}\right] \\
&= -\frac{B}{2}\max_{\|\lambda\|_2= R}\mathop{\mathbb{E}}_{\mathcal{T}_{z,z'}\sim\zeta}\left[\sqrt{\sum_{i=1}^{d}\lambda_i^2(z_i-z_i')^2}\right] \\
&= -B\max_{\|\lambda\|_2= R}\mathop{\mathbb{E}}_{\mathcal{T}_{z,z'}\sim\zeta}\left[\sqrt{\sum_{i\in J_C}\lambda_i^2\mathbb{1}[z_i\neq z_i']}\right], \qquad (8.70)
\end{aligned}$$

where $\mathbb{1}[z_i \neq z_i']$ is a Boolean function, mapping True to 1 and False to 0.

Let $\phi_\zeta^* = U\Lambda^* Q^{-1}$ with corresponding λ^*. Now, we use contradiction to prove for any $j,k \in J_C$, we have $\lambda_j^* = \lambda_k^*$. W.l.o.g., suppose $\lambda_j^* < \lambda_k^*$,

$$\begin{aligned}
&\mathcal{L}_{sup}(\phi_\zeta^*) \\
&= -B\mathop{\mathbb{E}}_{\mathcal{T}_{z,z'}\sim\zeta}\left[\sqrt{\lambda_j^{*2}\mathbb{1}[z_j\neq z_j'] + \lambda_k^{*2}\mathbb{1}[z_k\neq z_k'] + \sum_{i\in J_C\setminus\{j,k\}}\lambda_i^{*2}\mathbb{1}[z_i\neq z_i']}\right] \\
&= -B\Bigg\{p(z_j\neq z_j', z_k\neq z_k')\mathop{\mathbb{E}}_{\mathcal{T}_{z,z'}\sim\zeta}\left[\sqrt{\lambda_j^{*2}+\lambda_k^{*2}+\sum_{i\in J_C\setminus\{j,k\}}\lambda_i^{*2}\mathbb{1}[z_i\neq z_i']}\,\middle|\, z_j\neq z_j', z_k\neq z_k'\right] \\
&\quad + p(z_j= z_j', z_k\neq z_k')\mathop{\mathbb{E}}_{\mathcal{T}_{z,z'}\sim\zeta}\left[\sqrt{\lambda_k^{*2}+\sum_{i\in J_C\setminus\{j,k\}}\lambda_i^{*2}\mathbb{1}[z_i\neq z_i']}\,\middle|\, z_j= z_j', z_k\neq z_k'\right] \\
&\quad + p(z_j\neq z_j', z_k= z_k')\mathop{\mathbb{E}}_{\mathcal{T}_{z,z'}\sim\zeta}\left[\sqrt{\lambda_j^{*2}+\sum_{i\in J_C\setminus\{j,k\}}\lambda_i^{*2}\mathbb{1}[z_i\neq z_i']}\,\middle|\, z_j\neq z_j', z_k= z_k'\right]\Bigg\}.
\end{aligned}$$

By symmetric Assumption 8.4.1 and non-degenerate Assumption 8.4.2, we have $p(z_j = z'_j, z_k \neq z'_k) = p(z_j \neq z'_j, z_k = z'_k) > 0$, and

$$
\begin{aligned}
&\mathop{\mathbb{E}}_{\mathcal{T}_{z,z'}\sim\zeta}\left[\sqrt{\lambda_k^{*2}+\sum_{i\in J_{\mathcal{C}}\setminus\{j,k\}}\lambda_i^{*2}\mathbb{1}[z_i\neq z'_i]}\middle| z_j = z'_j, z_k \neq z'_k\right] \\
&+\mathop{\mathbb{E}}_{\mathcal{T}_{z,z'}\sim\zeta}\left[\sqrt{\lambda_j^{*2}+\sum_{i\in J_{\mathcal{C}}\setminus\{j,k\}}\lambda_i^{*2}\mathbb{1}[z_i\neq z'_i]}\middle| z_j \neq z'_j, z_k = z'_k\right] \\
=&\mathop{\mathbb{E}}_{\mathcal{T}_{z,z'}\sim\zeta}\left[\sqrt{\lambda_k^{*2}+\sum_{i\in J_{\mathcal{C}}\setminus\{j,k\}}\lambda_i^{*2}\mathbb{1}[z_i\neq z'_i]}\middle| z_j = z'_j, z_k \neq z'_k\right] \\
&+\mathop{\mathbb{E}}_{\mathcal{T}_{z,z'}\sim\zeta}\left[\sqrt{\lambda_j^{*2}+\sum_{i\in J_{\mathcal{C}}\setminus\{j,k\}}\lambda_i^{*2}\mathbb{1}[z_i\neq z'_i]}\middle| z_k \neq z'_k, z_j = z'_j\right] \\
<&2\mathop{\mathbb{E}}_{\mathcal{T}_{z,z'}\sim\zeta}\left[\sqrt{\frac{\lambda_j^{*2}+\lambda_k^{*2}}{2}+\sum_{i\in J_{\mathcal{C}}\setminus\{j,k\}}\lambda_i^{*2}\mathbb{1}[z_i\neq z'_i]}\middle| z_j = z'_j, z_k \neq z'_k\right] \\
=&\mathop{\mathbb{E}}_{\mathcal{T}_{z,z'}\sim\zeta}\left[\sqrt{\frac{\lambda_j^{*2}+\lambda_k^{*2}}{2}+\sum_{i\in J_{\mathcal{C}}\setminus\{j,k\}}\lambda_i^{*2}\mathbb{1}[z_i\neq z'_i]}\middle| z_j = z'_j, z_k \neq z'_k\right] \\
&+\mathop{\mathbb{E}}_{\mathcal{T}_{z,z'}\sim\zeta}\left[\sqrt{\frac{\lambda_j^{*2}+\lambda_k^{*2}}{2}+\sum_{i\in J_{\mathcal{C}}\setminus\{j,k\}}\lambda_i^{*2}\mathbb{1}[z_i\neq z'_i]}\middle| z_k \neq z'_k, z_j = z'_j\right].
\end{aligned}
$$

where two equality follows Assumption 8.4.1 and the inequality follows Jensen's inequality. Let $\phi' = U\Lambda' Q^{-1}$ with corresponding λ', where $\lambda'_j = \lambda'_k = \sqrt{\frac{\lambda_j^{*2}+\lambda_k^{*2}}{2}}$ and for any $i \in J_{\mathcal{C}} \setminus \{j,k\}$, $\lambda'_i = \lambda^*_i$. We have $\|\phi'\|_F = \|\phi^*_\zeta\|_F$ and $\mathcal{L}_{sup}(\phi^*_\zeta) > \mathcal{L}_{sup}(\phi')$ which is a contradiction as we have ϕ^*_ζ is the optimal solution. Thus, for any $j,k \in J_{\mathcal{C}}$, we have $\lambda^*_j = \lambda^*_k$ and we finish the proof under simple calculation. □

Now, we are ready to analyze consistency and diversity under this linear case study.

Consistency

The intuition is that ζ not only covers $\mathcal{C}_0$ but contains too much unrelated information. Recall that the consistent term in Definition 3.3.3 is $\kappa = \sup_{\mathcal{T}_0\subseteq\mathcal{C}_0}\left[\mathcal{L}_{sup}(\mathcal{T}_0,\phi^*_\zeta) - \mathcal{L}_{sup}(\mathcal{T}_0,\phi^*_0)\right]$.

We first define some notation we will use later. Let ζ_0 be a multitask finetuning tasks distribution over $\mathcal{C}_0 \times \mathcal{C}_0$ and denote the corresponding optimal representation model as ϕ^*_0. Suppose for any target task $\mathcal{T}_0$ contains two latent classes z, z' from $\mathcal{C}_0$. W.l.o.g., denote z, z' differ in n_0 entries ($1 \leq n_0 \leq k_0$), whose $n_{\mathcal{C}}$ entries fall in $L_{\mathcal{C}}$, where $0 \leq n_{\mathcal{C}} \leq n_0$. Then, we get the lemma below:

Lemma 8.4.4. *Assume Assumption 8.4.1 and Assumption 8.4.2. We have*

$$
\kappa = \sup_{\mathcal{T}_0\subseteq\mathcal{C}_0}\left[\mathcal{L}_{sup}(\mathcal{T}_0,\phi^*_\zeta) - \mathcal{L}_{sup}(\mathcal{T}_0,\phi^*_0)\right] = BR\left(\sqrt{\frac{n_0}{k_0}} - \sqrt{\frac{n_{\mathcal{C}}}{k_{\mathcal{C}}}}\right). \tag{8.71}
$$

Proof of Theorem 8.4.4. Recall $1 \leq n_0 \leq k_0$ and $0 \leq n_{\mathcal{C}} \leq n_0$. By Theorem 8.4.3, we have $\phi^*_\zeta = U\Lambda^* Q^{-1}$, where U is any orthonormal matrix, $\Lambda^* = \mathrm{diag}(\lambda^*)$. For any $i \in J_{\mathcal{C}}$, $\lambda^*_i = \frac{R}{\sqrt{k_{\mathcal{C}}}}$ and $\lambda^*_i = 0$ otherwise. We also have $\phi^*_0 = U_0\Lambda^*_0 Q^{-1}$, where U_0 is any orthonormal matrix, $\Lambda^*_0 = \mathrm{diag}(\lambda^{0,*})$. For any $i \in J_0$, $\lambda^{0,*}_i = \frac{R}{\sqrt{k_0}}$ and $\lambda^{0,*}_i = 0$

otherwise. Thus, we have

$$\kappa = \sup_{\mathcal{T}_0 \subseteq \mathcal{C}_0} \left[\mathcal{L}_{sup}(\mathcal{T}_0, \phi_\zeta^*) - \mathcal{L}_{sup}(\mathcal{T}_0, \phi_0^*)\right] \tag{8.72}$$

$$= BR\left(\sqrt{\frac{n_0}{k_0}} - \sqrt{\frac{n_\mathcal{C}}{k_\mathcal{C}}}\right). \tag{8.73}$$

□

Let $n'_\mathcal{C} = k_\mathcal{C} - n_\mathcal{C}$. Note this $k_\mathcal{C}$ is an increasing factor if $\mathcal{C}$ contains more features. Moreover, $n_\mathcal{C}$ is the number of features encoded by both target and training data, representing the information of target data covered by training data, $n_\mathcal{C}$ increases as more target information covered by training data, the loss will decrease. $n'_\mathcal{C}$ is the number of features encoded in training data but not encoded by target data, representing the un-useful information, $n'_\mathcal{C}$ increases as more un-related information is covered by training data, the loss will increase.

Diversity

We first review some definitions in Definition 3.3.2. The **averaged representation difference** for two model $\phi, \tilde{\phi}$ on a distribution ζ over tasks is

$$\bar{d}_\zeta(\phi, \tilde{\phi}) := \mathop{\mathbb{E}}_{\mathcal{T}\sim\zeta}\left[\mathcal{L}_{sup}(\mathcal{T}, \phi) - \mathcal{L}_{sup}(\mathcal{T}, \tilde{\phi})\right] = \mathcal{L}_{sup}(\phi) - \mathcal{L}_{sup}(\tilde{\phi}). \tag{8.74}$$

The **worst-case representation difference** between representations $\phi, \tilde{\phi}$ on the family of classes $\mathcal{C}_0$ is

$$d_{\mathcal{C}_0}(\phi, \tilde{\phi}) := \sup_{\mathcal{T}_0 \subseteq \mathcal{C}_0} \left|\mathcal{L}_{sup}(\mathcal{T}_0, \phi) - \mathcal{L}_{sup}(\mathcal{T}_0, \tilde{\phi})\right|. \tag{8.75}$$

We say the model class Φ has ν-diversity for ζ and $\mathcal{C}_0$ if for any $\phi \in \Phi$ and ϕ_ζ^*,

$$d_{\mathcal{C}_0}(\phi, \phi_\zeta^*) \le \bar{d}_\zeta(\phi, \phi_\zeta^*)/\nu. \tag{8.76}$$

To find the minimum value of ν in Definition 3.3.2, we need further information about ζ. For simplicity, we have a fixed distance assumption, e.g., uniformly sampling from $\{(+1, +1, -1), (+1, -1, +1), (-1, +1, +1)\}$. Then, we consider two different cases below. We consider that all $\mathcal{T}_0 \subseteq \mathcal{C}_0$ such containing z, z' that differ in only 1 entry.

Assumption 8.4.5 (Fixed Distance)**.** *We assume for any multitask finetuning tasks distribution ζ, for any two latent classes $(z, z') \sim \zeta$, we have z, z' differ in n_k entries.*

Case $L_\mathcal{C} \neq J_0$. In this case, $J_0 \setminus L_\mathcal{C} \neq \emptyset$, we have the features learned in multitask finetuning that do not cover all features used in the target task. Then, we have the following lemma, which means if $L_\mathcal{C} \neq J_0$ we can have infinitesimal ν to satisfy the diversity definition.

Lemma 8.4.6. *Assume Assumption 8.4.1, Assumption 8.4.2 and Assumption 8.4.5. When $L_\mathcal{C} \neq J_0$, we have $\nu \to 0$.*

Proof of Theorem 8.4.6. As features in $\mathcal{C}_0$ not covered by $\mathcal{C}$, we can always find a $\mathcal{T}_0$ such containing z, z' that only differ in entries in $J_0 \setminus L_\mathcal{C}$, we say as entry $\tilde{i}$.

By Theorem 8.4.3, we have $\phi_\zeta^* = U\Lambda^* Q^{-1}$, where U is any orthonormal matrix, $\Lambda^* = \mathrm{diag}(\lambda^*)$. For any $i \in J_\mathcal{C}$, $\lambda_i^* = \frac{R}{\sqrt{k_\mathcal{C}}}$ and $\lambda_i^* = 0$ otherwise. We have $\mathcal{L}_{sup}(\mathcal{T}_0, \phi_\zeta^*) = 0$ and by Eq. 8.70,

$$\mathcal{L}_{sup}(\phi_\zeta^*) = -B \mathop{\mathbb{E}}_{\mathcal{T}_{z,z'}\sim\zeta}\left[\sqrt{\sum_{i\in J_\mathcal{C}} \lambda_i^{*2} \mathbb{1}[z_i \neq z'_i]}\right] \tag{8.77}$$

$$= -BR\sqrt{\frac{n_k}{k_\mathcal{C}}}. \tag{8.78}$$

On the other hand, for any $\phi \in \Phi$, we have $\mathcal{L}_{sup}(\mathcal{T}_0, \phi) = -B|\lambda_{\tilde{i}}|$. Thus, we have

$$\begin{aligned}
\nu &= \min_{\phi\in\Phi} \frac{\mathcal{L}_{sup}(\phi) - \mathcal{L}_{sup}(\phi^*_\zeta)}{\left|\mathcal{L}_{sup}(\mathcal{T}_0, \phi) - \mathcal{L}_{sup}(\mathcal{T}_0, \phi^*_\zeta)\right|} \\
&= \min_{\phi\in\Phi} \frac{\mathcal{L}_{sup}(\phi) + BR\sqrt{\frac{n_k}{k_\mathcal{C}}}}{B|\lambda_{\tilde{i}}|} \\
&= \min_{\phi\in\Phi} \frac{-B \mathop{\mathbb{E}}_{\mathcal{T}_{z,z'}\sim\zeta}\left[\sqrt{\sum_{i\in J_\mathcal{C}} \lambda_i^2 \mathbb{1}[z_i \neq z'_i]}\right] + BR\sqrt{\frac{n_k}{k_\mathcal{C}}}}{B|\lambda_{\tilde{i}}|} \\
&\leq \frac{-\mathop{\mathbb{E}}_{\mathcal{T}_{z,z'}\sim\zeta}\left[\sqrt{\sum_{i\in J_\mathcal{C}} \frac{R^2-\lambda_i^2}{k_\mathcal{C}} \mathbb{1}[z_i \neq z'_i]}\right] + R\sqrt{\frac{n_k}{k_\mathcal{C}}}}{|\lambda_{\tilde{i}}|} \\
&= \frac{-\sqrt{\frac{(R^2-\lambda_{\tilde{i}}^2)n_k}{k_\mathcal{C}}} + R\sqrt{\frac{n_k}{k_\mathcal{C}}}}{|\lambda_{\tilde{i}}|},
\end{aligned} \tag{8.79}$$

where the first inequality is by constructing a specific ϕ. Note that Eq. 8.79 $\to 0$ when $|\lambda_{\tilde{i}}| \to 0$. ϕ is constructed as: for any $i \in J_\mathcal{C}$, $\lambda_i = \sqrt{\frac{R^2-\lambda_{\tilde{i}}^2}{k_\mathcal{C}}}$ and $|\lambda_{\tilde{i}}| \to 0$. Thus, we finish the proof. □

Case $L_\mathcal{C} = J_0$. In this case $J_0 \setminus L_\mathcal{C} = \emptyset$, we have all features in $\mathcal{C}_0$ covered by $\mathcal{C}$.

Lemma 8.4.7. *Assume Assumption 8.4.1, Assumption 8.4.2 and Assumption 8.4.5. When all $\mathcal{T}_0 \subseteq \mathcal{C}_0$ such containing z, z' that differ in only 1 entry and $L_\mathcal{C} = J_0$, we have ν is lower bounded by some constant $\tilde{c} = \sqrt{n_k}\left(1 - \sqrt{\frac{1}{k_\mathcal{C}(k_\mathcal{C}-1)}}\left(\sqrt{n_k(n_k-1)} + k_\mathcal{C} - n_k\right)\right)$.*

Proof of Theorem 8.4.7. We say the differ entry in $\mathcal{T}_0$ as entry $\tilde{i}$. By Theorem 8.4.3, we have $\phi^*_\zeta = U\Lambda^* Q^{-1}$, where U is any orthonormal matrix, $\Lambda^* = \text{diag}(\lambda^*)$. For any $i \in J_\mathcal{C}$, $\lambda_i^* = \frac{R}{\sqrt{k_\mathcal{C}}}$ and $\lambda_i^* = 0$ otherwise. By Eq. 8.70, we have $\mathcal{L}_{sup}(\mathcal{T}_0, \phi^*_\zeta) = -BR\sqrt{\frac{n_0}{k_\mathcal{C}}}$ and $\mathcal{L}_{sup}(\phi^*_\zeta) = -BR\sqrt{\frac{n_k}{k_\mathcal{C}}}$.

On the other hand, for any $\phi \in \Phi$, we have $\mathcal{L}_{sup}(\mathcal{T}_0, \phi) = -B|\lambda_{\tilde{i}}|$. Thus, by Assumption 8.4.1, we have

$$\begin{aligned}
\nu &= \min_{\mathcal{T}_0\subseteq\mathcal{C}_0, \phi\in\Phi} \frac{\mathcal{L}_{sup}(\phi) - \mathcal{L}_{sup}(\phi^*_\zeta)}{\left|\mathcal{L}_{sup}(\mathcal{T}_0, \phi) - \mathcal{L}_{sup}(\mathcal{T}_0, \phi^*_\zeta)\right|} \\
&= \min_{\mathcal{T}_0\subseteq\mathcal{C}_0, \phi\in\Phi} \frac{\mathcal{L}_{sup}(\phi) + BR\sqrt{\frac{n_k}{k_\mathcal{C}}}}{|-B|\lambda_{\tilde{i}}| + BR\sqrt{\frac{1}{k_\mathcal{C}}}|} \\
&= \min_{\mathcal{T}_0\subseteq\mathcal{C}_0, \phi\in\Phi} \frac{-B \mathop{\mathbb{E}}_{\mathcal{T}_{z,z'}\sim\zeta}\left[\sqrt{\sum_{i\in J_\mathcal{C}} \lambda_i^2 \mathbb{1}[z_i \neq z'_i]}\right] + BR\sqrt{\frac{n_k}{k_\mathcal{C}}}}{|-B|\lambda_{\tilde{i}}| + BR\sqrt{\frac{1}{k_\mathcal{C}}}|} \\
&= \min_{\mathcal{T}_0\subseteq\mathcal{C}_0, \phi\in\Phi} \frac{-\mathop{\mathbb{E}}_{\mathcal{T}_{z,z'}\sim\zeta}\left[\sqrt{\lambda_{\tilde{i}}^2 \mathbb{1}[z_{\tilde{i}} \neq z'_{\tilde{i}}] + \sum_{i\in J_\mathcal{C}\setminus\{\tilde{i}\}} \frac{R^2-\lambda_i^2}{k_\mathcal{C}-1} \mathbb{1}[z_i \neq z'_i]}\right] + R\sqrt{\frac{n_k}{k_\mathcal{C}}}}{|-|\lambda_{\tilde{i}}| + R\sqrt{\frac{1}{k_\mathcal{C}}}|} \\
&= \min_{\mathcal{T}_0\subseteq\mathcal{C}_0, \phi\in\Phi} \frac{-\left[\frac{n_k}{k_\mathcal{C}}\sqrt{\lambda_{\tilde{i}}^2 + \frac{R^2-\lambda_{\tilde{i}}^2}{k_\mathcal{C}-1}(n_k-1)} + \frac{k_\mathcal{C}-n_k}{k_\mathcal{C}}\sqrt{\frac{n_k(R^2-\lambda_{\tilde{i}}^2)}{k_\mathcal{C}-1}}\right] + R\sqrt{\frac{n_k}{k_\mathcal{C}}}}{|-|\lambda_{\tilde{i}}| + R\sqrt{\frac{1}{k_\mathcal{C}}}|} \\
&= \sqrt{n_k}\left(1 - \sqrt{\frac{1}{k_\mathcal{C}(k_\mathcal{C}-1)}}\left(\sqrt{n_k(n_k-1)} + k_\mathcal{C} - n_k\right)\right),
\end{aligned} \tag{8.80}$$

where the last equality take $\lambda_{\tilde{i}} = 0$. □

8.4.3 Proof of Main Results

Proof of Theorem 3.3.6. Note that $R = B = n_0 = k_0 = 1, n_k = 2$.

We see that ζ satisfies Assumption 8.4.1, Assumption 8.4.2 and Assumption 8.4.5. We finish the proof by Theorem 8.4.4, Theorem 8.4.6 and Theorem 8.4.7 with some simple calculations. □

Thus, we can link our diversity and consistency parameters to the number of features in z encoded by training tasks or target tasks. Based on this intuition, we propose a selection algorithm, where selection is based on x, we want to select data that encodes more relevant features of z, this can be achieved by comparing x from target data and training data either using cosine similarity or KDE.

8.5 Vision Experimental Results

We first provide a summary of dataset and protocal we use, we provide details in following sections.

Datasets and Models. We use four widely used few-shot learning benchmarks: miniImageNet [Vinyals et al., 2016], tieredImageNet [Ren et al., 2018], DomainNet [Peng et al., 2019] and Meta-dataset [Triantafillou et al., 2020], following the protocol in Chen et al. [2021b]; Tian et al. [2020b]. We use exemplary foundation models with different pretraining schemes (MoCo-v3 [Chen et al., 2021a], DINO-v2 [Oquab et al., 2023], and supervised learning with ImageNet [Russakovsky et al., 2015]) and architectures (ResNet [He et al., 2016] and ViT [Dosovitskiy et al., 2021]).

Experiment Protocol. We consider few-shot tasks consisting of N classes with K support samples and Q query samples per class (known as N-way K-shot). The goal is to classify the query samples into the N classes based on the support samples. Tasks used for finetuning are constructed by samples from the training split. Each task is formed randomly by sampling 15 classes, with every class drawing 1 or 5 support samples and 10 query samples. Target tasks are similarly constructed, yet from the test set. We follow [Chen et al., 2021b] for multitask finetuning and target task adaptation. During multitask finetuning, we update all parameters in the model using a nearest centroid classifier, in which all samples are encoded, class centroids are computed, and cosine similarity between a query sample and those centroids are treated as the class logits. For adaptation to a target task, we only retain the model encoder and consider a similar nearest centroid classifier. This experiment protocol applies to all three major experiments (Sections 3.4.1 to 3.4.3).

8.5.1 Datasets

The miniImageNet dataset is a common benchmark for few-shot learning. It contains 100 classes sampled from ImageNet, then is randomly split into 64, 16, and 20 classes as training, validation, and testing set respectively.

The tieredImageNet dataset is another widely used benchmark for few-shot learning. It contains 608 classes from 34 super-categories sampled from ImageNet. These categories are then subdivided into 20 training categories with 351 classes, 6 validation categories with 97 classes, and 8 testing categories with 160 classes

DomainNet is the largest domain adaptation benchmark with about 0.6 million images. It consists of around 0.6 million images of 345 categories from 6 domains: clipart (clp), infograph (inf), quickdraw (qdr), real (rel) and sketch (skt). We split it into 185, 65, 100 classes as training, validation, and testing set respectively. We conduct experiments on Sketch (skt) subsets.

Meta-Dataset encompasses ten publicly available image datasets covering a wide array of domains: ImageNet-1k, Omniglot, FGVC-Aircraft, CUB-200-2011, Describable Textures, QuickDraw, FGVCx Fungi, VGG Flower, Traffic Signs, and MSCOCO. Each of these datasets is split into training, validation, and testing subsets. For additional information on the Meta-Dataset can be found in Appendix 3 of Triantafillou et al. [2020].

8.5.2 Experiment Protocols

Our evaluation and the finetuning process take the form of few-shot tasks, where a target task consists of N classes with K support samples and Q query samples in each class. The objective is to classify the query samples into the N classes based on the support samples. To accomplish this, we take the support samples in each class and feed them through an image encoder to obtain representations for each sample. We then calculate the average of these representations within

each class to obtain the centroid of each class. For a given query sample x, we compute the probability that x belongs to class y based on the cosine similarity between the representation of x and the centroid of class y.

In our testing stage, we constructed 1500 target tasks, each consisting of 15 classes randomly sampled from the test split of the dataset. Within each class, we randomly selected 1 or 5 of the available images as shot images and 15 images as query images. These tasks are commonly referred to as 1-shot or 5-shot tasks. We evaluated the performance of our model on these tasks and reported the average accuracy along with a 95% confidence interval.

During multitask finetuning, the image encoder is directly optimized on few-shot classification tasks. To achieve this, we construct multitasks in the same format as the target tasks and optimize from the same evaluation protocol. Specifically, we create a total of 200 finetuning tasks, each task consists of 15 classes sampled from the train split of data, where each class contains 1 support image and 9 query images, resulting in 150 images per task. The classes in a finetuning task are sampled from the train split of the data.

To ensure a fair comparison with the finetuning baseline, we used the same training and testing data, as well as batch size, and applied standard finetuning. During standard finetuning, we added a linear layer after the encoder and trained the model. We also utilized the linear probing then finetuning (LP-FT) technique proposed by Kumar et al. [2022], which has been shown to outperform finetuning alone on both in-distribution and out-of-distribution data. In the testing stage, we removed the linear layer and applied the same few-shot testing pipeline to the finetuned encoders.

For task selection, we employ the CLIP ViT-B image encoder to obtain image embeddings. We assess consistency by measuring the cosine similarity of the mean embeddings and we evaluate diversity through a coverage score derived from the ellipsoid formula outlined in Section 3.3.2.

For optimization, we use the SGD optimizer with momentum 0.9, the learning rate is 1e-5 for CLIP and moco v3 pretrained models, and is 2e-6 for DINO v2 pretrained models. The models were finetuned over varying numbers of epochs in each scenario until they reached convergence.

8.5.3 Existence of Task Diversity

Task diversity is crucial for the foundation model to perform well on novel classes in target tasks.

In this section, we prove for task satisfying consistency, greater diversity in the related data can help reduce the error on the target task. Specifically, for the target task, where the target tasks data originates from the test split of a specific dataset, we utilized the train split of the same dataset as the finetuning tasks data. Then finetuning tasks satisfied consistency. In experiments, we varied the number of classes accessible to the model during the finetuning stage, while keeping the total sample number the same. This serves as a measure of the diversity of training tasks.

miniImageNet and Omniglot

We show the results of CLIP encoder on miniImageNet and Omniglot. We vary the number of classes model access to in finetuning stage. The number of classes varies from all classes, i.e., 64 classes, to 8 classes. Each task contains 5 classes. For finetuning tasks, each class contains 1 shot image and 10 query images. For target tasks, each class contains the 1-shot image and 15 query images.

# limited classes	64	32	16	8	0
Accuracy	90.02 ± 0.15	88.54 ± 1.11	87.94 ± 0.22	87.07 ± 0.20	83.03 ± 0.24

Table 8.1: Class diversity on ViT-B32 backbone on miniImageNet.

Table 8.1 shows the accuracy of ViT-B32 across different numbers of classes during the finetuning stage. The "Class 0" represents direct evaluation without any finetuning. We observe that finetuning the model leads to an average accuracy improvement of 4%. Furthermore, as the diversity of classes increases, we observe a corresponding increase in performance. This indicates that incorporating a wider range of classes during the finetuning process enhances the model's overall accuracy.

For task diversity, we also use dataset Omniglot [Lake et al., 2015]. The Omniglot dataset is designed to develop more human-like learning algorithms. It contains 1623 different handwritten characters from 50 different alphabets. The 1623 classes are divided into 964, 301, and 358 classes as training, validation, and testing sets respectively. We sample multitask in finetuning stage from training data and the target task from testing data.

# limited classes	964	482	241	50	10	0
Accuracy	95.35 ± 0.14	95.08 ± 0.14	94.29 ± 0.15	88.48 ± 0.20	80.26 ± 0.24	74.69 ± 0.26

Table 8.2: Class diversity on ViT-B32 backbone on Omniglot.

Table 8.2 shows the accuracy of ViT-B32 on different numbers of classes in finetuning stage, where class 0 indicates direct evaluation without finetuning. Finetuning improves the average accuracy by 5.5%. As class diversity increases, performance increases.

tieredImageNet

We then show results on tieredImageNet across learning settings for the ViT-B backbone. We follow the same setting where we restrain each task that contains 15 classes.

Pretrained	351	175	43	10
DINOv2	84.74	82.75	82.60	82.16
CLIP	68.57	67.70	67.06	63.52
Supervised	89.97	89.69	89.19	88.92

Table 8.3: The performance of the ViT-B backbone using different pretraining methods on tieredImagenet, varying the number of classes accessible to the model during the finetuning stage. Each column represents the number of classes within the training data.

We found that using more classes from related data sources during finetuning improves accuracy. This result indicates that upon maintaining consistency, a trend is observed where increased diversity leads to an enhancement in performance.

8.5.4 Ablation Study

In Section 3.4 and the result in Table 3.2, we utilize the train split from the same dataset to construct the finetuning data. It is expected that the finetuning data possess a diversity and consistency property, encompassing characteristics that align with the test data while also focusing on its specific aspects.

In the following ablation study, we explore the relationship between the diversity and consistency of data in finetuning tasks, sample complexity, and finetuning methods. We seek to answer the following questions: Does multitask finetuning benefit only from certain aspects? How do these elements interact with each other?

Violate both consistency and diversity: Altering Finetuning Task Data with Invariant Sample Complexity

In this portion, we examine the performance when the model is finetuned using data completely unrelated to the target task data. With the same finetuning sample complexity, the performance cannot be compared to the accuracy we have currently attained.

In this section, we present the performance of MoCo v3 with a ViT-B backbone on the DomainNet dataset. We finetuned the model using either ImageNet data or DomainNet train-split data and evaluated its performance on the test-split of DomainNet. We observed that finetuning the model with data selected from the DomainNet train-split resulted in improved performance on the target task. This finding aligns with our expectations and highlights the significance of proper finetuning data selection.

When considering the results presented in Table 8.4, we also noticed that for MoCo v3 with a ResNet50 backbone and DINO v2 with a ViT-S backbone, multitask finetuning on ImageNet led to a decrease in model performance compared to direct adaptation. This suggests that inappropriate data selection can have a detrimental effect on the final model performance. This conclusion is also supported by the findings of Kumar et al. [2022].

Violating consistency while retaining diversity: The Trade-Off between Task Consistency and Sample Complexity

Finetuning tasks with superior data are expected to excel under identical complexity, a natural question can be proposed: Does additional data enhance performance? Our results in this section negate this question. Testing the model on the DomainNet test-split, we employ two settings. In the first setting, we finetune the model on the DomainNet train-split.

pretrained	backbone	FT data	Accuracy
MoCo v3	ViT-B	ImageNet	24.88 (0.25)
		DomainNet	32.88 (0.29)
	ResNet50	ImageNet	27.22 (0.27)
		DomainNet	33.53 (0.30)
DINO v2	ViT-S	ImageNet	51.69 (0.39)
		DomainNet	61.57 (0.40)
	ViT-B	ImageNet	62.32 (0.40)
		DomainNet	68.22 (0.40)
Supervised	ViT-B	ImageNet	31.16 (0.31)
		DomainNet	48.02 (0.38)
	ResNet50	ImageNet	29.56 (0.28)
		DomainNet	39.09 (0.34)

Table 8.4: Finetuning data selection on model performance. FT data: dataset we select for multitask finetuning. Report the accuracy on the test-split of DomainNet.

In the second, the model is finetuned with a combination of the same data from DomainNet as in the first setting, along with additional data from ImageNet.

Within our theoretical framework, mixing data satisfies diversity but fails consistency. The finetuning data, although containing related information, also encompasses excessive unrelated data. This influx of unrelated data results in a larger consistency parameter κ in our theoretical framework, adversely impacting model performance on the target task. We offer empirical evidence to affirm our theoretical conclusion.

Pretrained	DomainNet	DomainNet + ImageNet
DINOv2	68.22	66.93
CLIP	64.97	63.48
Supervised	48.02	43.76

Table 8.5: Results evaluating on DomainNet test-split using ViT-B backbone. First column shows performance where model finetune on data from DomainNet train-split alone, second column shows the performance of the model finetuned using a blend of the same data from DomainNet, combined with additional data from ImageNet.

Table 8.5 shows mixed data of domainNet and ImageNet will doesn't provide the same advantages as using only DomainNet data. In this case, an increasing in data does not necessarily mean better performance.

Diversity and Consistency of Task Data and Finetuning Methods

To provide a more comprehensive understanding of the impact of task data and finetuning methods on model performance, we conduct additional experiments, utilizing varying finetuning methods and data. The model is tested on the DomainNet test split. We employ either multitask finetuning or standard finetuning, where a linear layer is added after the pretrained model. This linear layer maps the representations learned by encoders to the logits. The data of finetuning tasks derive from either the DomainNet train-split or ImageNet.

In Table 8.6, we detail how data quality and finetuning methods of tasks impact the ultimate performance. Standard finetuning (SFT) with unrelated data diminishes performance compared to direct adaptation (col-1 vs col-2). On the other hand, multitask finetuning using unrelated data (ImageNet), or SFT with related data (DomainNet), both outperform direct adaptation. However, multitask finetuning with unrelated data proves more beneficial than the latter (col-3 vs col-4). The peak performance is attained through multitask finetuning on related data (col-5).

Pretrained	1 Adaptation	2 ImageNet (SFT)	3 ImageNet (Ours)	4 DomainNet (SFT)	5 DomainNet (Ours)
DINOv2	61.65	59.80	62.32	61.84	68.22
CLIP	46.39	46.50	58.94	47.72	64.97
Supervised	28.70	28.52	31.16	30.93	48.02

Table 8.6: Results evaluating on DomainNet test-split using ViT-B backbone. Adaptation: Direction adaptation without finetuning; SFT: Standard finetuning; Ours: Our multitask finetuning. Col-1 shows performance without any finetuning, Col-2,3,4,5 shows performance with different finetuning methods and data.

Pretrained	Selection	INet	Omglot	Acraft	CUB	QDraw	Fungi	Flower	Sign	COCO
CLIP	All	60.87	70.53	31.67	66.98	40.28	34.88	80.80	37.82	33.71
	Selected	60.87	**77.93**	**32.02**	**69.15**	**42.36**	**36.66**	**80.92**	**38.46**	**37.21**
DINOv2	All	83.04	72.92	36.52	94.01	49.65	52.72	98.54	34.59	47.05
	Selected	83.04	**80.29**	**36.91**	**94.12**	**52.21**	**53.31**	**98.65**	**36.62**	**50.09**
MoCo v3	All	59.62	60.85	18.72	40.49	40.96	32.65	59.60	33.94	33.42
	Selected	59.62	**63.08**	**19.03**	**40.74**	**41.16**	**32.89**	**59.64**	**35.25**	**33.51**

Table 8.7: Results evaluating our task selection algorithm on Meta-dataset using ViT-B backbone.

Ablation Study on Task Selection Algorithm

We show a simplified diagram for task selection in Figure 3.2.

We first provide some details of Table 3.1. We first create an array of finetuning tasks, and then apply our task selection algorithm to these tasks. Specifically, we design 100 finetuning tasks by randomly selecting 15 classes, each providing 1 support sample and 10 query samples. The target tasks remain consistent with those discussed in Section 3.4. For a more comprehensive analysis of our algorithm, we performed ablation studies on the task selection algorithm, concentrating solely on either consistency or diversity, while violating the other. **Violate Diversity**: If the algorithm terminates early without fulfilling the stopping criteria, the data utilized in finetuning tasks fails to encompass all the attributes present in the target data. This leads to a breach of the diversity principle. **Violate Consistency**: Conversely, if the algorithm persists beyond the stopping criteria, the finetuning tasks become overly inclusive, incorporating an excessive amount of unrelated data, thus breaching the consistency.

This section details an ablation study on task selection for the dataset, we implement our task selection process on a meta-dataset, treating each dataset as a distinct task and choosing datasets to serve as data sources for the finetuning tasks. We show the result in Table 8.7.

Table 8.7 indicates that maintaining both consistency and diversity in the task selection algorithm is essential for optimal performance. This is evident from the comparison between the Random selection and the our approach, where the latter often shows improved performance across multiple datasets. ImageNet as the target task is an exception where the two approaches give the best results. Due to its extensive diversity, all samples from all other datasets are beneficial for finetuning. Consequently, the task selection algorithm tends to select all the candidate tasks.

8.5.5 Task Selection Algorithm on DomainNet

We verify our task selection algorithm by applying it on DomainNet. Here, the mini-ImageNet test-split is regarded as the target task source, and diverse domains (such as clipart (clp), infograph (inf), quickdraw (qdr), real (rel), and sketch (skt)) are considered as sources for finetuning tasks. We view different domain datasets as distinct finetuning tasks. With 6 domains in focus, our objective is to select a subset that optimizes model performance. We systematically apply Algorithm 1. Initially, we calculate the cosine similarity of mean embeddings between each domain and target tasks, ordering them from most to least similar: real, painting, sketch, clipart, infograph, and quickdraw. Sequentially adding datasets in this order, the process continues until the diversity score (1 over Mahalanobis distance) stops exhibiting significant increase.

As we can see in Figure 8.1, the diversity does not increase when we just select *real* and *painting* as our finetuning task data. For a comprehensive analysis, each combination is finetuned and the model performance accuracy on the target task is displayed.

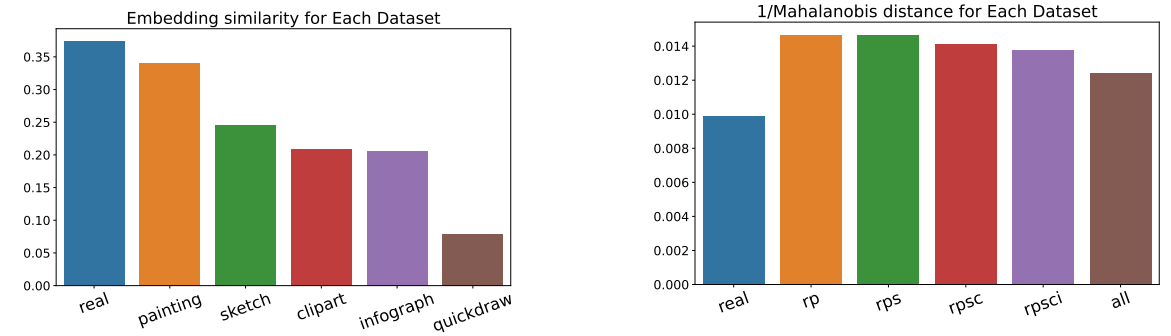

(a) Mean embedding similarity for each data sort from most similar to least similar.

(b) Diversity score when adding task one by one, where *rp*: *real* and *painting*; *rps*: *real* and *painting* and *sketch* and so on.

Figure 8.1: Dataset selection based on consistency and diversity on domainNet. Figure 8.1a shows the consistency. Figure 8.1b shows the diversity.

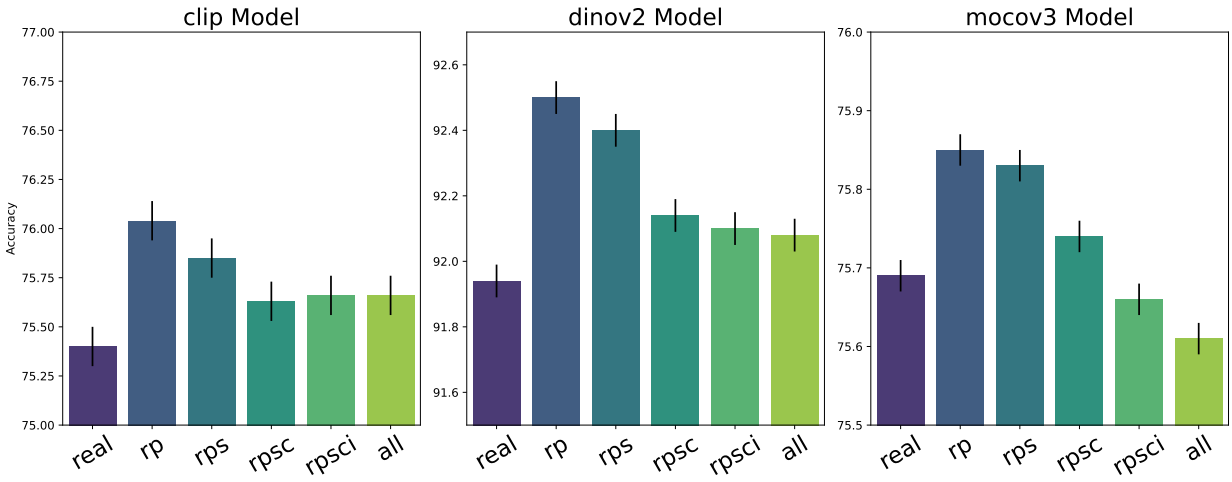

Figure 8.2: Finetuning with different selection of domain datasets, where *rp*: *real* and *painting*; *rps*: *real* and *painting* and *sketch* and so on.

As we can see in Figure 8.2,the accuracy aligns with the conclusions drawn based on consistency and diversity. Remarkably, only *real* and *painting* suffice for the model to excel on the target task.

8.5.6 More Results with CLIP Encoder

In this section, we show additional results on CLIP [Radford et al., 2021] model.

We can observe from Table 8.8 standard finetuning improves performance compared to direct adaptation. However, our proposed multitask finetuning approach consistently achieves even better results than the standard baseline.

Task (M) vs Sample (m). We vary the task size and sample size per task during finetuning. We verify the trend of different numbers of tasks and numbers of images per task. Each task contains 5 classes. For finetuning tasks, $m = 50$ indicates each class contains the 1-shot image and 9-query images. $m = 100$ indicates each class contains 2-shot and 18-query images. $m = 200$ indicates each class contains 4-shot and 36-query images. $M = m = 0$ indicates direct evaluation without finetuning. For target tasks, each class contains the 1-shot image and 15 query images.

Table 8.9 shows the results on the pretrained CLIP model using the ViT backbone. For direct adaptation without finetuning, the model achieves 83.03% accuracy. Multitask finetuning improves the average accuracy at least by 6%.

		miniImageNet		tieredImageNet		DomainNet	
backbone	**method**	**1-shot**	**5-shot**	**1-shot**	**5-shot**	**1-shot**	**5-shot**
CLIP-ViTB32	Direct Adaptation	68.41 (0.54)	87.43 (0.15)	59.55 (0.21)	79.51 (0.27)	46.48 (0.37)	72.01 (0.29)
	Standard FT	69.39 (0.30)	88.39 (0.15)	61.20 (0.37)	80.65 (0.27)	47.72 (0.37)	72.82 (0.29)
	Multitask FT (Ours)	**78.62** (0.15)	**93.22** (0.11)	**68.57** (0.37)	**84.79** (0.22)	**64.97** (0.39)	**80.49** (0.25)
CLIP-ResNet50	Direct Adaptation	61.31 (0.31)	82.03 (0.18)	51.76 (0.36)	71.40 (0.30)	40.55 (0.36)	64.90 (0.31)
	Standard FT	63.15 (0.31)	83.45 (0.17)	55.77 (0.35)	75.28 (0.29)	43.77 (0.38)	67.30 (0.31)
	Multitask FT (Ours)	**67.03** (0.30)	**85.09** (0.17)	**57.56** (0.36)	**75.80** (0.28)	**52.67** (0.39)	**72.19** (0.30)

Table 8.8: **Comparison on 15-way classification.** Average few-shot classification accuracies (%) with 95% confidence intervals clip encoder.

Task (M) \ **Sample (m)**	0	50	100	200
0	83.03 ± 0.24			
200		89.07 ± 0.20	89.95 ± 0.19	$\mathbf{90.09 \pm 0.19}$
400		89.31 ± 0.19	$\mathbf{90.11 \pm 0.19}$	90.70 ± 0.18
800		$\mathbf{89.71 \pm 0.19}$	90.27 ± 0.19	90.80 ± 0.18

Table 8.9: Accuracy with a varying number of tasks and samples (ViT-B32 backbone).

For a fixed number of tasks or samples per task, increasing samples or tasks improves accuracy. These results suggest that the total number of samples ($M \times m$) will determine the overall performance, supporting our main theorem.

Few-shot Effect. We perform experiments on the few-shot effects of finetuning tasks. We aim to evaluate whether increasing the number of few-shot images in the finetuning task leads to significant improvements. Each finetuning task consists of 5 classes, and we maintain a fixed number of 10 query images per class while gradually increasing the number of shot images, as illustrated in Table 8.10. As for the target tasks, we ensure each class contains 1 shot image and 15 query images for evaluation.

# shot images	20	10	5	1	0
Accuracy	91.03 ± 0.18	90.93 ± 0.18	90.54 ± 0.18	90.02 ± 0.15	83.03 ± 0.24

Table 8.10: Few-shot effect on ViT-B32 backbone on miniImageNet.

Table 8.10 displays the accuracy results of ViT-B32 when varying the number of few-shot images in the finetuning tasks. We observe that increasing the number of few-shot images, thereby augmenting the sample size within each task, leads to improved performance. This finding is quite surprising, considering that the finetuning tasks and target tasks have different numbers of shot images. However, this aligns with our understanding of sample complexity, indicating that having access to more training examples can enhance the model's ability to generalize and perform better on unseen data.

8.5.7 Sample Complexity on Performance for tieredImageNet

We provide a table and visualization of the trend of the number of tasks and the number of samples per task for the MoCo v3 ViT model on tieredImageNet in Table 8.11 and Figure 8.3.

As demonstrated in the paper, we have observed that increasing the number of tasks generally leads to performance improvements, while keeping the number of samples per task constant. Conversely, when the number of samples per task is increased while maintaining the same number of tasks, performance also tends to improve. These findings emphasize the positive relationship between the number of tasks and performance, as well as the influence of sample size within each task.

8.5.8 Full results for Effectiveness of Multitask Finetuning

In this section, we provide another baseline in complement to the results in Section 3.4.3.

Task (M) \ Sample (m)	150	300	450	600
200	68.32 (0.35)	71.42 (0.35)	73.84 (0.35)	75.58 (0.35)
400	71.41 (0.35)	75.60 (0.35)	77.57 (0.34)	78.66 (0.34)
600	73.85 (0.35)	77.59 (0.34)	79.04 (0.33)	79.76 (0.33)
800	75.56 (0.35)	78.68 (0.34)	79.78 (0.33)	80.26 (0.33)

Table 8.11: Accuracy with a varying number of tasks and samples (ViT-B32 backbone).

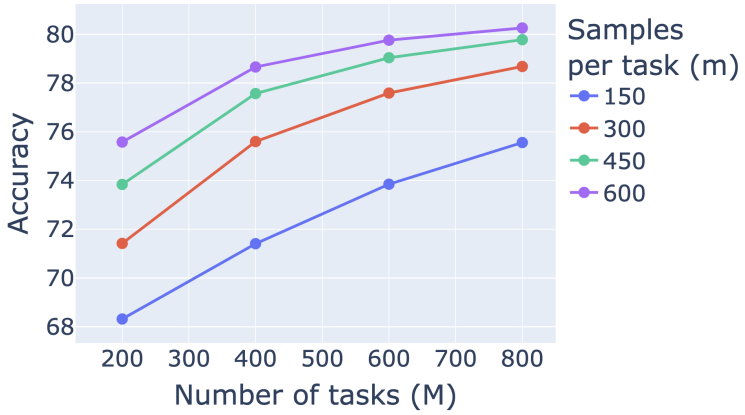

Figure 8.3: Finetuning using tieredImageNet train-split, test on test-split.

We incorporated the Model-Agnostic Meta-Learning (MAML) algorithm, as outlined by Finn et al. [2017], as another baseline for our few-shot tasks. MAML operates in a two-step process: it initially updates parameters based on within-episode loss (the inner loop), then it evaluates and updates loss based on learned parameters (the outer loop). We follow the pipeline in Triantafillou et al. [2020] to implement MAML for few-shot tasks. We show results in Table 8.12.

Table 8.12 reveals that MAML exhibits variable performance across different settings. For instance, it outperforms both Adaptation and Standard FT methods in scenarios like MoCo v3 ViT-B on miniImageNet, DomainNet, and ResNet 50 on supervised training for tieredImageNet. However, its performance is less impressive in other contexts, such as DINOv2 ViT-B on miniImageNet and ViT-B on supervised training for miniImageNet. This variability in performance is attributed to the constraints of our few-shot tasks, where the limited number of support samples restricts the model's capacity to adapt to new tasks. Despite these fluctuations, our multitask finetuning approach consistently surpasses the mentioned baselines, often by a significant margin, across all evaluated scenarios.

			miniImageNet		tieredImageNet		DomainNet	
pretrained	**backbone**	**method**	**1-shot**	**5-shot**	**1-shot**	**5-shot**	**1-shot**	**5-shot**
MoCo v3	ViT-B	Adaptation	75.33 (0.30)	92.78 (0.10)	62.17 (0.36)	83.42 (0.23)	24.84 (0.25)	44.32 (0.29)
		Standard FT	75.38 (0.30)	92.80 (0.10)	62.28 (0.36)	83.49 (0.23)	25.10 (0.25)	44.76 (0.27)
		MAML	79.26 (0.28)	93.02 (0.08)	67.96 (0.32)	84.66 (0.19)	28.91 (0.39)	51.12 (0.28)
		Ours	**80.62** (0.26)	**93.89** (0.09)	**68.32** (0.35)	**85.49** (0.22)	**32.88** (0.29)	**54.17** (0.30)
	ResNet50	Adaptation	68.80 (0.30)	88.23 (0.13)	55.15 (0.34)	76.00 (0.26)	27.34 (0.27)	47.50 (0.28)
		Standard FT	68.85 (0.30)	88.23 (0.13)	55.23 (0.34)	76.07 (0.26)	27.43 (0.27)	47.65 (0.28)
		MAML	69.28 (0.26)	88.78 (0.12)	55.31 (0.32)	75.51 (0.19)	27.53 (0.39)	47.73 (0.28)
		Ours	**71.16** (0.29)	**89.31** (0.12)	**58.51** (0.35)	**78.41** (0.25)	**33.53** (0.30)	**55.82** (0.29)
DINO v2	ViT-S	Adaptation	85.90 (0.22)	95.58 (0.08)	74.54 (0.32)	89.20 (0.19)	52.28 (0.39)	72.98 (0.28)
		Standard FT	86.75 (0.22)	95.76 (0.08)	74.84 (0.32)	89.30 (0.19)	54.48 (0.39)	74.50 (0.28)
		MAML	86.67 (0.24)	95.54 (0.08)	74.63 (0.34)	89.60 (0.19)	52.72 (0.34)	73.35 (0.28)
		Ours	**88.70** (0.22)	**96.08** (0.08)	**77.78** (0.32)	**90.23** (0.18)	**61.57** (0.40)	**77.97** (0.27)
	ViT-B	Adaptation	90.61 (0.19)	97.20 (0.06)	82.33 (0.30)	92.90 (0.16)	61.65 (0.41)	79.34 (0.25)
		Standard FT	91.07 (0.19)	97.32 (0.06)	82.40 (0.30)	93.07 (0.16)	61.84 (0.39)	79.63 (0.25)
		MAML	90.77 (0.18)	97.20 (0.08)	82.54 (0.32)	92.88 (0.19)	62.30 (0.39)	79.01 (0.28)
		Ours	**92.77** (0.18)	**97.68** (0.06)	**84.74** (0.30)	**93.65** (0.16)	**68.22** (0.40)	**82.62** (0.24)
Supervised pretraining on ImageNet	ViT-B	Adaptation	94.06 (0.15)	97.88 (0.05)	83.82 (0.29)	93.65 (0.13)	28.70 (0.29)	49.70 (0.28)
		Standard FT	95.28 (0.13)	98.33 (0.04)	86.44 (0.27)	94.91 (0.12)	30.93 (0.31)	52.14 (0.29)
		MAML	95.35 (0.12)	98.50 (0.08)	86.79 (0.32)	94.72 (0.19)	30.53 (0.39)	52.21 (0.28)
		Ours	**96.91** (0.11)	**98.76** (0.04)	**89.97** (0.25)	**95.84** (0.11)	**48.02** (0.38)	**67.25** (0.29)
	ResNet50	Adaptation	81.74 (0.24)	94.08 (0.09)	65.98 (0.34)	84.14 (0.21)	27.32 (0.27)	46.67 (0.28)
		Standard FT	84.10 (0.22)	94.81 (0.09)	74.48 (0.33)	88.35 (0.19)	34.10 (0.31)	55.08 (0.29)
		MAML	82.07 (0.28)	94.12 (0.08)	75.69 (0.32)	89.30 (0.19)	35.10 (0.39)	56.51 (0.28)
		Ours	**87.61** (0.20)	**95.92** (0.07)	**77.74** (0.32)	**89.77** (0.17)	**39.09** (0.34)	**60.60** (0.29)

Table 8.12: **Results of few-shot image classification.** We report average classification accuracy (%) with 95% confidence intervals on test splits. Adaptation: Direction adaptation without finetuning; Standard FT: Standard finetuning; MAML: MAML algorithm in Finn et al. [2017]; Ours: Our multitask finetuning; 1-/5-shot: number of labeled images per class in the target task.

8.6 NLP Experimental Results

We first provide a summary of the experimental setting and results in the below subsection. Then we provide details in the following subsections.

8.6.1 Summary

To further validate our approach, we conducted prompt-based finetuning experiments on masked language models, following the procedure outlined in Gao et al. [2021a].

Datasets and Models. We consider a collection of 14 NLP datasets, covering 8 single-sentence and 6 sentence-pair English tasks. This collection includes tasks from the GLUE benchmark [Wang et al., 2018a], as well as 7 other popular sentence classification tasks. The objective is to predict the label based on a single sentence or a sentence-pair. Specifically, the goal is to predict sentiments for single sentences or to estimate the relationship between sentence pairs. Each of the datasets is split into training and test set. See details in Section 8.6.2. We experiment with a pretrained model RoBERTa [Liu et al., 2019].

Experiment Protocols. We consider prompt-based finetuning for language models [Gao et al., 2021a]. This approach turns a prediction task into a masked language modeling problem, where the model generates a text response to a given task-specific prompt as the label. Our experiment protocol follows Gao et al. [2021a]. The experiments are divided into 14 parallel experiments, each corresponding to a dataset. For the few-shot experiment, we use test split data as the target task data and sample 16 examples per class from the train split as finetuning data. The evaluation metric is measured by prompt-based prediction accuracy.

During the testing stage, we conduct experiments in zero-shot and few-shot settings for a given dataset. In the zero-shot setting, we directly evaluate the model's prompt-based prediction accuracy. In the few-shot setting, we finetune the model using support samples from the same dataset and assess its accuracy on the test split. For multitask finetuning,

	SST-2 (acc)	SST-5 (acc)	MR (acc)	CR (acc)	MPQA (acc)	Subj (acc)	TREC (acc)	CoLA (Matt.)
Prompt-based zero-shot	83.6	35.0	80.8	79.5	67.6	51.4	32.0	2.0
Multitask FT zero-shot	**92.9**	37.2	86.5	88.8	73.9	55.3	36.8	-0.065
Prompt-based FT†	92.7 (0.9)	47.4 (2.5)	87.0 (1.2)	90.3 (1.0)	84.7 (2.2)	**91.2** (1.1)	84.8 (5.1)	**9.3** (7.3)
Multitask Prompt-based FT	92.0 (1.2)	**48.5** (1.2)	86.9 (2.2)	90.5 (1.3)	**86.0** (1.6)	89.9 (2.9)	83.6 (4.4)	5.1 (3.8)
+ task selection	92.6 (0.5)	47.1 (2.3)	**87.2** (1.6)	**91.6** (0.9)	85.2 (1.0)	90.7 (1.6)	**87.6** (3.5)	3.8 (3.2)

	MNLI (acc)	MNLI-mm (acc)	SNLI (acc)	QNLI (acc)	RTE (acc)	MRPC (F1)	QQP (F1)
Prompt-based zero-shot	50.8	51.7	49.5	50.8	51.3	61.9	49.7
Multitask FT zero-shot	63.2	65.7	61.8	65.8	74.0	81.6	63.4
Prompt-based FT†	68.3 (2.3)	70.5 (1.9)	77.2 (3.7)	64.5 (4.2)	69.1 (3.6)	74.5 (5.3)	65.5 (5.3)
Multitask Prompt-based FT	70.9 (1.5)	73.4 (1.4)	**78.7** (2.0)	71.7 (2.2)	**74.0** (2.5)	**79.5** (4.8)	67.9 (1.6)
+ task selection	**73.5** (1.6)	**75.8** (1.5)	77.4 (1.6)	**72.0** (1.6)	70.0 (1.6)	76.0 (6.8)	**69.8** (1.7)

Table 8.13: **Results of few-shot learning with NLP benchmarks.** All results are obtained using RoBERTa-large. We report mean (and standard deviation) of metrics over 5 different splits. †: Result in Gao et al. [2021a]; FT: finetuning; task selection: select multitask data from customized datasets.

we select support samples from other datasets and construct tasks for prompt-based finetuning. We then evaluate the performance of the finetuned model on the target task. More details can be found in Section 8.6.3.

Task Selection. We select datasets by using task selection algorithm of feature vectors, which are obtained by computing the representations of each dataset and analyzing their relationship. We first obtain text features for each data point in the dataset. We select few-shot samples for generating text features. For each example, we replace the masked word with the true label in its manual template, then we forward them through the BERT backbone. Then, we compute the first principal component to obtain a feature vector for each dataset. Dataset selection provides certain improvements on some datasets, as elaborated below. Further details can be found in Section 8.6.4.

Results. Our results are presented in Table 8.13. Again, our method outperforms direct adaptation on target tasks across most datasets. For zero-shot prediction, our method provides improvements on all datasets except CoLA. Our multitask finetuning approach results in performance improvements on 12 out of 15 target tasks for few-shot prediction, with the exceptions being SST-2, Subj, and CoLA. CoLA is also reported by Gao et al. [2021a] as an exception that contains non-grammatical sentences that are outside of the distribution of the pretrained language model. SST-2 already achieves high accuracy in zero-shot prediction, and our model performs best in such setting. Subj is unique in that its task is to predict whether a given sentence is subjective or objective, therefore multitasking with few-shot samples from other datasets may not provide significant improvement for this task.

8.6.2 Datasets and Models

The text dataset consisted of 8 single-sentence and 6 sentence-pair English tasks, including tasks from the GLUE benchmark [Wang et al., 2018a], as well as 7 other popular sentence classification tasks (SNLI [Bowman et al., 2015], SST-5 [Socher et al., 2013], MR [Pang and Lee, 2005], CR [Hu and Liu, 2004], MPQA [Wiebe et al., 2005], Subj [Pang and Lee, 2004], TREC [Voorhees and Tice, 2000]). The objective was to predict the label based on a single sentence or a sentence-pair. Specifically, for single sentences, we aimed to predict their semantics as either positive or negative, while for sentence-pairs, we aimed to predict the relationship between them. We experiment with the pretrained model `RoBERTa`. We have 14 datasets in total. We split each dataset into train and test split, see details below. We experiment with the pretrained model `RoBERTa`.

We follow Gao et al. [2021a] in their train test split. We use the original development sets of SNLI and datasets from GLUE for testing. For datasets such as MR, CR, MPQA, and Subj that require a cross-validation evaluation, we randomly select 2,000 examples for testing and exclude them from training. For SST5 and TREC, we utilize their official test sets.

To construct multitask examples from support samples, we gather support samples from all datasets except the testing dataset. For each task, we randomly select ten support samples and prompt-based finetuning the model.

Task	Template	Label words
SST-2	<S_1> It was [MASK] .	positive: great, negative: terrible
SST-5	<S_1> It was [MASK] .	v.positive: great, positive: good, neutral: okay, negative: bad, v.negative: terrible
MR	<S_1> It was [MASK] .	positive: great, negative: terrible
CR	<S_1> It was [MASK] .	positive: great, negative: terrible
Subj	<S_1> This is [MASK] .	subjective: subjective, objective: objective
TREC	[MASK] : <S_1>	abbreviation: Expression, entity: Entity, description: Description human: Human, location: Location, numeric: Number
COLA	<S_1> This is [MASK] .	grammatical: correct, not_grammatical: incorrect
MNLI	<S_1> ? [MASK] , <S_2>	entailment: Yes, netural: Maybe, contradiction: No
SNLI	<S_1> ? [MASK] , <S_2>	entailment: Yes, netural: Maybe, contradiction: No
QNLI	<S_1> ? [MASK] , <S_2>	entailment: Yes, not_entailment: No
RTE	<S_1> ? [MASK] , <S_2>	entailment: Yes, not_entailment: No
MRPC	<S_1> [MASK] , <S_2>	equivalent: Yes, not_equivalent: No
QQP	<S_1> [MASK] , <S_2>	equivalent: Yes, not_equivalent: No

Table 8.14: Manual templates and label words that we used in our experiments, following Gao et al. [2021a].

8.6.3 Experiment Protocols

Gao et al. [2021a] proposed a prompt-based finetuning pipeline for moderately sized language models such as `BERT`, `RoBERTa`. Prompt-based prediction converts the downstream prediction task as a (masked) language modeling problem, where the model directly generates a textual response also known as a label word, to a given prompt defined by a task-specific template. As an illustration, consider the SST-2 dataset, which comprises sentences expressing positive or negative sentiment. The binary classification task can be transformed into a masked prediction problem using the template `<S>, it was <MASK>.`, where `<S>` represents the input sentence and `<MASK>` is the label word (e.g., "great" or "terrible") that the model is supposed to predict, see full templates in Table 8.14. Prompt-based finetuning updates the model with prompt-based prediction loss for a given example, such as a sentence or sentence-pair.

To conduct the few-shot experiment, we use all data from the test split as the target task data for each dataset, and sample 16 examples per class from the train split as the support samples. The experiments are divided into 14 parallel experiments, with each corresponding to one dataset. The evaluation accuracy is measured as the prompt-based prediction accuracy. We subsampled 5 different sets of few-shot examples to run replicates experiments and report average performance.

During the testing stage, for a given dataset (e.g. QNLI), we consider the entire test split as the target task and divide the experiment into zero-shot and few-shot settings. In the zero-shot setting, we directly evaluate the model by measuring the accuracy of prompt-based predictions. In the few-shot setting, we first prompt-based finetune the model with support samples from the same dataset (QNLI) and then evaluate the accuracy on the test split. This experimental protocol follows the same pipeline as described in Gao et al. [2021a].

To perform multitask finetuning for a target task on a particular dataset (e.g. QNLI), we select support samples from other datasets (e.g. SST-2, Subj, QQP, etc.) as finetuning examples. We construct tasks using these examples and apply the same prompt-based finetuning protocol to multitask finetune the model on these tasks. Finally, we evaluate the performance of the finetuned model on the target task.

8.6.4 Task Selection

The importance of the relationship between the data used in the training tasks and the target task cannot be overstated in multitask finetuning. Our theory measures this relationship through diversity and consistency statements, which require that our finetuning data are diverse enough to capture the characteristics of the test data, while still focusing on the specific regions where the test data aligns. We visualize this diversity and relationship through the feature maps of the datasets.

To visualize the relationship between feature vectors of different datasets, we first obtain text features for each data point in the dataset. We select few-shot samples for generating text features. For each example, we replace the masked word with the true label in its manual template, then we forward them through the `BERT` backbone. The reason for using `BERT` over `RoBERTa` is that the latter only has masked token prediction in pretraining, the `[CLS]` in pretrained `RoBERTa`

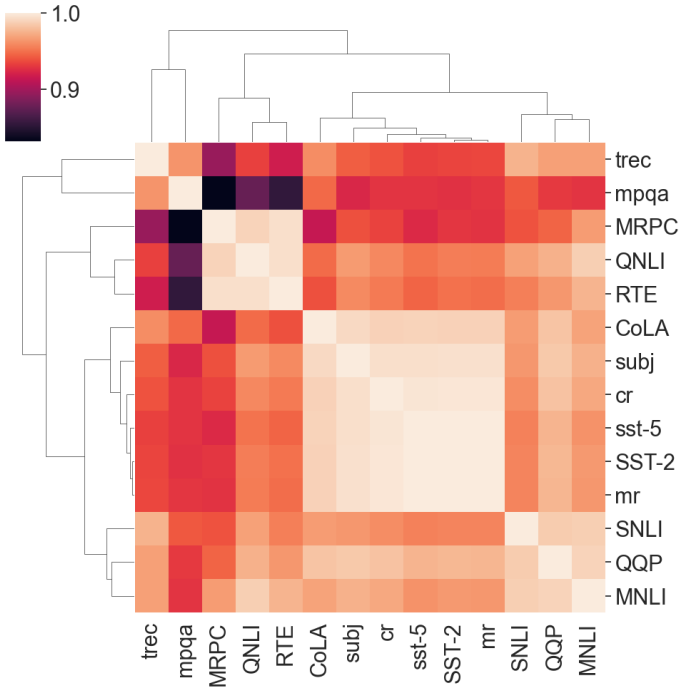

Figure 8.4: Linear similarity among features vectors among 14 language datasets.

cola: mr, cr,sst-2,sst-5,subj
sst-2: cola,mr, cr,sst-5,subj,
mrpc: qnli, rte
qqp: snli, mnli
mnli: snli, qqp
snli: qqp, mnli
qnli: mrpc, rte
rte: mrpc, qnli
mr: cola, cr,sst-2,sst-5,subj
sst-5: cola,mr, cr,sst-2,subj
subj: cola,mr, cr,sst-2,sst-5
trec: mpqa
cr: cola,mr,sst-2,sst-5,subj
mpqa: trec

Table 8.15: Dataset selection.

model might not contain as much sentence information as BERT. Then, we compute the first principal component to obtain a feature vector for each dataset. We illustrate the relationship between these feature vectors in Figure 8.4.

We further perform training data selection based on the task selection algorithm among the feature vectors, the selected dataset is shown in table Table 8.15.

By performing task selection, we observed further improvements in multitask prompt-based finetuning on MR, CR, TREC, MNLI, QNLI, and QQP datasets. However, it's worth noting that the CoLA dataset is an exception, as it involves predicting the grammaticality of sentences, and its inputs may include non-grammatical sentences that are outside the

	SST-2 (acc)	SST-5 (acc)	MR (acc)	CR (acc)	MPQA (acc)	Subj (acc)	TREC (acc)	CoLA (Matt.)
Prompt-based zero-shot	83.6	35.0	80.8	79.5	67.6	51.4	32.0	2.0
Multitask FT zero-shot	**92.9**	37.2	86.5	88.8	73.9	55.3	36.8	-0.065
+ task selection	92.5	34.2	87.1	88.7	71.8	72.0	36.8	0.001
Prompt-based FT†	92.7 (0.9)	47.4 (2.5)	87.0 (1.2)	90.3 (1.0)	84.7 (2.2)	**91.2** (1.1)	84.8 (5.1)	**9.3** (7.3)
Multitask Prompt-based FT	92.0 (1.2)	**48.5** (1.2)	86.9 (2.2)	90.5 (1.3)	**86.0** (1.6)	89.9 (2.9)	83.6 (4.4)	5.1 (3.8)
+ task selection	92.6 (0.5)	47.1 (2.3)	**87.2** (1.6)	**91.6** (0.9)	85.2 (1.0)	90.7 (1.6)	**87.6** (3.5)	3.8 (3.2)

	MNLI (acc)	MNLI-mm (acc)	SNLI (acc)	QNLI (acc)	RTE (acc)	MRPC (F1)	QQP (F1)
Prompt-based zero-shot	50.8	51.7	49.5	50.8	51.3	61.9	49.7
Multitask FT zero-shot	63.2	65.7	61.8	65.8	74.0	81.6	63.4
+ task selection	62.4	64.5	65.5	61.6	64.3	75.4	57.6
Prompt-based FT†	68.3 (2.3)	70.5 (1.9)	77.2 (3.7)	64.5 (4.2)	69.1 (3.6)	74.5 (5.3)	65.5 (5.3)
Multitask Prompt-based FT	70.9 (1.5)	73.4 (1.4)	**78.7** (2.0)	71.7 (2.2)	**74.0** (2.5)	**79.5** (4.8)	67.9 (1.6)
+ task selection	**73.5** (1.6)	**75.8** (1.5)	77.4 (1.6)	**72.0** (1.6)	70.0 (1.6)	76.0 (6.8)	**69.8** (1.7)

Table 8.16: **Results of few-shot learning with NLP benchmarks.** All results are obtained using RoBERTa-large. We report the mean (and standard deviation) of metrics over 5 different splits. †: Result in Gao et al. [2021a] in our paper; FT: finetuning; task selection: select multitask data from customized datasets.

distribution of masked language models, as noted in Gao et al. [2021a]. Overall, our approach shows promising results for multitask learning in language tasks.

Full Results with Task Selection

To complement task selection in Table 8.13, we provide full results here and explain each method thoroughly.

We first elaborate on what each method did in each stage. During the testing stage, we conducted experiments in zero-shot and few-shot settings for a given dataset following Gao et al. [2021a], who applied prompt-based methods on moderately sized language models such as RoBERTa. Prompt-based finetuning method updates the model with prompt-based prediction loss for a given example. The given example can either be from a testing dataset or other datasets.

Table 8.16 shows our multitask finetuning and task selection provide helps on target tasks, as detailed in Section 8.6.1. We will elaborate on what each method did in the "Multitask fintuning phase" and "Downstream phase".

In the "Multitask fintuning phase": For prompt-based zero-shot (col-1) and prompt-based FT (col-4) we do not finetune any model. For Multitask Prompt-based finetuning (col-2,3,5,6), we conduct prompt-based finetuning methods using finetuning(auxiliary) tasks. The data of tasks are from datasets other than testing datasets. For instance, consider a model designated to adapt to a dataset (say SST-2), we choose data from other datasets (mr, cr, etc.) and combine these data together and form multiple auxiliary tasks, these tasks updated the model using prompt-based finetuning methods. In the "downstream phase" where we adapt the model: In the zero-shot setting (col-1,2,3), we directly evaluate the model's prompt-based prediction accuracy. In the few-shot setting (col-4,5,6), we finetune the model using shot samples from the same dataset (sst-2) and assess its accuracy on the test split.

Additional Results on simCSE

We present our results using the same approach as described in our paper. However, we used a different pretrained loss, namely simCSE, as proposed by Gao et al. [2021c]. However, the results are not promising, The reason is simCSE is trained with a contrastive loss instead of masked language prediction, making it less suitable for prompt-based finetuning.

8.7 Vision Language Tasks

Pretrained vision-language as another type of foundation model has achieved tremendous success across various downstream tasks. These models, such as CLIP [Radford et al., 2021] and ALIGN [Jia et al., 2021], align images and text in a shared space, enabling zero-shot classification in target tasks. Finetuning such models has resulted in state-of-the-art accuracy in several benchmarks.

	SST-2 (acc)	SST-5 (acc)	MR (acc)	CR (acc)	MPQA (acc)	Subj (acc)	TREC (acc)	CoLA (Matt.)
Prompt-based zero-shot	50.9	19.3	50	50	50	50.4	**27.2**	0
Multitask FT zero-shot	51.3	13.8	50	50	50	50.6	18.8	0
Prompt-based FT†	**51.8**(2.6)	20.5 (6.1)	**50.6** (0.8)	50.8 (1.1)	52.3 (1.9)	**55.4** (3.7)	19.8 (7.3)	0.8 (0.9)
Multitask Prompt-based FT	50.6 (0.7)	**22.1** (6.2)	50.5 (1.0)	51.5 (1.7)	**53.4** (2.7)	51.0 (1.4)	26.4 (8.5)	**0.9** (1.3)
+ task selection	51.7 (1.7)	19.7 (5.6)	**50.6** (0.8)	**51.6** (1.6)	52.3 (2.7)	54.7 (2.5)	23.2 (9.9)	0.5 (0.7)

	MNLI (acc)	MNLI-mm (acc)	SNLI (acc)	QNLI (acc)	RTE (acc)	MRPC (F1)	QQP (F1)
Prompt-based zero-shot	35.4	35.2	33.8	50.5	47.3	1.4	1.5
Multitask FT zero-shot	35.4	35.2	33.6	49.5	47.3	53.8	53.8
Prompt-based FT†	32.9 (0.8)	33.0 (0.7)	33.7 (0.6)	**50.6** (1.4)	48.7 (3.7)	**79.2** (4.1)	53.5 (2.7)
Multitask Prompt-based FT	32.5 (0.6)	32.5 (0.7)	33.5 (0.4)	**50.6** (2.4)	50.0 (2.0)	76.3 (6.5)	**54.2** (0.8)
+ task selection	**33.2** (1.2)	**33.2** (1.1)	**35.0** (0.8)	50.3 (0.4)	**51.8** (2.0)	72.2 (10.8)	52.9 (3.0)

Table 8.17: Our main results using simCSE [Gao et al., 2021c]. We report mean (and standard deviation) performance over 5 splits of few-shot examples. FT: fine-tuning; task selection: select multitask data from customized dataset.

Vision-language model enables the classification of images through prompting, where classification weights are calculated by a text encoder. The text encoder inputs text prompts containing class information, and outputs features aligned with features from the vision encoder in the same space.

However, standard finetuning can be affected by minor variations underperforming direct adaptation [Kumar et al., 2022; Wortsman et al., 2022]. Additionally, standard finetuning can be computationally expensive, as it requires training the model on a large amount of target task data.

We perform our multitask finetuning pipeline on the vision-language model and observe certain improvements. It's worth mentioning although the vision-language model is pretrained using contrastive learning, the model does not align with our framework. Vision-language model computes contrastive loss between image and text encoder, whereas our pretraining pipeline formulates the contrastive loss between the same representation function ϕ for positive and negative sample pairs. Despite the discrepancy, we provide some results below.

8.7.1 Improving Zero-shot Performance

We investigate the performance of CLIP models in a zero-shot setting, following the established protocol for our vision tasks. Each task includes 50 classes, with one query image per class. We employ text features combined with class information as the centroid to categorize query images within the 50 classes. During adaptation, we classify among randomly selected classes in the test split, which consists of 50 classes.

We experimented with our methods on tieredImageNet and DomainNet. The text template utilized in *tieredImageNet* was adapted from the CLIP documentation. In adaptation, we classify among all classes in the test split (160 classes in tieredImageNet and 100 classes in DomainNet). For text features on tieredImageNet, we use 8 templates adapted from CLIP `a photo of a {}, itap of a {}, a bad photo of the {}, a origami {}, a photo of the large {}, a {} in a video game, art of the {}, a photo of the small {}`. For templates on *DomainNet*, we simply use `a photo of a {}`. In the DomainNet The text template used for this experiment is `"a photo of {}"`. We perform Locked-Text Tuning, where we fixed the text encoder and update the vision encoder alone.

Backbone	Method	tieredImageNet	DomainNet
ViT-B	Adaptation	84.43 (0.25)	70.93 (0.32)
	Ours	84.50 (0.25)	73.31 (0.30)
ResNet50	Adaptation	81.01 (0.28)	63.61 (0.34)
	Ours	81.02 (0.27)	65.55 (0.34)

Table 8.18: Multitask finetune on zero-shot performance with CLIP model.

Table 8.18 demonstrates that CLIP already exhibits a high level of zero-shot performance. This is due to the model classifying images based on text information rather than relying on another image from the same class, which enables the model to utilize more accurate information to classify among query images. We show the effectiveness of zero-shot accuracy in tieredImageNet and DomainNet. It is worth highlighting that our multitask finetuning approach enhances the model's zero-shot performance, particularly on the more realistic DomainNet dataset. We have observed that our multitask finetuning pipeline yields greater improvements for tasks on which the model has not been extensively trained.

8.7.2 Updating Text Encoder and Vision Encoder

We also investigated whether updating the text encoder will provide better performance. On the tieredImageNet dataset, We finetune the text encoder and vision encoder simultaneously using the contrastive loss, following the protocol in Goyal et al. [2023].

Method	Zero-shot	Multitask finetune
Accuracy	84.43 (0.25)	85.01 (0.76)

Table 8.19: Multitask finetune on zero-shot performance with ViT-B32 backbone on tieredImageNet.

In Table 8.19, we observed slightly better improvements compared to updating the vision encoder alone. We anticipate similar performance trends across various datasets and backbone architectures. We plan to incorporate these findings into our future work.

8.7.3 CoCoOp

We also multitask finetune the vision language model following the protocol outlined in Zhou et al. [2022a]. This approach involved prepending an image-specific token before the prompt to enhance prediction accuracy. To generate this token, we trained a small model on the input image. We evaluate the performance of our model on all classes in the test split, which corresponds to a 160-way classification task. This allows us to comprehensively assess the model's ability to classify among a large number of categories.

Method	Zero-shot	Multitask finetune
ViT-B32	69.9	71.4

Table 8.20: Multitask finetune on zero-shot performance with ViT-B32 backbone on tieredImageNet.

Table 8.20 showed the result of the performance of the CoCoOp method. We observed an improvement of 1.5% in accuracy on direct adaptation.

Chapter 9

Appendix of Chapter 4

In this appendix, we provide more empirical settings and results for logical tasks in Section 9.1 and linguistic translation tasks in Section 9.2. We provide a theory for confined support and model scalability, along with a case study of a toy model in Section 9.3. We provide full proof in Section 9.4.

9.1 Logical Tasks

9.1.1 Task Setup

We provide a comprehensive explanation of logical composite tasks below. Examples can be seen in Table 9.1.

- **(A) + (B) Capitalization & Swap**, as in Section 4.2.
- **(A) + (C) Capitalization & Two Sum.** Given words of numerical numbers, * represents the operation of capitalizing, @ represents summing the two numbers.
- **(G) + (H) Modular & Two Sum Plus.** Given numerical numbers, @ represents the operation of taking modular, # represents to sum the two numbers and then plus one.
- **(A) + (F) Capitalization & Plus One.** If numerical numbers are given, plus one; if words are given, capitalize the word; if both are given, perform both operations.

Among these, **(A) + (F)** performs the two operations on separable parts of the test inputs (i.e., separable composite task).

Tasks	Simple Task	Simple Task	Composite
(A) + (B)	input: * apple output: APPLE	input: (farm frog) output: frog farm	input: (* bell * ford) output: FORD BELL
(A) + (C)	input: ** (five)* output: FIVE	input: *twenty @ eleven* output: thirty-one	input: ** (thirty-seven @ sixteen)* output: FIFTY-THREE
(G) + (H)	input: 15 @ 6 output: 3	input: 12 # 5 output: 18	input: 8 # 9 @ 7 Ouput: 4
(A) + (F)	input: 435 output: 436	input: cow output: COW	input: 684 cat output: 685 CAT

Table 9.1: Examples of the four logical composite tasks. Note that in **(G) + (H)**, the output of the composite task can be either 4 or 11 depending on the order of operations, and we denote both as correct.

We design our logical tasks following the idea of math reasoning and logical rules. The details are shown in Table 9.1. Our numerical numbers in Table 4.2 are uniformly randomly chosen from 1 to 1000. The words of numbers in task **(C)** are uniformly randomly chosen from one to one hundred. The words representing objects in Table 4.2 are uniformly randomly chosen from class names of ImageNet after dividing the phrase (if any) into words. We randomly chose 100 examples in composite testing data in our experiments and replicated the experiments in each setting three times. We fixed the number of in-context examples as $K = 10$ as demonstrations.

9.1.2 Experimental Setup

We use exact match accuracy to evaluate the performance between sequence outputs. The calculation of exact match accuracy divided the number of matched words by the length of ground truth.

For Llama models, we use official Llama1 and Llama2 models from Meta [Touvron et al., 2023a], we use open_llama_3b_v2 from open OpenLlama [Geng and Liu, 2023]. For GPT models, we use GPT2-large from OpenAI [Radford et al., 2019], and we use GPT-neo models for GPT models in other scales from EleutherAI [Black et al., 2021].

We've experimented with prompt demonstrations. Instructional prompts do help ChatGPT and Claude3 (although we haven't quantified the accuracy in large-scale experiments), but they offer limited benefits for current open-source models. On the other hand, we did not have prompt tuning or any other parameter updates during our evaluation.

In our experiments, we provided the model with instructions. Here are instructions of Figure 4.1, which were prepended to ICL examples. We refer to our codebase for full instructions and results.

> * is a function before words for swapping the position of 2 words, # is another function after words for capitalizing letters of words.

9.1.3 Results

We show a visualization of some logical task accuracy along the increasing to model scale, complement to Table 4.4.

We also include results for the more recent model Llama3 [Meta, 2024] on the part of our logical tasks to demonstrate the idea. We show results in Table 9.2.

	Tasks	Llama3 8B	Llama3 70B
(A) + (B)	Capitalization	100	100
	swap	100	100
	Compose	52	72
	Com. in-context	97	100
(A) + (F)	Capitalization	100	100
	PlusOne	100	100
	Compose	88	100
	Com. in-context	100	100

Table 9.2: Results evaluating composite tasks on Llama3. The accuracy is shown in %.

As shown in the Table 9.2, for the *separable composite tasks* which are relatively easy for model to solve **(A) + (F)**, the models show strong compositional ability: the composite accuracy is high, improves with increasing scale, and eventually reaches similar performance as the *gold standard* composite in-context setting. For composite tasks with sequential reasoning steps **(A) + (B)**, the model has poor performance on a small scale but has increased performance on an increased model scale. Providing composed examples as in-context demonstrations will help the model understand and solve the composite tasks well.

9.2 Formal Language Translation Tasks

Our translation tasks mainly follow the compositional generalization tasks in COFE [An et al., 2023b]. The details can be found in Section 4 in An et al. [2023a]. We directly take the source grammar $\mathcal{G}_s$ in COGS, which mimics the English natural language grammar, and reconstruct the target grammar $\mathcal{G}_t$ in COGS to be chain-structured.

We follow the Primitive coverage principle proposed by An et al. [2023b] that primitives contained in each test sample should be fully covered by in-context examples. Here, primitives refer to the basic, indivisible elements of expressions,

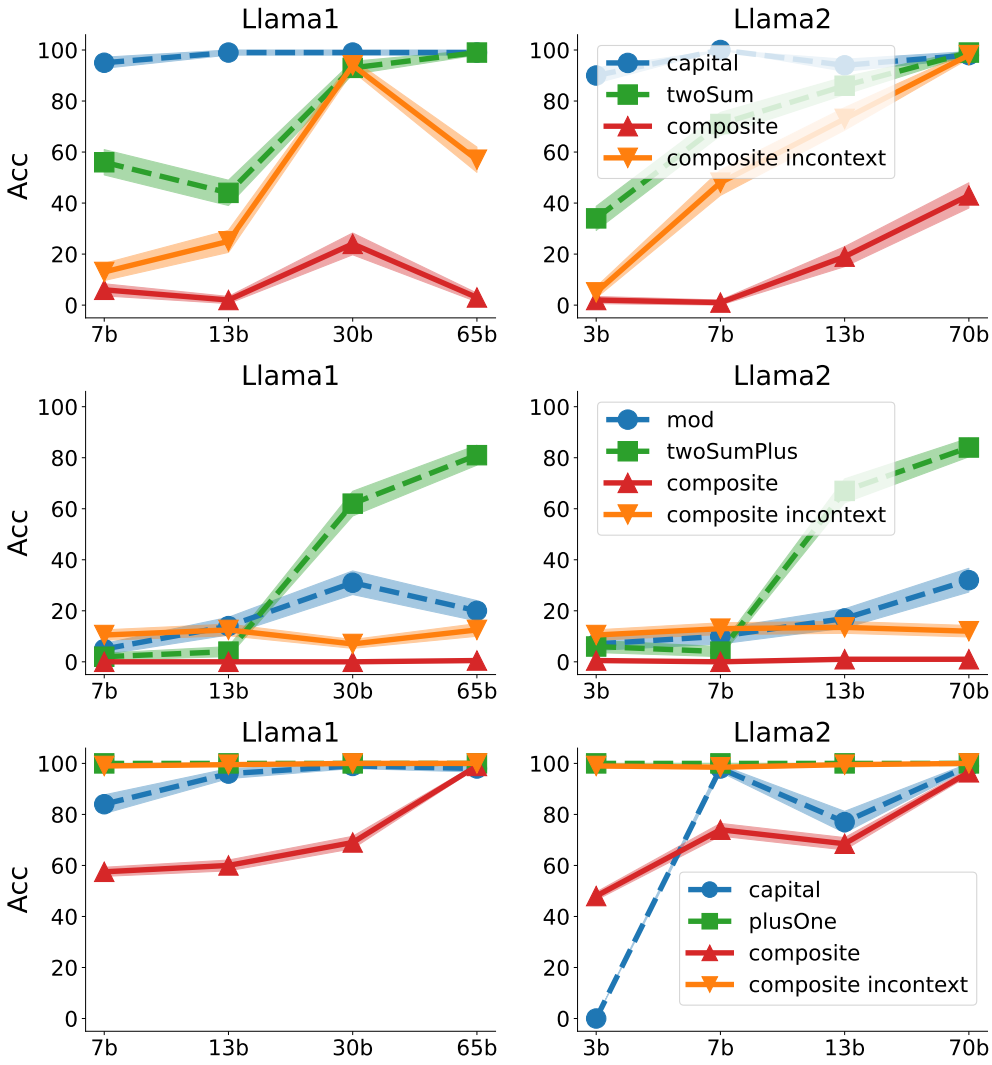

Figure 9.1: The accuracy v.s. model scale on composite logical rule tasks. Dashed lines: simple tasks. Solid lines: composite tasks. Rows: **(A) + (C)** Capitalization & Two Sum; **(G) + (H)** Modular & Two Sum Plus; **(A) + (F)** Capitalization & Plus One. Columns: different models. Lines: performance in different evaluation settings, i.e., the two simple tasks, the composite setting, and the composite in-context setting (examples for the last two are shown in Table 4.1).

including subjects, objects, and verbs. Note that multiple sets of in-context examples can meet these criteria for each test case. Across all experimental conditions, we maintain a consistent number of test instances at 800.

We use the word error rate (WER) as the metric. It measures the differences between 2 sentences. It measures the minimum number of editing operations (deletion, insertion, and substitution) required to transform one sentence into another and is common for speech recognition or machine translation evaluations. The computation of WER is divided by the number of operations by the length of ground truth.

In formal language tasks, as mentioned in Section 4.3.2, we change the original target grammar of COGS to be chain-structured. In Table 9.3, we list some examples with the original target grammar and the new chain-structured grammar.

- First, to distinguish the input and output tokens, we capitalize all output tokens (e.g., from “rose” to “ROSE”).
- Second, we replace the variables (e.g., “x_1”) in the original grammar with their corresponding terminals (e.g., “ROSE”).

Original Target Grammar	Chain-Structured Target Grammar
rose (x_1) AND help . theme (x_3 , x_1) AND help . agent (x_3 , x_6) AND dog (x_6)	HELP (DOG, ROSE, NONE)
* captain (x_1) ; eat . agent (x_2 , x_1)	EAT (CAPTION, NONE, NONE)
* dog (x_4) ; hope . agent (x_1 , Liam) AND hope . ccomp (x_1 , x_5) AND prefer . agent (x_5 , x_4)	HOPE (LIAM, NONE, NONE) CCOMP PREFER (DOG, NONE, NONE)

Table 9.3: Demonstration in An et al. [2023a] showing examples with the original grammar and the new chain-structured grammar.

- Then, we group the terminals of AGENT (e.g., "DOG"), THEME (e.g., "ROSE"), and RECIPIENT with their corresponding terminal of PREDICATE (e.g., "HELP") and combine this group of terminals in a function format, i.e., "PREDICATE (AGENT, THEME, RECIPIENT)". If the predicate is not equipped with an agent, theme, or recipient in the original grammar, the corresponding new non-terminals (i.e., AGENT, THEME, and RECIPIENT, respectively) in the function format above will be filled with the terminal NONE (e.g., "HELP (DOG, ROSE, NONE)"). Such a function format is the minimum unit of a CLAUSE.
- Finally, each CLAUSE is concatenated with another CLAUSE by the terminal CCOMP (e.g., "HOPE (LIAM, NONE, NONE) CCOMP PREFER (DOG, NONE, NONE)").

Task	In-context Example	Testing Example
Passive to Active	The book was squeezed . SQUEEZE (NONE , BOOK , NONE)	Sophia squeezed the donut . SQUEEZE (SOPHIA , DONUT , NONE)
Object to Subject	Henry liked a cockroach in a box . LIKE (HENRY , IN (COCKROACH , BOX)	A cockroach inflated a boy . INFLATE (COCKROACH , BOY , NONE)
Composite Task	The book was squeezed . SQUEEZE (NONE , BOOK , NONE) Henry liked a cockroach in a box . LIKE (HENRY , IN (COCKROACH , BOX)	A cockroach squeezed the hedgehog . SQUEEZE (COCKROACH , hedgehog , NONE)

Table 9.4: Testing examples of Passive to Active and Object to Subject, red text shows the verbs changing from passive to active voice in simple tasks, and blue text shows the nouns from objective to subjective.

Task		Example
Phrase Recombination	Input	The baby on a tray in the house screamed .
	Output	SCREAM (ON (BABY , IN (TRAY , HOUSE)) , NONE , NONE)
Longer Chain	Input	A girl valued that Samuel admired that a monkey liked that Luna liked that Oliver respected that Savannah hoped that a penguin noticed that Emma noticed that the lawyer noticed that a cake grew .
	Output	VALUE (GIRL , NONE , NONE) \ CCOMP ADMIRE (SAMUEL , NONE , NONE) \ CCOMP LIKE (MONKEY , NONE , NONE) \ CCOMP LIKE (LUNA , NONE , NONE) \ CCOMP RESPECT (OLIVER , NONE , NONE) \ CCOMP HOPE (SAVANNAH , NONE , NONE) \ CCOMP NOTICE (PENGUIN , NONE , NONE) \ CCOMP NOTICE (EMMA , NONE , NONE) \ CCOMP NOTICE (LAWYER , NONE , NONE) \ CCOMP GROW (NONE , CAKE , NONE)
Composite Task	Input	The baby on a tray in the house valued that Samuel admired that a monkey liked that Luna liked that Oliver respected that Savannah hoped that a penguin noticed that Emma noticed that the lawyer noticed that a cake grew .
	Output	VALUE (ON (BABY , IN (TRAY , HOUSE) , NONE , NONE) \ CCOMP ADMIRE (SAMUEL , NONE , NONE) \ CCOMP LIKE (MONKEY , NONE , NONE) \ CCOMP LIKE (LUNA , NONE , NONE) \ CCOMP RESPECT (OLIVER , NONE , NONE) \ CCOMP HOPE (SAVANNAH , NONE , NONE) \ CCOMP NOTICE (PENGUIN , NONE , NONE) \ CCOMP NOTICE (EMMA , NONE , NONE) \ CCOMP NOTICE (LAWYER , NONE , NONE) \ CCOMP GROW (NONE , CAKE , NONE)

Table 9.5: Testing examples of Phrase Recombination and Longer Chain, red text shows the phrase serving as primitives in sentences in simple tasks, and blue text shows the logical structures as sub-sentences in long sentences.

In the following, we provide a detailed explanation of our two composite tasks in translation tasks.

Passive to Active and Object to Subject Transformation. Based on the generalization tasks identified in Kim and Linzen [2020]), we select two distinct challenges for our study as two simple tasks. *Passive to Active*: Transitioning sentences from Passive to Active voice. *Object to Subject*: Changing the focus from Object to Subject using common nouns. These tasks serve as the basis for our composite task, where both transformations are applied simultaneously to the same sentence. Examples illustrating this dual transformation can be found in Table 9.4.

Enhanced Phrase Subject with Longer Chain. COFE proposed two compositional generalization tasks (Figure 2 in An et al. [2023b]): *Phrase Recombination (PhraReco)*: integrate a prepositional phrase (e.g., "A in B") into a specific grammatical role (e.g., "subject", "object"); *Longer Chain (LongChain)*: Extend the tail of the logical form in sentences. We consider these two generalization tasks as two simple tasks, merging them to form a composite task. In particular, we substitute the sentence subject in the Longer Chain task with a prepositional phrase from the Phrase Recombination task, creating a more complex task structure. Detailed examples of this combined task can be found in Table 9.5.

9.3 Theory for Confined Support

9.3.1 Compositional Ability with Model Scale

We then show that if simple tasks have confined support, the compositional ability of language models will increase as the model scale increases. We demonstrate this by showing that the accuracy of the model on each simple task improves with a larger model scale.

Note that the optimal solutions of the parameter matrices are W^{*PV} and W^{*KQ}. We naturally consider that the rank of the parameter matrices W^{*PV} and W^{*KQ} can be seen as a measure of the model's scale. A higher rank in these matrices implies that the model can process and store more information, thereby enhancing its capability. We state the following theorem.

Theorem 9.3.1. *Suppose a composite task satisfies confined support. Suppose that we have* $(x_1, y_1, \ldots, x_N, y_N, x_q)$ *as a testing input prompt and the corresponding* W *where* $y_i = Wx_i$*. As rank* r *decreases,* $\mathbb{E}_{W,x_1,\cdots,x_N}[Acc_\theta]$ *will have a smaller upper bound.*

Theorem 9.3.1 shows the expected accuracy of a model on composite tasks is subjected to a lower upper bound as the scale of the model diminishes. This conclusion explains why scaling up helps the performance when the model exhibits compositional ability for certain tasks (those we call "separable composite tasks"). One common characteristic of these tasks is their inputs display confined supports within the embeddings. This is evidenced by the model's decent performance on tasks as presented in Table 4.4 and Figure 4.3, where inputs are composed of parts.

9.3.2 Case Study of Confined Support

Our theoretical conclusion shows the model behavior regarding input embedding. It states that the model will have compositional ability if tasks are under confined support of input embedding. To illustrate such theoretical concepts and connect them to empirical observations, we specialize the general conclusion to settings that allow easy interpretation of disjoint. In this section, we provide a toy linear case study on classification tasks, showing how confined support on embedding can be decomposed and composite tasks can be solved. We assume $\delta = \epsilon = 0$ in the following simple example.

Consider that there are only two simple tasks for some random objects with the color red and blue and the shape square and round: (1) binary classification based on the color red and blue. (2) binary classification based on shape: circle and square. However, during evaluation, the composite task is a four-class classification, including red circle, red square, blue circle, and blue square.

Then we have two simple tasks $K = 2$. Consider the input embedding $x = (a, b)$, where $a \in \mathbb{R}^2, b \in \mathbb{R}^2, d = 4$. Consider $W = \begin{pmatrix} 1 & -1 & 0 & 0 \\ 0 & 0 & 1 & -1 \end{pmatrix}$ and $y = Wx$.

Consider the inputs from simple and composite tasks as:

- Task 1: Red: $x_1 = (1, 0, 0, 0), y_1 = (1, 0)$ and blue: $x_2 = (0, 1, 0, 0), y_2 = (-1, 0)$.
- Task 2: Circle $x_3 = (0, 0, 1, 0)$ $y_3 = (0, 1)$ and square $x_4 = (0, 0, 0, 1)$ $y_4 = (0, -1)$.

- Composed task: red circle $x_5 = (1, 0, 1, 0), y_5 = (1, 1)$, red square $x_6 = (1, 0, 0, 1), y_6 = (1, -1)$, blue circle $x_7 = (0, 1, 1, 0)$ $y_7 = (-1, 1)$ and blue square $x_8 = (0, 1, 0, 1)$ $y_8 = (-1, -1)$.

Suppose that we have the optimal solution $\hat{y}_q$ as in Eq. 9.1. Given $x_q = (1, 0, 1, 0)$ as a testing input for a red circle example, During the test, we have different predictions given different in-context examples:

1. Given only examples from Task 1 (red and blue): $[(x_1, y_1), (x_2, y_2)]$, we have $\widehat{y}_q = (1, 0)$ can only classify the color as red.
2. Given only examples from Task 2 (square and circle): $[(x_4, y_4), (x_3, y_3)]$, we have $\widehat{y}_q = (0, 1)$ only classify the shape as a circle.
3. Given a mixture of examples from Task 1 and 2 (red and circle): $[(x_1, y_1), (x_3, y_3)]$, we have $\widehat{y}_q = (1, 1)$ can classify as red and circle.

We can see that in the final setting, the model shows compositional ability. This gives a concrete example for the analysis in Theorem 4.4.4.

9.4 Deferred Proof

In this section, we provide a formal setting and proof. We first formalize our model setup.

9.4.1 Linear self-attention networks.

These networks are widely studied [Von Oswald et al., 2023; Akyürek et al., 2023; Mahankali et al., 2023; Garg et al., 2022; Zhang et al., 2023b; Shi et al., 2023d]. Following them, we consider the following linear self-attention network with parameters $\theta = (W^{PV}, W^{KQ})$:

$$f_{\text{LSA},\theta}(E) = E + W^{PV} E \cdot \frac{E^\top W^{KQ} E}{N}.$$

The prediction of the model for x_q is $\hat{y}_q = [f_{\text{LSA},\theta}(E)]_{(d+1):(d+K),N+1}$, the bottom rightmost sub-vector of $f_{\text{LSA},\theta}(E)$ with length K. Let

$$W^{PV} = \begin{pmatrix} W_{11}^{PV} & W_{12}^{PV} \\ (W_{21}^{PV})^\top & W_{22}^{PV} \end{pmatrix} \in \mathbb{R}^{(d+K)\times(d+K)}, W^{KQ} = \begin{pmatrix} W_{11}^{KQ} & W_{12}^{KQ} \\ (W_{21}^{KQ})^\top & W_{22}^{KQ} \end{pmatrix} \in \mathbb{R}^{(d+K)\times(d+K)},$$

where $W_{11}^{PV} \in \mathbb{R}^{d\times d}$, $W_{12}^{PV}, W_{21}^{PV} \in \mathbb{R}^{d\times K}$, and $W_{22}^{PV} \in \mathbb{R}^{K\times K}$; similar for W^{KQ}. Then the prediction is

$$\widehat{y}_q = \begin{pmatrix} (W_{21}^{PV})^\top & W_{22}^{PV} \end{pmatrix} \begin{pmatrix} \frac{EE^\top}{N} \end{pmatrix} \begin{pmatrix} W_{11}^{KQ} \\ (W_{21}^{KQ})^\top \end{pmatrix} x_q. \tag{9.1}$$

We observe only part of the parameters affect our prediction, so we treat the rest of them as zero in our analysis.

9.4.2 Proof of Compositional Ability under Confined Support

Here, we provide the proof of our main conclusion regarding Theorem 4.4.4 and Section 4.4.2.

Without abuse of notation, we denote $U = W_{11}^{KQ}, u = W_{22}^{PV}$.

We also add some mild assumptions.

1. The covariance matrix Λ of simple tasks will have the same trace to prevent the scale effect of different simple tasks.
2. The spectral norm of Λ is bounded on both sides $m \le \|\Lambda\| \le M$.

We first introduce the lemma where the language model only pretrained on one simple task ($K = 1$). The pretraining loss $L(\theta)$ can be refactored, and the solution will have a closed form. We further discuss the following.

Lemma 9.4.1 (Lemma 5.3 in Zhang et al. [2023b]). *Let* $\Gamma := \left(1 + \frac{1}{N}\right)\Lambda + \frac{1}{N}\operatorname{tr}(\Lambda) I_{d\times d} \in \mathbb{R}^{d\times d}$. *Let*

$$\tilde{\ell}(U, u) = \operatorname{tr}\left[\frac{1}{2} u^2 \Gamma \Lambda U \Lambda U^\top - u \Lambda^2 U^\top\right]$$

Then

$$\min_{\theta} L(\theta) = \min_{U,u} \tilde{\ell}(U,u) + C = -\frac{1}{2}\operatorname{tr}[\Lambda^2\Gamma^{-1}] + C$$

where C is a constant independent with θ. For any global minimum of $\tilde{\ell}$, we have $uU = \Gamma^{-1}$.

As the above lemma construction, we denote the optimal solution as W^{*PV} and W^{*KQ}. Taking one solution as $U = \Gamma^{-1}, u = 1$, we observe the minimizer of global training loss is of the form:

$$W^{*PV} = \begin{pmatrix} 0_{d\times d} & 0_d \\ 0_d^\top & 1 \end{pmatrix}, W^{*KQ} = \begin{pmatrix} \Gamma^{-1} & 0_d \\ 0_d^\top & 0 \end{pmatrix}. \tag{9.2}$$

We then prove our main theory Theorem 4.4.4 in Section 4.4.2, we first re-state below:

Theorem 4.4.4. *Consider distinct tasks k and g with corresponding examples $\mathcal{S}_k, \mathcal{S}_g$. If two tasks have confined support, and Assumption 4.4.2 is true, then with high probability, the model has the compositional ability as defined in Definition 4.4.1. Moreover,*

$$Acc_\theta(\mathcal{S}_k) + Acc_\theta(\mathcal{S}_g) \le Acc_\theta(\mathcal{S}_{k\cup g}).$$

Proof of Theorem 4.4.4. WLOG, consider two simple tasks, $K = 2$. We have $x = (a, b)$, where $a \in \mathbb{R}^{d_1}, b \in \mathbb{R}^{d_2}, d_1 + d_2 = d$. Since x only has large values on certain dimensions, it's equivalent to just consider corresponding dimensions in w, i.e., for simple task 1, we have $w^{(1)} = (w_a, w_{\delta b})$, for simple task 2, we have $w^{(2)} = (w_{\delta a}, w_b)$.

We have $x \sim \Lambda$, where:

$$\Lambda = \begin{pmatrix} \Lambda_{\mathbb{K}\mathbb{K}} & \Lambda_{\mathbb{K}\mathbb{G}} \\ \Lambda_{\mathbb{G}\mathbb{K}} & \Lambda_{\mathbb{G}\mathbb{G}} \end{pmatrix}$$

- Task 1: $x = (a, 0_{d_2})^\top + (0, b_\delta)^\top, y = (w_a^\top a, 0) + (0, w_{\delta b}^\top b_\delta)$.
- Task 2: $x = (0_{d_1}, b)^\top + (a_\delta, 0_{d_2})^\top, y = (0, w_b^\top b) + (w_{\delta a}^\top a_\delta), 0)$.
- Composed task: $x = (a, b)^\top + (a_\delta, b_\delta)^\top, y = (w_a^\top a, w_b^\top b) + (w_{\delta a}^\top a_\delta, w_{\delta b}^\top b_\delta)$.

The form of E is,

$$E := \begin{pmatrix} a_1 & a_2 & \dots & a_N & a_q \\ b_1 & b_2 & \dots & b_N & b_q \\ y_1 & y_2 & \dots & y_N & 0 \end{pmatrix} + E_r \in \mathbb{R}^{(d+2)\times(N+1)}.$$

where E_r represents the values caused by residual dimensions whose entries are bounded by δ.

Following Equation (4.3) in Zhang et al. [2023b], we have

$$EE^\top = \frac{1}{N}\begin{pmatrix} \sum_{i=1}^N a_i a_i^\top + a_q a_q^\top & \sum_{i=1}^N a_i b_i^\top + a_q b_q^\top & \sum_{i=1}^N a_i y_i^\top \\ \sum_{i=1}^N b_i a_i^\top + b_q a_q^\top & \sum_{i=1}^N b_i b_i^\top + b_q b_q^\top & \sum_{i=1}^N b_i y_i^\top \\ \sum_{i=1}^N y_i a_i^\top & \sum_{i=1}^N y_i b_i^\top & \sum_{i=1}^N y_i y_i^\top \end{pmatrix} + \delta \cdot o(EE^\top).$$

The W^{PV} can be presented in block matrix

$$W^{PV} = \begin{pmatrix} W_{11}^{PV} & W_{12}^{PV} & W_{13}^{PV} \\ (W_{21}^{PV})^\top & W_{22}^{PV} & W_{23}^{PV} \\ (W_{31}^{PV})^\top & (W_{32}^{PV})^\top & W_{33}^{PV} \end{pmatrix} \in \mathbb{R}^{(d_1+d_2+2)\times(d_1+d_2+2)}$$

We can apply Lemma 9.4.1 into optimization and recall

$$W^{*KQ} = \begin{pmatrix} \Gamma_{all}^{-1} & 0_d \\ 0_d^\top & 0 \end{pmatrix}.$$

where $\Gamma_{all}^{-1} \in \mathbb{R}^{(d_1+d_2)\times(d_1+d_2)}$. Consider two tasks only related to disjoint dimension of x, we also have $\sigma(\Lambda_{\mathbb{K}\mathbb{G}}) = \sigma(\Lambda_{\mathbb{G}\mathbb{K}}) \le \epsilon$. Denote

$$\Lambda = \tilde{\Lambda} + \Lambda_r$$

where

$$\tilde{\Lambda} = \begin{pmatrix} \Lambda_{\mathbb{K}\mathbb{K}} & \\ & \Lambda_{\mathbb{G}\mathbb{G}} \end{pmatrix}, \Lambda_r = \begin{pmatrix} & \Lambda_{\mathbb{K}\mathbb{G}} \\ \Lambda_{\mathbb{G}\mathbb{K}} & \end{pmatrix}$$

We apply Lemma 9.4.1 Recall $\Gamma := \left(1 + \frac{1}{N}\right)\Lambda + \frac{1}{N}\operatorname{tr}(\Lambda) I_{d\times d} \in \mathbb{R}^{d\times d}$, we have:

$$\begin{aligned} \Gamma &= \left(1 + \frac{1}{N}\right)\tilde{\Lambda} + \frac{1}{N}\operatorname{tr}(\tilde{\Lambda}) I_{d\times d} + \left(1 + \frac{1}{N}\right)\Lambda_r \\ &= \tilde{\Gamma} + \Gamma_r \end{aligned}$$

where denote $\Gamma_r = \left(1 + \frac{1}{N}\right)\Lambda_r$. We have:

$$\Gamma^{-1} = \tilde{\Gamma}^{-1} - \tilde{\Gamma}^{-1}\Gamma_r\tilde{\Gamma}^{-1} + \mathcal{O}(\Gamma_r)$$

We denote

$$\tilde{\Gamma} = \begin{pmatrix} \Gamma_1 & 0 \\ 0 & \Gamma_2 \end{pmatrix},$$

where $\Gamma_1 = \left(1 + \frac{1}{N}\right)\Lambda_{\mathbb{K}\mathbb{K}} + \frac{1}{N}\operatorname{tr}(\Lambda) I_{d_1} \in \mathbb{R}^{d_1\times d_1}$ and $\Gamma_2 = \left(1 + \frac{1}{N}\right)\Lambda_{\mathbb{G}\mathbb{G}} + \frac{1}{N}\operatorname{tr}(\Lambda) I_{d_2} \in \mathbb{R}^{d_2\times d_2}$. Then we have;

$$\Gamma^{-1} = \begin{pmatrix} \Gamma_1^{-1} & 0 \\ 0 & \Gamma_2^{-1} \end{pmatrix} + A$$

where $\sigma(A) \le 2m^2\epsilon$.

Then, It's similar to applying Lemma 9.4.1 for pretraining separately into dimensions corresponding to different tasks. We solve similarly to W_{KQ}.

We have:

$$f_\theta(E) = \begin{pmatrix} 0_{d_1\times d_1} & 0_{d_1\times d_2} & 0_{d_1\times 2} \\ 0_{d_2\times d_1} & 0_{d_2\times d_2} & 0_{d_2\times 2} \\ 0_{2\times d_1} & 0_{2\times d_2} & I_2 \end{pmatrix} EE^\top \begin{pmatrix} \Gamma_1^{-1} & 0_{d_1\times d_2} & 0_{d_1\times 2} \\ 0_{d_2\times d_1} & \Gamma_2^{-1} & 0_{d_2\times 2} \\ 0_{2\times d_1} & 0_{2\times d_2} & 0_{2\times 2} \end{pmatrix} \begin{pmatrix} a_q \\ b_q \\ 0 \end{pmatrix} + \tilde{A} \tag{9.3}$$

$$\hat{y}_q = \frac{1}{N}\left(\sum_{i=1}^N y_i a_i^\top, \sum_{i=1}^N y_i b_i^\top, \sum_{i=1}^N y_i y_i^\top\right) \begin{pmatrix} \Gamma_1^{-1} a_q \\ \Gamma_2^{-1} b_q \\ 0 \end{pmatrix} + v \tag{9.4}$$

$$= \left(\frac{1}{N}\sum_{i=1}^N y_i a_i^\top\right)\Gamma_1^{-1} a_q + \left(\frac{1}{N}\sum_{i=1}^N y_i b_i^\top\right)\Gamma_2^{-1} b_q + v \tag{9.5}$$

$$= \frac{1}{N}\begin{pmatrix} a_q^\top \Gamma_1^{-1} \sum_{i=1}^N y_i^{(1)} a_i \\ b_q^\top \Gamma_2^{-1} \sum_{i=1}^N y_i^{(2)} b_i \end{pmatrix} + v. \tag{9.6}$$

where $\tilde{A}$ representing residual matrix whose norm can be bounded by $\mathcal{O}(m^2\epsilon\delta)$ Recall $x \sim N(0, \Lambda)$, then with high probability each entry in v will be bounded by $Cm^2\delta\epsilon$ for some constant C.

WLOG, we write residual vectors as 0 vector for simplicity of notation, and only consider residuals for estimations $\hat{y}$. Note that we composed example $x = (a, b)^\top$, $y = (w_a^\top a, w_b^\top b)$. For simplicity, we write $\hat{w}_a = \frac{1}{N}\Gamma_1^{-1}\sum_{i=1}^N y_i^{(1)} a_i$, similarly, $\hat{w}_b = \frac{1}{N}\Gamma_2^{-1}\sum_{i=1}^N y_i^{(2)} b_i$.

Given in-context examples from one simple task only, consider that we have N examples from simple task 1, $\mathcal{S}_1 = \left[\{(a_i, 0), y_i\}_{i=1}^N\right]$. We have $\hat{w}^{(1)} = (\hat{w}_a, 0_{d_2}), \hat{w}^{(2)} = (0_d)$, and we also have $\hat{y}_q = (\hat{y}_q^{(1)}, 0)^\top$, where $\hat{y}_q^{(1)} = a_q^\top\Gamma_1^{-1}\left(\frac{1}{N}\sum_{i=1}^N y_i^{(1)} a_i\right) + Cm^2\delta\epsilon$. We have $\operatorname{Acc}_\theta(\mathcal{S}_1) = \frac{\mathbb{1}\left(\widetilde{y}_q^{(1)} = y_q^{(1)}\right)}{2}$.

Similarly, for N in-context examples only from task 2, we have $\hat{w}^{(1)} = (0_d), \hat{w}^{(2)} = (0_{d_1}, \hat{w}_b)$, $\hat{y}_q = (0, \hat{y}_q^{(2)})^\top$, where $\hat{y}_q^{(2)} = a_q^\top\Gamma_2^{-1}\left(\frac{1}{N}\sum_{i=1}^N y_i^{(2)} b_i\right) + Cm^2\delta\epsilon$. We have $\operatorname{Acc}_\theta(\mathcal{S}_2) = \frac{\mathbb{1}\left(\widetilde{y}_q^{(2)} = y_q^{(2)}\right)}{2}$.

Then we have $\mathcal{S}_{1\cup 2}$ contains $2N$ in-context examples from both tasks, specifically, we have N from task 1 and rest from task 2. We have $\hat{w}^{(1)} = (\hat{w}_a/2, 0_{d_2}), \hat{w}^{(2)} = (0_{d_1}, \hat{w}_b/2)$, $\hat{y}_q = (\hat{y}_q^{(1)}, \hat{y}_q^{(2)})^\top$.

Since $y_{\tau,q}^{(k)} = \text{sgn}(\langle w_\tau, x_{\tau,q}\rangle)$, $\widetilde{y}_{\tau,q}^{(k)} = \text{sgn}\left(\widehat{y}_{\tau,q}^{(k)}\right)$, following the proof of Lemma 9.4.2, where Acc_θ only concerns the direction of $\hat{w}$ and w, we have $\text{Acc}_\theta(\mathcal{S}_{1\cup 2}) = \frac{\mathbb{1}\left(\widetilde{y}_q^{(1)}=y_q^{(1)}\right)+\mathbb{1}\left(\widetilde{y}_q^{(2)}=y_q^{(2)}\right)}{2}$.

Extending the above analysis into any of two simple tasks, when the composite task integrates them, we have

$$\text{Acc}_\theta(\mathcal{S}_k) + \text{Acc}_\theta(\mathcal{S}_g) \leq \text{Acc}_\theta(\mathcal{S}_{k\cup g}). \tag{9.7}$$

□

We then prove Section 4.4.2, and we first restate it below.

If two tasks do not have confined support, there exists one setting in which we have

$$\text{Acc}_\theta(\mathcal{S}_k) = \text{Acc}_\theta(\mathcal{S}_g) = \text{Acc}_\theta(\mathcal{S}_{k\cup g}).$$

Proof of Section 4.4.2. WLOG, consider two simple tasks, $K = 2$. We have $x = (a, b)$, where $a \in \mathbb{R}^{d_1}, b \in \mathbb{R}^{d_2}, d_1 + d_2 = d$. Consider the setting where w also have the same active dimensions, i.e., for simple task 1, we have $w^{(1)} = (w_a, 0)$, for simple task 2, we have $w^{(2)} = (0, w_b)$.

We have $x \sim \Lambda$. Consider tasks are overlapping on all dimensions, where:

- Task 1: $x = (a^{(1)}, b^{(1)})^\top$, $y = (w_a^\top a^{(1)}, w_b^\top b^{(1)})$.
- Task 2: $x = (a^{(2)}, b^{(2)})^\top$, $y = (w_a^\top a^{(2)}, w_b^\top b^{(2)})$.
- Composed task: $x = (a, b)^\top$, $y = (w_a^\top a, w_b^\top b)$.

Similarly, we have:

$$\hat{y}_q = \frac{1}{N}\left(\sum_{i=1}^N y_i a_i^\top, \sum_{i=1}^N y_i b_i^\top, \sum_{i=1}^N y_i y_i^\top\right)\begin{pmatrix}\Gamma_1^{-1} a_q \\ \Gamma_2^{-1} b_q \\ 0\end{pmatrix} \tag{9.8}$$

$$= \left(\frac{1}{N}\sum_{i=1}^N y_i a_i^\top\right)\Gamma_1^{-1} a_q + \left(\frac{1}{N}\sum_{i=1}^N y_i b_i^\top\right)\Gamma_2^{-1} b_q \tag{9.9}$$

$$= \frac{1}{N}\begin{pmatrix} a_q^\top \Gamma_1^{-1} \sum_{i=1}^N y_i^{(1)} a_i + b_q^\top \Gamma_2^{-1} \sum_{i=1}^N y_i^{(1)} b_i \\ a_q^\top \Gamma_1^{-1} \sum_{i=1}^N y_i^{(2)} a_i + b_q^\top \Gamma_2^{-1} \sum_{i=1}^N y_i^{(2)} b_i \end{pmatrix}. \tag{9.10}$$

Note that composed example $x = (a, b)^\top$, $y = (w_1^\top a, w_2^\top b)$.

When in-context examples are from a simple task, we have N examples from simple task 1, $\mathcal{S}_1 = \left[\left\{(a_i^{(1)}, b_i^{(1)}), y_i\right\}_{i=1}^N\right]$, and $\hat{y}_q$ has the same form as Eq. 9.10, similarly, for task 2.

Suppose $\mathcal{S}_{1\cup 2}$ contains $2N$ examples from both tasks, where N from task 1 and rest from task 2. We have

$$\hat{y}_q = \frac{1}{2N}\begin{pmatrix} a_q^\top \Gamma_1^{-1} \sum_{i=1}^N y_i^{(1)} a_i + b_q^\top \Gamma_2^{-1} \sum_{i=1}^N y_i^{(1)} b_i \\ a_q^\top \Gamma_1^{-1} \sum_{i=1}^N y_i^{(2)} a_i + b_q^\top \Gamma_2^{-1} \sum_{i=1}^N y_i^{(2)} b_i \end{pmatrix}. \tag{9.11}$$

We finish the proof by checking that Eq. 9.10 and Eq. 9.11 share the same direction.

□

9.4.3 Proof of Compositional Ability with Model Scale

Here, we provide the proof of our conclusions in Theorem 9.3.1 in Section 9.3.1 with respect to model performance and model scale. We first introduce a lemma under the $K = 1$ setting.

Accuracy under $K = 1$

When $K = 1$, we can give an upper bound of accuracy by Λ and Γ. Taking into account the optimal solution in Eq. 9.2, we have the following accuracy lemma.

Lemma 9.4.2. *Consider $K = 1$ and $x_q \sim \mathcal{N}(0, I_d)$. When $N > C$, where C is a constant, we have*

$$\mathbb{E}_{w_\tau, x_1, \cdots, x_N}\left[Acc_\theta\right] \leq \operatorname{tr}(\Gamma^{-1}\Lambda).$$

Proof of Lemma 9.4.2. Since $K = 1$, the problem reduces to the linear regression problem in ICL. Consider the solution form in Lemma 9.4.1, we have

$$\hat{y}_q = x_q^\top \frac{1}{N}\Gamma^{-1}\sum_{i=1}^{N}\langle w_\tau, x_i\rangle x_i$$

We re-write the form as $\hat{y}_q = x_q^\top \hat{w}$. Following Equation (4.3) in Zhang et al. [2023b], we have:

$$\hat{w} = \frac{1}{N}\Gamma^{-1}\sum_{i=1}^{N}\langle w_\tau, x_i\rangle x_i.$$

Recall the definition of Acc_θ and $y_{\tau,q}^{(k)} = \text{sgn}(\langle w_\tau, x_{\tau,q}\rangle)$, $\widetilde{y}_{\tau,q}^{(k)} = \text{sgn}\left(\widehat{y}_{\tau,q}^{(k)}\right) = \text{sgn}(\langle \hat{w}, x_{\tau,q}\rangle)$, for any $\alpha > 0$, we have:

$$\mathbb{E}_{w_\tau, x_1, \cdots, x_N, x_q}\left[\text{Acc}_\theta\right] = P\left(\langle x_q, w_\tau\rangle > 0, \langle x_q, \alpha\hat{w}\rangle > 0\right) + P\left(\langle x_q, w_\tau\rangle < 0, \langle x_i, \alpha\hat{w}\rangle < 0\right).$$

Denote hyperplane orthogonal to w as $\mathcal{P}_w$ and similar to $\mathcal{P}_{\hat{w}}$. Recall that x_q is independent of other samples. We have the expectation conditioned on $w_\tau, x_1, \cdots, x_N$ is the probability that x_q falls out of the angle between $\mathcal{P}_w$ and $\mathcal{P}_{\hat{w}}$. Denote the angle between w and $\hat{w}$ as $\widetilde{\theta}$. As x_q is uniform along each direction (uniform distribution or isotropic Gaussian), then the probability is $1 - \frac{|\widetilde{\theta}|}{\pi}$ given $w_\tau, x_1, \cdots, x_N$. Then $\mathbb{E}_{w_\tau, x_1, \cdots, x_N}\left[\text{Acc}_\theta\right] = \mathbb{E}_{w_\tau, x_1, \cdots, x_N}\left[1 - \frac{|\widetilde{\theta}|}{\pi}\right]$. Note that

$$\mathbb{E}_{w_\tau, x_1, \cdots, x_N}\left[\cos(\widetilde{\theta})\right] = \left\langle \frac{w_\tau}{\|w_\tau\|_2}, \frac{\hat{w}}{\|\hat{w}\|_2}\right\rangle.$$

As, we can choose α, w.l.o.g, we take $\|w_\tau\| = \|\hat{w}\| = 1$, then we have

$$\mathbb{E}_{w_\tau, x_1, \cdots, x_N}\left[\cos(\widetilde{\theta})\right] = \mathbb{E}_{w_\tau}\left[\mathbb{E}_{x_1, \cdots, x_N}\left[\langle w_\tau, \hat{w}\rangle \,|w_\tau\right]\right].$$

Given w_τ, we have

$$\begin{aligned} E[\hat{w}|w_\tau] &= \frac{1}{N}\Gamma^{-1}\sum_{i=1}^{N} E\left[\langle w_\tau, x_i\rangle x_i | w_\tau\right] \\ &= \frac{1}{N}\Gamma^{-1}\sum_{i=1}^{N}\Lambda w_\tau \\ &= \Gamma^{-1}\Lambda w_\tau. \end{aligned}$$

Then, we have

$$\begin{aligned} E_{w_\tau}\left[\langle \hat{w}, w_\tau\rangle\right] &= \left\langle \Gamma^{-1}\Lambda w_\tau^\top, w_\tau\right\rangle \\ &= \operatorname{tr}(\Gamma^{-1}\Lambda). \end{aligned}$$

Thus, we have

$$\mathbb{E}\cos(\widetilde{\theta}) = \operatorname{tr}(\Gamma^{-1}\Lambda) \tag{9.12}$$

$$\mathbb{E}\left[\text{Acc}_\theta\right] = \mathbb{E}\left[1 - \frac{|\widetilde{\theta}|}{\pi}\right]. \tag{9.13}$$

Note that when $\theta \leq \frac{\pi}{6}$, we have $1 - \frac{|\widetilde{\theta}|}{\pi} \leq \cos(\theta)$. Thus, as $N > C$ where C is constant, we have $\hat{w}$ and w_τ are closed and satisfy $\theta \leq \frac{\pi}{6}$. Then we get the statement. □

Model scale on composite tasks

Here, we present proof for model scale and performance on composite tasks. Recall we consider the rank of W^{*PV} and W^{*KQ} as a measure of the model's scale.

We first introduce a lemma about U as an optimal full-rank solution.

Lemma 9.4.3 (Corollary A.2 in Zhang et al. [2023b]). *The loss function $\tilde{\ell}$ in Lemma 9.4.1 satisfies*

$$\min_{U\in\mathbb{R}^{d\times d},u\in\mathbb{R}} \tilde{\ell}(U,u) = -\frac{1}{2}\operatorname{tr}[\Lambda^2\Gamma^{-1}],$$

where $U = c\Gamma^{-1}, u = \frac{1}{c}$ for any non-zero constant c are minimum solution. We also have

$$\tilde{\ell}(U,u) - \min_{U\in\mathbb{R}^{d\times d},u\in\mathbb{R}} \tilde{\ell}(U,u) = \frac{1}{2}\left\|\Gamma^{\frac{1}{2}}\left(u\Lambda^{\frac{1}{2}}U\Lambda^{\frac{1}{2}} - \Lambda\Gamma^{-1}\right)\right\|_F^2. \tag{9.14}$$

As the scale of the model decreases, the rank of U also reduces, leading to an optimal reduced rank solution $\widetilde{U}$. Our findings reveal that this reduced rank $\widetilde{U}$ can be viewed as a truncated form of the full-rank solution U. This implies that smaller-scale models are essentially truncated versions of larger models, maintaining the core structure but with reduced complexity.

Recall Λ is the covariance matrix, we have eigendecomposition $\Lambda = QDQ^\top$, where Q is an orthonormal matrix containing eigenvectors of Λ and D is a sorted diagonal matrix with non-negative entries containing eigenvalues of Λ, denoting as $D = \operatorname{diag}([\lambda_1,\ldots,\lambda_d])$, where $\lambda_1 \geq \cdots \geq \lambda_d \geq 0$. We introduce the lemma below.

Lemma 9.4.4 (Optimal rank-r solution). *Recall the loss function $\tilde{\ell}$ in (Lemma 9.4.1). Let*

$$U^*, u^* = \operatorname*{arg\,min}_{U\in\mathbb{R}^{d\times d},\operatorname{rank}(U)\leq r,u\in\mathbb{R}} \tilde{\ell}(U,u).$$

Then $U^* = cQV^*Q^\top, u = \frac{1}{c}$, where c is any non-zero constant and $V^* = \operatorname{diag}([v_1^*,\ldots,v_d^*])$ is satisfying for any $i \leq r, v_i^* = \frac{N}{(N+1)\lambda_i + \operatorname{tr}(D)}$ and for any $i > r, v_i^* = 0$.

Then, we proof the Lemma 9.4.4

Proof of Lemma 9.4.4. Note that,

$$\begin{aligned}
\operatorname*{arg\,min}_{U\in\mathbb{R}^{d\times d},\operatorname{rank}(U)\leq r,u\in\mathbb{R}} \tilde{\ell}(U,u) &= \operatorname*{arg\,min}_{U\in\mathbb{R}^{d\times d},\operatorname{rank}(U)\leq r,u\in\mathbb{R}} \tilde{\ell}(U,u) - \min_{U\in\mathbb{R}^{d\times d},u\in\mathbb{R}} \tilde{\ell}(U,u) \\
&= \operatorname*{arg\,min}_{U\in\mathbb{R}^{d\times d},\operatorname{rank}(U)\leq r,u\in\mathbb{R}} \left(\tilde{\ell}(U,u) - \min_{U\in\mathbb{R}^{d\times d},u\in\mathbb{R}} \tilde{\ell}(U,u)\right).
\end{aligned}$$

Thus, we may consider Eq. 9.14 in Lemma 9.4.3 only. On the other hand, we have

$$\begin{aligned}
\Gamma &= \left(1+\frac{1}{N}\right)\Lambda + \frac{1}{N}\operatorname{tr}(\Lambda)I_{d\times d} \\
&= \left(1+\frac{1}{N}\right)QDQ^\top + \frac{1}{N}\operatorname{tr}(D)QI_{d\times d}Q^\top \\
&= Q\left(\left(1+\frac{1}{N}\right)D + \frac{1}{N}\operatorname{tr}(D)I_{d\times d}\right)Q^\top.
\end{aligned}$$

We denote $D' = \left(1+\frac{1}{N}\right)D + \frac{1}{N}\operatorname{tr}(D)I_{d\times d}$. We can see $\Lambda^{\frac{1}{2}} = QD^{\frac{1}{2}}Q^\top, \Gamma^{\frac{1}{2}} = QD'^{\frac{1}{2}}Q^\top$, and $\Gamma^{-1} = QD'^{-1}Q^\top$. We denote $V = uQ^\top UQ$. Since Γ and Λ are commutable and the Frobenius norm (F-norm) of a matrix does not change after multiplying it by an orthonormal matrix, we have Eq. 9.14 as

$$\begin{aligned}
\tilde{\ell}(U,u) - \min_{U\in\mathbb{R}^{d\times d},u\in\mathbb{R}} \tilde{\ell}(U,u) &= \frac{1}{2}\left\|\Gamma^{\frac{1}{2}}\left(u\Lambda^{\frac{1}{2}}U\Lambda^{\frac{1}{2}} - \Lambda\Gamma^{-1}\right)\right\|_F^2 \\
&= \frac{1}{2}\left\|\Gamma^{\frac{1}{2}}\Lambda^{\frac{1}{2}}\left(uU - \Gamma^{-1}\right)\Lambda^{\frac{1}{2}}\right\|_F^2 \\
&= \frac{1}{2}\left\|D'^{\frac{1}{2}}D^{\frac{1}{2}}\left(V - D'^{-1}\right)D^{\frac{1}{2}}\right\|_F^2.
\end{aligned}$$

As W^{KQ} is a matrix whose rank is at most r, we have V is also at most rank r. Then, we denote $V^* = \arg\min_{V\in\mathbb{R}^{d\times d},\mathrm{rank}(V)\leq r} \left\| D'^{\frac{1}{2}} D^{\frac{1}{2}} \left(V - D'^{-1}\right) D^{\frac{1}{2}} \right\|_F^2$. We can see that V^* is a diagonal matrix. Denote $D' = \mathrm{diag}([\lambda'_1, \ldots, \lambda'_d])$ and $V^* = \mathrm{diag}([v_1^*, \ldots, v_d^*])$. Then, we have

$$\left\| D'^{\frac{1}{2}} D^{\frac{1}{2}} \left(V - D'^{-1}\right) D^{\frac{1}{2}} \right\|_F^2 \tag{9.15}$$

$$= \sum_{i=1}^{d} \left(\lambda_i'^{\frac{1}{2}} \lambda_i \left(v_i^* - \frac{1}{\lambda'_i} \right) \right)^2 \tag{9.16}$$

$$= \sum_{i=1}^{d} \left(\left(1 + \frac{1}{N}\right) \lambda_i + \frac{\mathrm{tr}(D)}{N} \right) \lambda_i^2 \left(v_i^* - \frac{1}{\left(1 + \frac{1}{N}\right) \lambda_i + \frac{\mathrm{tr}(D)}{N}} \right)^2. \tag{9.17}$$

As V^* is the minimum rank r solution, we have that $v_i^* \geq 0$ for any $i \in [d]$ and if $v_i^* > 0$, we have $v_i^* = \frac{1}{\left(1+\frac{1}{N}\right)\lambda_i + \frac{\mathrm{tr}(D)}{N}}$. Denote $g(x) = \left(\left(1 + \frac{1}{N}\right) x + \frac{\mathrm{tr}(D)}{N}\right) x^2 \left(\frac{1}{\left(1+\frac{1}{N}\right)x + \frac{\mathrm{tr}(D)}{N}} \right)^2 = x^2 \left(\frac{1}{\left(1+\frac{1}{N}\right)x + \frac{\mathrm{tr}(D)}{N}} \right)$. It is easy to see that $g(x)$ is an increasing function on $[0, \infty)$. Now, we use contradiction to show that V^* only has non-zero entries in the first r diagonal entries. Suppose $i > r$, such that $v_i^* > 0$, then we must have $j \leq r$ such that $v_j^* = 0$ as V^* is a rank r solution. We find that if we set $v_i^* = 0, v_j^* = \frac{1}{\left(1+\frac{1}{N}\right)\lambda_j + \frac{\mathrm{tr}(D)}{N}}$ and all other values remain the same, Eq. 9.17 will strictly decrease as $g(x)$ is an increasing function on $[0, \infty)$. Thus, here is a contradiction. We finish the proof by $V^* = uQ^\top U^* Q$. □

We then ready to prove the Theorem 9.3.1 in Section 9.3.1, we first re-state it below.

Theorem 9.3.1. *Suppose a composite task satisfies confined support. Suppose that we have $(x_1, y_1, \ldots, x_N, y_N, x_q)$ as a testing input prompt and the corresponding W where $y_i = Wx_i$. As rank r decreases, $\mathbb{E}_{W,x_1,\cdots,x_N}[Acc_\theta]$ will have a smaller upper bound.*

Proof of Theorem 9.3.1. We first prove in a simple task setting ($K = 1$), that the accuracy will have such a conclusion. By Lemma 9.4.2, consider $x_q \sim \mathcal{N}(0, I_d)$. When $N > C$, where C is a constant, we have

$$\mathbb{E}_{w_\tau,x_1,\cdots,x_N}[\mathrm{Acc}_\theta] \leq \mathrm{tr}(\Gamma^{-1}\Lambda).$$

Recall Lemma 9.4.4. WLOG, we take $c = 1$. We have

$$\begin{aligned} \mathrm{tr}(\Gamma^{-1}\Lambda) &= \mathrm{tr}\left(QV^*DQ\right) \\ &= \sum_{i=1}^{r} \frac{N}{N + 1 + \sum_{j=1}^{r} \frac{\lambda_j}{\lambda_i}}, \end{aligned}$$

where second equation comes from Lemma 9.4.4.

Under the confined support setting, the same conclusion holds since Eq. 9.7 in the proof of Theorem 4.4.4.

□